

A PNEUMATIC SENSOR FOR
GRINDING WHEEL CONDITION MONITORING

A PNEUMATIC SENSOR FOR GRINDING WHEEL CONDITION MONITORING

By

KEVIN M. TANAKA, B.Eng.Mgt.

A Thesis Submitted to the School of Graduate Studies
in Partial Fulfillment of the Requirements for the Degree
Master of Applied Science

McMaster University

McMaster University © Copyright by Kevin M. Tanaka, July 2013

McMaster University, Hamilton, Ontario

MASTER OF APPLIED SCIENCE, Department of Mechanical Engineering

TITLE: A pneumatic sensor for grinding wheel condition
 monitoring

AUTHOR: Kevin M. Tanaka, B. Eng. Mgt. (McMaster University)

SUPERVISOR: Dr. Philip Koshy

NUMBER OF PAGES: xvi, 169

Abstract

Changes to the surface condition of a grinding wheel caused by excessive wear can result in geometric inaccuracy and severe thermal damage to a workpiece. As a precision metal removal process, grinding is typically a finishing operation and such errors are costly in both materials and lost time. Unfortunately grinding wheel performance is difficult to predict, and workpiece damage is commonly prevented by frequent dressing of the wheel surface. However, such over dressing is also costly in unnecessary machine down time and consumption of the grinding wheel. Monitoring systems have been developed in an effort to prevent damage to the workpiece and unnecessary dressing, but various difficulties have prevented any single system from achieving widespread application.

The following body of research focuses on the investigation and development of a pneumatic sensor for monitoring the surface condition of a grinding wheel. These sensors are relatively simple, robust and inexpensive, and well suited to in situ applications. While these sensors are traditionally used to measure displacement of static or quasi-static surfaces, research into dynamic applications has shown they can detect the features or topography of a moving surface. Inspired by these developments, a monitoring method employing both the static and dynamic measurement capabilities of the sensor is proposed with applications to both metal-bonded and vitrified grinding wheels.

Acknowledgements

As the author I would like to acknowledge the individuals and organizations that made this research possible.

I would like to thank my supervisor, Dr. Philip Koshy, for his encouragement, trust and support. His skill as an educator and commitment to his students and to this research made my experience as a graduate an exceptional one. I am grateful for his guidance and high expectations, which have pushed me, help me to grow, and made me a better thinker and problem solver. It is with the highest regard that I extend my gratitude to him and his relentless pursuit of innovative and interesting ideas.

My thanks are also extended to the technical staff of the mechanical engineering department; Terry, Jim, Joe, Mark, Mike and Ron, for their help in constructing and executing experiments, and for contributing to my education.

Finally I would like to acknowledge the generous support of the CANRIMT/NSERC, which made this research possible.

Table of Contents

1	Introduction.....	1
1.1	The Grinding Process	1
1.2	Grinding Wheel Construction	3
1.3	Current Monitoring Technology	6
1.4	Pneumatic sensors	8
2	Literature Review.....	12
2.1	Static and Dynamic Performance of Pneumatic Sensors	12
2.2	The Grinding Wheel Surface.....	18
2.2.1	Vitrified Grinding Wheels	18
2.2.2	Solid Bond Wheels	23
2.3	Existing Application of the Pneumatic Sensor to Grinding Wheels	29
3	Experimental Equipment and Setup.....	32
3.1	Monitoring Equipment	32
3.1.1	Hardware	32
3.1.2	Data Acquisition	35
3.2	Software	36
3.2.1	Data collection	36
3.2.2	Data processing	36

3.3	Machine Tool Setup	38
3.3.1	Grinding Machine	38
3.3.2	Grinding wheels	39
3.3.3	Additional Equipment.....	40
3.3.4	Positioning the Pneumatic Sensor.....	41
3.3.5	Additional Sensors	44
3.3.5.1	Accelerometer.....	44
3.3.5.2	Three-Component Dynamometer	45
3.4	Lathe.....	45
3.4.1	Pneumatic Sensor Mounting.....	48
3.4.2	Accelerometer	48
3.4.3	Coolant.....	49
3.5	Data Collection Method	50
4	Experimental Results and Discussion.....	53
4.1	Proof of concept	53
4.1.1	Initial Experimental Setup	53
4.1.2	Special Considerations.....	56
4.1.2.1	Effective Stand-Off Distance.....	56
4.1.2.2	Edge Effect	57

4.1.3	Initial Detection	59
4.1.4	Incremental Wear & MVA Modeling	61
4.2	Characterizing Surface to Sensor Relationships	67
4.2.1	Axial Sensitivity and Frequency Spacing	67
4.2.2	Deterministic Surfaces	70
4.2.3	Knurl Surface Modeling	81
4.2.3.1	Influence of Nozzle Diameter by Simulation	87
4.2.4	Detecting Nondeterministic Surfaces.....	88
4.2.5	Stand-off Distance and Dynamic Signal Amplitude.....	94
4.2.5.1	Increasing Stand-off Distance.....	97
4.2.5.2	Internal Pressure Effect.....	99
4.2.6	Maximum Stand-off Distance	101
4.2.7	Frequency Dependent Sensitivity	104
4.3	Quantifying the Dynamic Pressure Transducer Signal	109
4.3.1	Use of High Pass RMS	110
4.3.2	RMS Repeatability	111
4.3.3	Setting the Back Pressure Range	114
4.3.4	Principle of Dual Transducer Monitoring.....	116
4.4	Dressing.....	119

4.4.1	Metal Bond Wheel	120
4.4.1.1	Relative Change in High Pass RMS	124
4.4.2	Vitrified Wheel Dressing	126
4.5	Wear	130
4.5.1	Metal Bond Wheel	130
4.5.2	Vitrified Wheel	137
4.5.2.1	Grinding Burn	138
4.5.2.2	Long Term Wear.....	143
4.6	Measurement Variation by Axial Position of the Sensor	149
4.7	Effect of Coolant	152
5	Conclusions and Future Work	161
5.1	Conclusions	161
5.1.1	High Frequency Response	161
5.1.2	Dynamic Response and Maximum SOD	162
5.1.3	Monitoring Grinding Wheels	163
5.1.4	Effect of Coolant.....	163
5.2	Future Work	164
5.2.1	Improved Dynamic Response	164
5.2.1.1	Wheel Runout and Circularity	165

6	References.....	167
---	-----------------	-----

Table of Figures

Figure 1-1: Illustrations of the generic grinding process	2
Figure 1-2: Vitrified grinding wheel and magnified working surface.	5
Figure 1-3: Metal bond grinding wheel and magnified working surface.	5
Figure 1-4: Construction and operation of a pneumatic sensor for displacement ..	9
Figure 1-5: Characteristic relationship between back pressure and gap size.....	10
Figure 1-6: Projection of escape area on an uneven target surface.....	11
Figure 2-1: Decreasing air flow for increasing velocity of a rough surface	13
Figure 2-2: Air flow restriction by increasing roughness and nozzle diameter	14
Figure 2-3: Pressure fluctuations from a pore during a turning operation.....	16
Figure 2-4: Response of a pneumatic sensor identifying surface roughness	17
Figure 2-5: High initial wear for a range of crossfeed rates	20
Figure 2-6: High initial grinding forces for a vitrified grinding wheel.....	20
Figure 2-7: Illustration of semi glazed surface condition after dressing.....	21
Figure 2-8: Distribution of grain protrusion heights for varying grit sizes.....	24
Figure 2-9: Percent of wheel surface area made up of exposed abrasive grains ..	24
Figure 2-10: Brake Controlled Truing Device from Norton Abrasives.....	25
Figure 2-11: Abrasive from the truing wheel erodes bond material	26
Figure 2-12: Magnified image of a 170 grit metal bond grinding wheel.....	27
Figure 2-13: Typical wear flat developed on a diamond grain	28
Figure 2-14: Calibration curve from Maksoud <i>et al.</i>	30
Figure 3-1: The pneumatic sensor used in this research.	32

Figure 3-2: Control orifices.....	34
Figure 3-3: Blohm Planomat 408 CNC grinder at McMaster University.....	38
Figure 3-4: Removal of significant burrs from the nozzle tip.....	42
Figure 3-5: Setting bottom dead center.....	43
Figure 3-6: Accelerometer positioning.	44
Figure 3-7: Okuma Lathe at McMaster University.....	45
Figure 3-8: Shaft mounted aluminum disk test surface.	46
Figure 3-9: Sample of Diamond Knurled Surface	47
Figure 3-10: Pneumatic sensor mounting in lathe based experiments.....	48
Figure 3-11: Indirect coolant application and cleaning in lathe	49
Figure 3-12: Illustration of fixed stand-off distance reference	51
Figure 4-1: Distance and Back Pressure: Theoretical relationship.	55
Figure 4-2: Back pressure curve for a vitrified grinding wheel.....	56
Figure 4-3: Edge effects.....	58
Figure 4-4: Raw dynamic signal with and without rotating wheel surface	60
Figure 4-5: Frequency domain, dynamic response to a moving wheel surface....	61
Figure 4-6: Frequency domain, dynamic signal, with not moving wheel surface	61
Figure 4-7: Incremental wear for proof of concept.....	63
Figure 4-8: Score plot of PCA model for incremental wear.	64
Figure 4-9: Score plot of verified PCA model.....	65
Figure 4-10: A unique PCA model is created by each data set.....	66
Figure 4-11: Dynamic signal from at two axial locations.....	68

Figure 4-12: Equal spacing of frequencies generated by the wheel surface.	69
Figure 4-13: Knurled and smooth surface, frequency domain plot.	71
Figure 4-14: Helices formed by knurls in fine and medium diamond knurls.	72
Figure 4-15: Varying internal geometry and volume of the pneumatic sensor	75
Figure 4-16: Frequency of knurls shifts with increasing surface velocity	76
Figure 4-17: Frequency domain of straight, coarse knurl surface	76
Figure 4-18: Separation of frequency peaks due to knurling helices.....	77
Figure 4-19: 7-start thread in disk surface	78
Figure 4-20: Frequencies generated by multi-start thread for 20 and 30 m/s	79
Figure 4-21: Trimmed knurls.....	80
Figure 4-22: Amplitude of frequency response is reduced by trimming knurls ...	81
Figure 4-23: Model of knurled surface.	82
Figure 4-24: Knurl model of the escape area, 3 increments.	83
Figure 4-25: Model of knurled surface at nozzle perimeter, 40 increments	84
Figure 4-26: Frequency response to fine knurl at 20 m/s predicted by model	85
Figure 4-27: Frequency response predicted by model with no helix.....	86
Figure 4-28: Simulated effect of helices for 10 and 20 helices per rotation.....	87
Figure 4-29: Simulation of varying nozzle diameter	88
Figure 4-30: Frequency response to a grinding wheel and trimmed knurls	89
Figure 4-31: Separation of frequency peaks in metal bond grinding wheel	90
Figure 4-32: Signal separation at high frequency.	91
Figure 4-33: High sample rate signal in the frequency domain.....	92

Figure 4-34: Response to trued dressed surface condition	93
Figure 4-35: Raw dynamic signal for varying SOD	96
Figure 4-36: Increasing SOD on coarse, straight knurled surface.	98
Figure 4-37: Increases in average back pressure on straight, coarse knurl.....	100
Figure 4-38: Stand-off distance and actual average distance.....	101
Figure 4-39: Finding maximum SOD for a metal bond grinding wheel.....	102
Figure 4-40: High pass RMS response to stand-off distance, no velocity	103
Figure 4-41: Frequency domain signal for 20 and 30 m/s, vitrified wheel.....	105
Figure 4-42: Frequency peaks shifting with increasing surface velocity.....	106
Figure 4-43: PCA score plot of trued and dressed metal bond wheel.	108
Figure 4-44: Variable importance plot of trued to dressed PCA model.	108
Figure 4-45: Continuous monitoring of a metal bond grinding wheel, dressing	110
Figure 4-46: Spectrogram of the raw dynamic pressure transducer signal.....	112
Figure 4-47: Axial variation of high pass RMS values.....	114
Figure 4-48: Finding the average back pressure range.	116
Figure 4-49: Plotting of gauge and dynamic measurements, Pb-RMS curve.	118
Figure 4-50: Trued and dressed back pressure curves.	119
Figure 4-51: Pb-RMS curve for incremental dressing of a metal bond wheel ...	122
Figure 4-52: Interpolating High Pass RMS at multiple Pb values.....	124
Figure 4-53: High Pass RMS Normalized by initial surface value.....	125
Figure 4-54: Differential dressing of a vitrified grinding wheel.....	127
Figure 4-55: Pb-RMS curve for differential dressing of a vitrified wheel.	127

Figure 4-56: Changing average back pressure with dressing.	129
Figure 4-57: Pb-RMS curve for incremental wear of a metal bond wheel.	132
Figure 4-58: Changing average Pb with wear.....	133
Figure 4-59: Photograph of the worn grinding wheel surface.	134
Figure 4-60: Pulled grains produce a new, large feature.	135
Figure 4-61: Abrasion of bond material by chips.	135
Figure 4-62: Ground workpiece surface after final grinding pass.	136
Figure 4-63: Grinding wheel section worn by grinding burn.	139
Figure 4-64: Pb-RMS curve of grinding burn by vitrified wheel.	140
Figure 4-65: Grinding wheel surface as dressed and worn with grinding burn..	141
Figure 4-66: Wear flats and loading of the vitrified wheel by grinding burn....	142
Figure 4-67: Long term wear testing Pb-RMS curve.....	144
Figure 4-68: Dynamometer measurements of normal force.	146
Figure 4-69: Effect of axial position on pneumatic sensor measurements	151
Figure 4-70: Illustration of in-process setup.	153
Figure 4-71: Indirect coolant application in lathe.....	154
Figure 4-72: Straight knurls with no coolant and with coolant	155
Figure 4-73: Back pressure with coolant and intermittent clearing by air jet.....	156
Figure 4-74: Effect of coolant on vitrified wheel measurements.....	157
Figure 4-75: Effect of coolant on metal bond wheel measurements.....	158
Figure 4-76: Metal bond wheel dressing in the presence of coolant	159
Figure 5-1: Low pass filtered dynamic response	165

Table of Tables

Table 3-1: Pressure Sensors and Regulators	33
Table 3-2: Data Acquisition Cards.....	36
Table 3-3: Knurl geometry.....	47
Table 3-4: Sensor setup according to grinding wheel.....	50
Table 4-1: Grinding parameters for metal bond grinding wheel wear.....	131
Table 4-2: Grinding parameters for vitrified wheel grinding burn.	138
Table 4-3: Parameters for vitrified wheel long term wear testing.	143

*This work is dedicated to my loving family, my wife, and to the memory of my
grandmother, grandfather, and my father-in-law.*

1 Introduction

The following chapter presents the principal aspects of this research, and provides a discussion of the grinding process and grinding wheels. An overview of current methods used to monitor the grinding process for grinding burn and the need to dress is given, and the basic structure and operation of a pneumatic sensor are explained.

1.1 The Grinding Process

Grinding is an abrasive metal removal process, generally used on hard materials or to produce fine surface finishes and precise geometries as a finishing operation. As illustrated in Fig. 1-1, in grinding many thousands of small abrasive grains are bonded together to form a grinding wheel, which is rotated at a high speed to a surface velocity of 20 m/s or more and fed into a workpiece. Each of the abrasive grains on the surface of the wheel is a small cutting tool, shearing away a small amount of material. A grinding wheel may have hundreds of grains cutting at once, even at typical depths of cut, on the order of tens of micrometers. High velocity nozzles apply coolant directly to the area being ground to help reduce friction and control heat. Small pores between each grain help to draw in coolant and carry away the chips produced by each of the microscopic cuts.

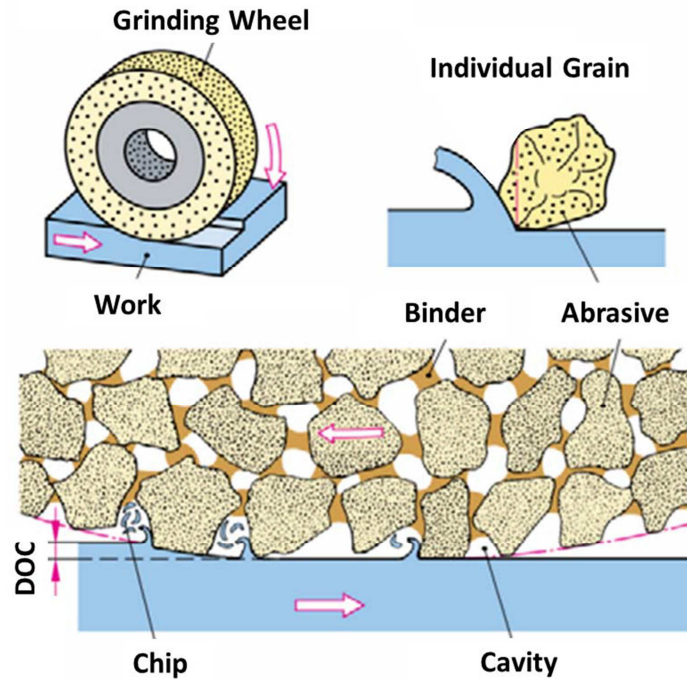


Figure 1-1: Illustrations of the generic grinding process and abrasive material removal [1]

Like any cutting tool, a grinding wheel will wear with continued use, compromising performance. The forces, heat and debris generated by grinding can negatively alter the wheel surface in a process generally referred to as grinding wheel wear. Grinding wheel wear can result in widespread loss of material from the edges and corners of the grinding wheel, altering its profile, or in the glazing of the wheel surface. Glazing arises from grains dulling and generating wear flats, and an over-accumulation of debris in the pores, functionally closing up the wheel surface. As this type of grinding wheel wear progresses, the force generated between individual grains and the workpiece can increase, and result in serious thermal damage to the workpiece known as grinding burn. To prevent damage to the workpiece or geometric errors, the

conditioning processes of truing and dressing are used to restore the surface of the grinding wheel.

Truing and dressing refer to the profiling and sharpening of the wheel surface respectively. The truing process removes abrasive and bond material from the grinding wheel in order to set the wheel profile and minimize runout. If it is required, truing always precedes dressing. Dressing works to sharpen and open up the wheel surface, removing the previously worn surface and generating new cutting edges by exposing fresh grains, or fracturing dull grains. In this way dressing is used to set the micro geometry of the wheel surface and is important in determining the performance and function of the grinding wheel.

Unlike conventional cutting tools, a grinding wheel has some capacity for self-sharpening. In an ideal case, as the grinding wheel wear progresses the increasing force between grains and the workpiece will eventually generate new cutting edges. This occurs when the force causes a worn grain to fracture or fractures the bonds holding a worn grain, resulting in grain pull out. A grain may fracture several times or not at all before falling away completely, depending on the application, wheel specifications and cutting conditions.

1.2 Grinding Wheel Construction

The volume of a grinding wheel is composed of abrasive grains, bond material and small voids. Abrasive grains are generally irregularly shaped crystals or ceramic particles, and are classified by composition and size. They are

typically between a quarter and half a millimeter in diameter, but may range from tens of micrometers up to a millimeter or more. Grinding wheels are typically 20 to 30 cm in diameter, and will contain grains of similar size connected to each other by a bonding material. The remainder of the wheel may be made up of voids, referred to as pores.

Grinding wheels are commonly one of two classes of bond type. Conventional grinding wheels commonly use a ceramic bonding material, which is heated to produce a vitrified wheel. These wheels are porous and can be made with varying degrees of hardness. Most commonly, these wheels are trued and dressed using a diamond dressing tool, which is fed into the rotating grinding wheel as in a turning operation. Metal bond wheels are the strongest solid bonded wheels and usually contain superabrasive grains such as diamond or cubic boron nitride (CBN), distributed within a layer of metal on the working surface of the grinding wheel. In this type of grinding wheel the abrasive grains protrude from the outer surface of the solid metal bond layer, and no additional space or pores between the grains is present. Resin may also be used as the bonding material with this type of wheel construction. Metal bond grinding wheels are typically trued and dressed by separate abrasive processes to remove or erode the bond material. Other bonding systems do exist, but are not as common, and are not examined in this research. Fig. 1-2 and 1-3 respectively show examples of the vitrified and metal bond grinding wheel construction and magnified images of their working surfaces.

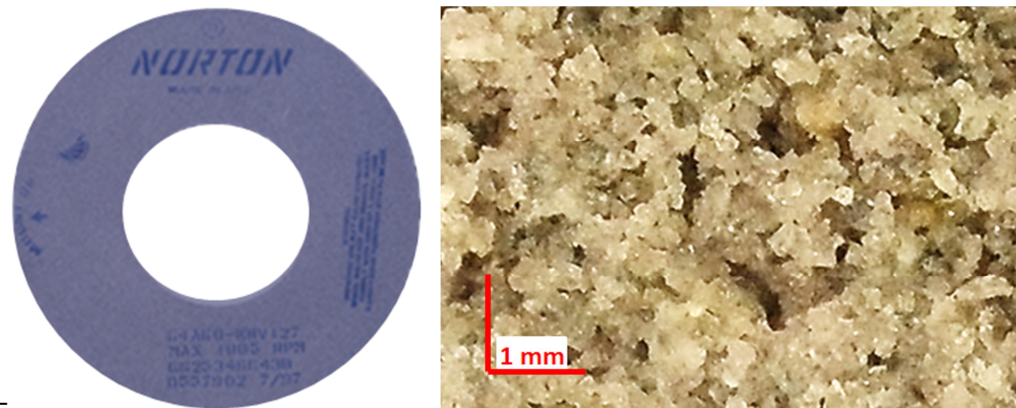


Figure 1-2: Vitrified grinding wheel [2] and magnified working surface.

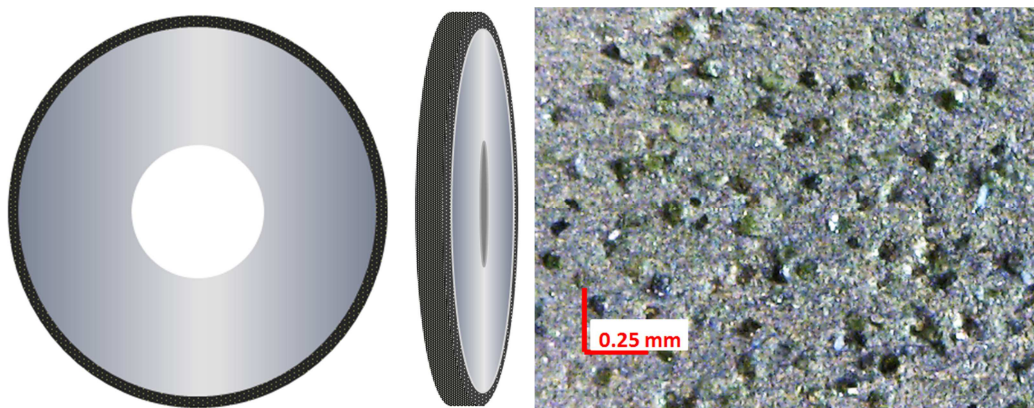


Figure 1-3: Metal bond grinding wheel and magnified working surface.

Thermal damage to workpieces from a worn grinding wheel can be costly because grinding is typically a finishing process. However, predicting grinding wheel performance is difficult, as it commonly varies from one wheel to the next, even with identical specifications. Workpiece damage can be prevented by frequent dressing, but such over dressing is costly due to unnecessary machine down time and consumption of the grinding wheel. Monitoring of the grinding wheel is therefore required, to both prevent damage and reduce unnecessary

dressings. However, unlike other conventional metal cutting tools such as milling tools, where the geometry of the cutting edge is specified, the size and geometry of grains and pores, and the orientation of each grain within the wheel is non-deterministic. The constant evolution of wheel surface condition is also unique to grinding, and with surface speeds typically at or above 20 m/s, monitoring of the wheel surface is a difficult challenge.

1.3 Current Monitoring Technology

A range of sensors and techniques are currently applied to the grinding process and wheel in an effort to prevent the expense of damaged workpieces and over dressing. The most common monitoring systems are indirect and take measurements of process related quantities such as forces or acoustic waves to empirically infer the condition of the wheel surface. The most promising indirect systems include the use of dynamometers, spindle power monitoring and acoustic emissions (AE) sensors. Direct monitoring methods are less common but take measurements straight from the wheel surface. One example is an optical method employing reflected laser light to detect wear flats on grains, which can be related to grinding forces and wear [3].

Various difficulties and barriers have prevented any single system from achieving widespread application. Some systems are simply not well suited for use in situ, where the grinding environment causes too much interference. Optical measurement systems suffer in this way, as the coolant and debris makes reliable

measurements difficult and various methods must be employed to shield both the sensor and the measured area of the grinding wheel [4].

Monitoring of the spindle power consumption or torque is easily accomplished by a variety of systems and sensor, and can be related to the cutting force. The ease with which spindle power can be measured is over shadowed by the fact that tangential grinding is force not heavily affected by wear [4].

Acoustic emission or AE sensors capture high frequency elastic waves and are adept at contact detection. This sensor can be implemented in a range of possible positions, both on the grinding wheel and the workpiece, and has previously been successful in the monitoring of dressing and the detection of wheel chatter [5,6]. Promising developments include the rapid and reliable identification of grinding burn, which has been shown to increase AE signal amplitude [7], and by using AE sensors as inputs, a neural network can quickly identify workpieces that have been damaged [8].

One of the most established and accepted sensors for monitoring grinding wheel wear is the force dynamometer. Typically, the workpiece is mounted on top of the dynamometer, and the cutting and feed forces are measured incrementally or continuously during the grinding process. The normal force between the grinding wheel and the workpiece can be used to monitor the development of wear flats and closing up of the wheel surface. While this makes them effective for protecting the surface integrity of the workpiece, dynamometers are too expensive for most enterprises as they typically cost tens of thousands of dollars.

In response to the difficulties experienced by current sensors, this research investigates the novel application of a pneumatic sensor as an inexpensive and effective in-process monitoring sensor for grinding wheel wear.

1.4 Pneumatic sensors

Pneumatic sensors are typically applied as static or quasi-static measurement tools for displacement. Also known as flapper-nozzle gauges, they are non-contact sensors relying on compressed air to monitor the distance between the sensor and a surface. This simple measurement tool is relatively inexpensive and well suited to in situ measurement applications as the equipment is both simple and robust.

The basic operation of a pneumatic sensor is illustrated in Fig. 1-4. The sensor chamber is supplied with air at a constant pressure P_s through a control orifice, and exits the chamber through a nozzle. The exiting air flow is restricted by the presence of a flat surface close to the nozzle tip, at a distance X_i . The restricted exit flow results in a back pressure P_b inside the sensor chamber, which is monitored by a sensitive pressure gauge. Changes to the distance are indicated by corresponding changes to the back pressure.

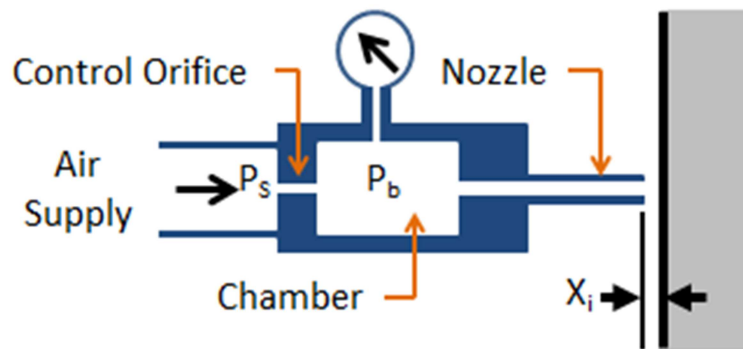


Figure 1-4: Construction and operation of a pneumatic sensor as a displacement indicator.

The back pressure in the pneumatic sensor has a non-linear response to changes in the gap size or distance X_i , as illustrated in Fig. 1-5. The back pressure and the sensitivity to a change in distance are both dependent on current distance from the surface. As a general description of this relationship the curve is roughly divided into three regions. The first region occurs when the nozzle tip is at or very near the surface. When the gap size is zero and the nozzle is sealed by the impinging surface, the back pressure in the chamber is equal to the supply pressure and there is no air flow. As the nozzle is moved away from the surface, the back pressure initially changes at a relatively slow rate, showing low sensitivity. The second region is where the back pressure is the most sensitive and is the desirable working range for measurements. Although still non-linear, the relationship between distance and back pressure is often approximated as linear for a short and defined range. In the third region, the dependence of the back pressure on the gap size decreases, and eventually reaches a minimum pressure with air flow only limited by the nozzle.

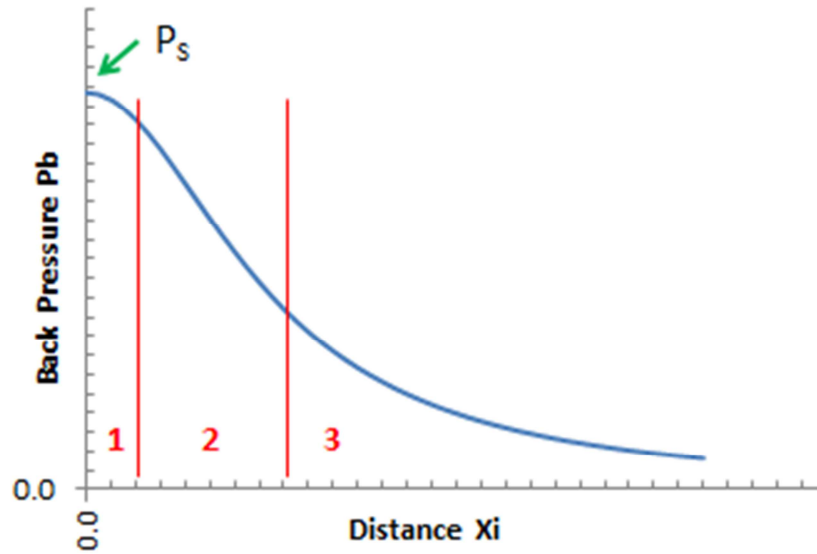


Figure 1-5: Characteristic relationship between back pressure and gap size.

While traditionally used to indicate distance or gap size, changes to the back pressure can also be applied to a moving surface to indicate the presence of surface features or roughness. This is possible because the back pressure is dependent on the area through which air can escape, and is given by the product of the perimeter of the nozzle and the distance between the nozzle and surface. For a flat target surface the escape area is therefore the circumference of the nozzle projected across the gap distance. Passing surface features such as bumps or pores can decrease or increase that area. Fig. 1-6 shows a nozzle passing over a step in the target surface, and the escape area for air flow is outlined by the dotted lines. As a step in the target surface passes under the nozzle, the total escape area

is altered by localized changes in gap size across a portion of the nozzle perimeter.

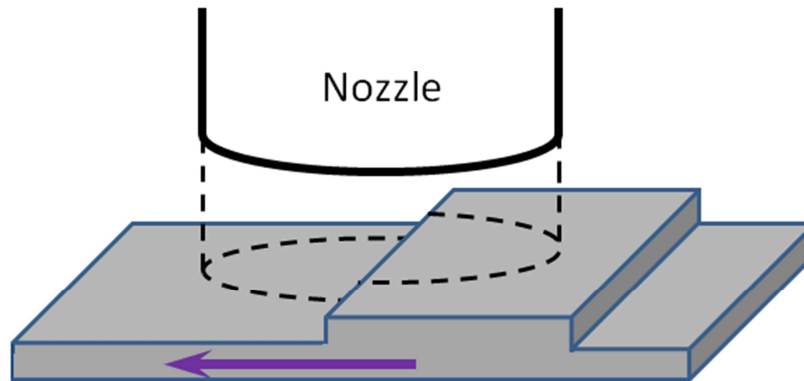


Figure 1-6: Projection of escape area on an uneven target surface.

This principle has allowed pneumatic sensors to be successfully used on moving surfaces for surface porosity detection [9]. The same geometric effect applies to detection of smaller features or assessment of surface topography, which create a partial blockage of the escape area and thus restricts the flow of air.

Going forward, this current research will focus on the development of the pneumatic sensor as a monitoring tool for the grinding process. It is to be determined if a pneumatic sensor is capable of detecting a wheel surface at operating speeds and conditions relevant to grinding, and if monitoring of the wheel surface condition is possible.

2 Literature Review

This chapter expands on the topics discussed in the Introduction, and highlights the current state of development of pneumatic sensors prior to this research, as well as the composition and changing topography of the grinding wheel surface. A review of important works relating to the operation and nature of the pneumatic sensor when applied to moving surfaces and grinding wheels is provided.

2.1 Static and Dynamic Performance of Pneumatic Sensors

Research by Wager [10] examines distance X_i measurements from still and moving surfaces, and documents the effect of surface roughness and surface velocity on air flow velocity. The experiments are comparable to the previously discussed pneumatic sensor employing back pressure measurements, and also included the use of opposing twin nozzles to eliminate the effects of run out when testing at high rotational velocities. Testing on a smooth disk, the surface velocity was shown to have no effect on the ability of the sensor to measure distance, other than the physical expansion of the disk due to rotation for surface velocities of up to 76 m/s. The testing was repeated using surfaces of varying roughness, up to 1350 $\mu\text{in CLA}$, initially reporting that for surface velocities up to 30.48 m/s, the roughness has little effect. However, by reducing the nozzle diameter from 2.67 to

1.17 mm both surface roughness and velocity could be related to changes in the indicated distance, Fig. 2-1.

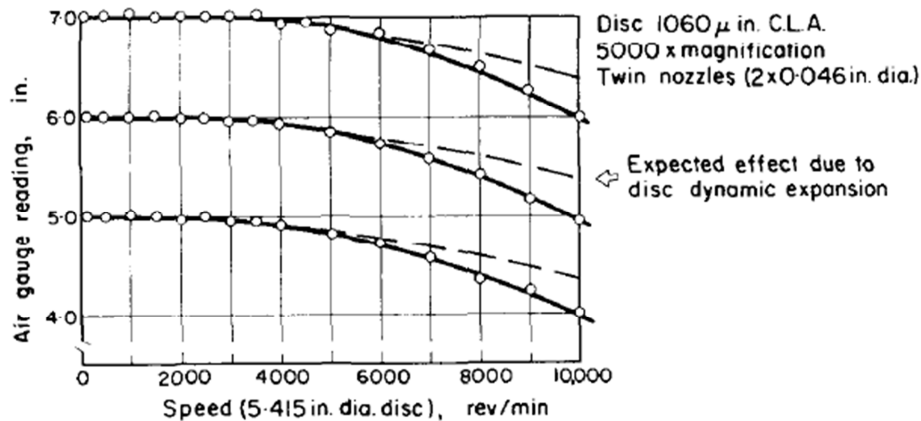


Figure 2-1: Decreasing air flow due to increasing rotating surface velocity of a rough surface [10]

Experimental results show air flow from the sensor was increasingly restricted by increasing surface roughness and velocity, but was only reported to occur at approximately 30.48 m/s or greater, and for roughness values greater than 500 μ in CLA. Air flow restriction is shown to be more pronounced for smaller nozzle diameters by the experimental results in Fig. 2-2 [10], examining a range of diameters as small as 0.7874 mm, at a surface speed of 71.5 m/s.

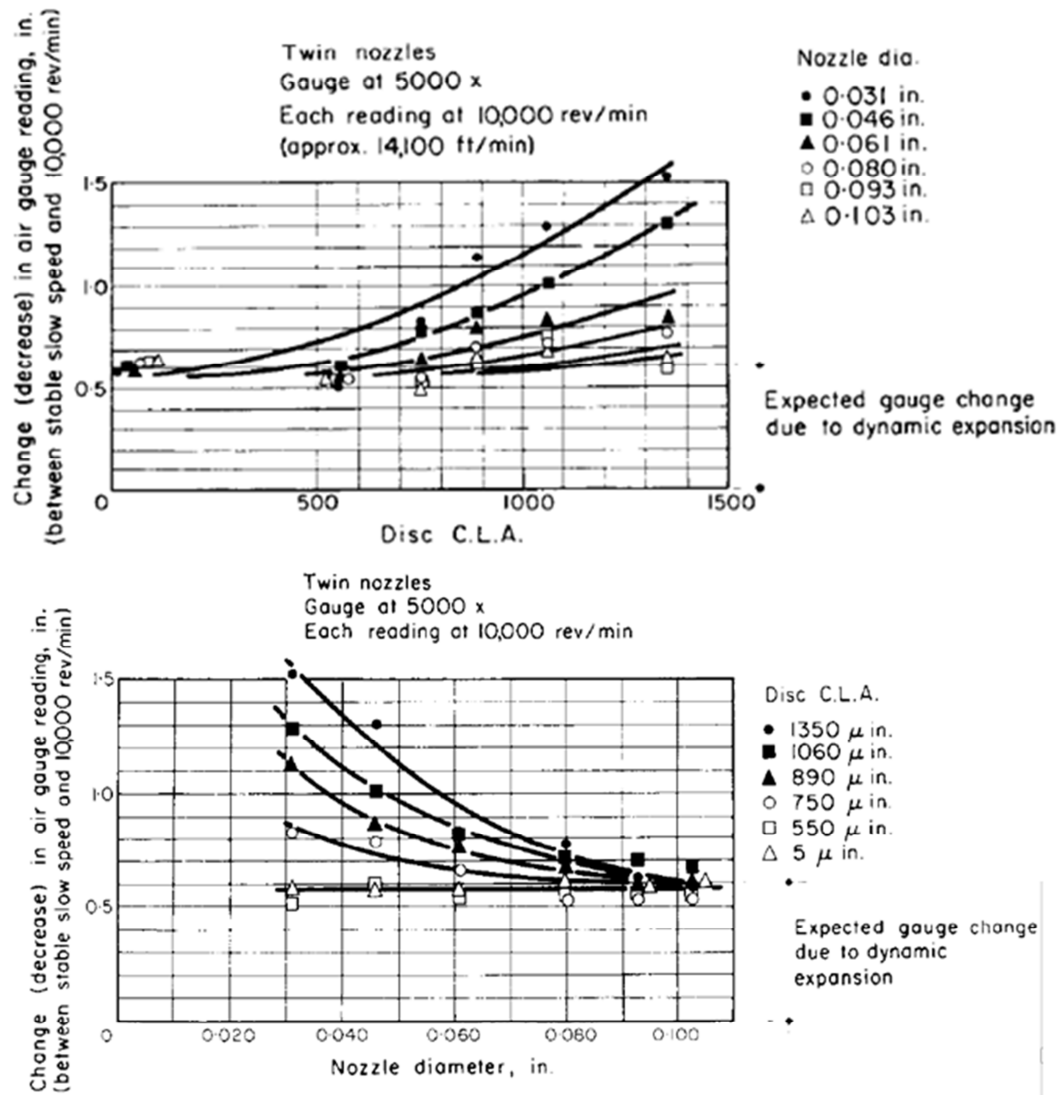


Figure 2-2: Air flow restriction due to increasing surface roughness and nozzle diameter [10].

While these results may suggest such a system could be used for roughness measurements on high speed surfaces, nominal values of flow or back pressure cannot distinguish between a change in actual distance and a change in surface roughness. This ambiguity makes it unsuitable for monitoring the condition of a grinding wheel. Wager concludes that surface roughness has little

effect on distance measurements, and that pneumatic sensors can be reliably used to monitor position on fast moving, rough surfaces, including grinding wheels [10]. The implication of this conclusion is that a steady air flow rate and back pressure may be maintained in grinding applications for a variety of wheel speeds and conditions.

Measurements of surface roughness and the detection of surface features has previously been accomplished by properly equipping a pneumatic sensor to respond quickly to very short or high frequency pressure fluctuations. Research works by Rucki *et al.* [11,12] have highlighted the importance of a small chamber size and high back pressure for increased dynamic performance. Similarly, Grandy *et al.* [13] showed that increasing the supply pressure will increase the amplitude of the pneumatic sensor's response. It has also been found that the relative sizes of the control orifice and nozzle diameters contribute to determining the rise time of the sensor, and that while a relatively small control orifice can enhance sensitivity for distance measurements, they lengthen the rise time [12].

Success has been achieved for detecting and characterizing surface roughness by using a dynamic pressure transducer to capture rapid fluctuations in the back pressure. Surfaces as fine as $0.1\mu\text{m } Ra$ [13,14] can be identified, and small pores, 0.6-1.6 mm in diameter have been detected at surface velocities of 50-200 m/min [9].

As detailed by Menzies *et al.* [9] the detection of surface porosity is made possible by a brief increase in escape area as the porosity passes under the nozzle.

The resulting time domain signal taken from a dynamic pressure transducer shows that a unique burst is generated in response to each pore. The example shown below is for porosity detected during a turning operation, Fig. 2-3. The ability to generate a unique response to each surface feature is an important capability in regards to the monitoring of a grinding wheel.

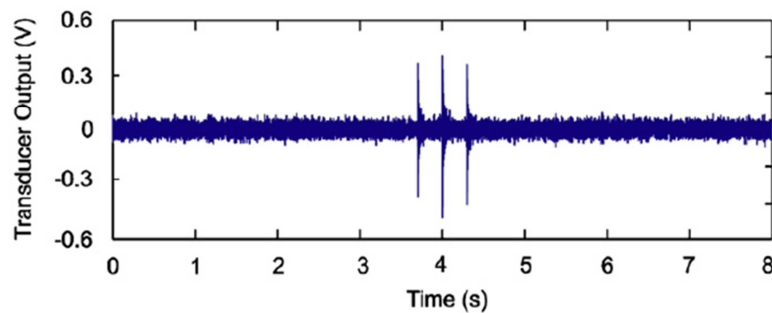


Figure 2-3: Pressure fluctuations from a pore during a turning operation at 100 m/min [9].

Grandy *et al.* [13] extracted more detailed information from the dynamic pressure transducer signal for surface roughness assessment. Specifically by examining signal frequency and amplitude to determine the wavelength and amplitude respectively for machined surfaces, Fig. 2-4.

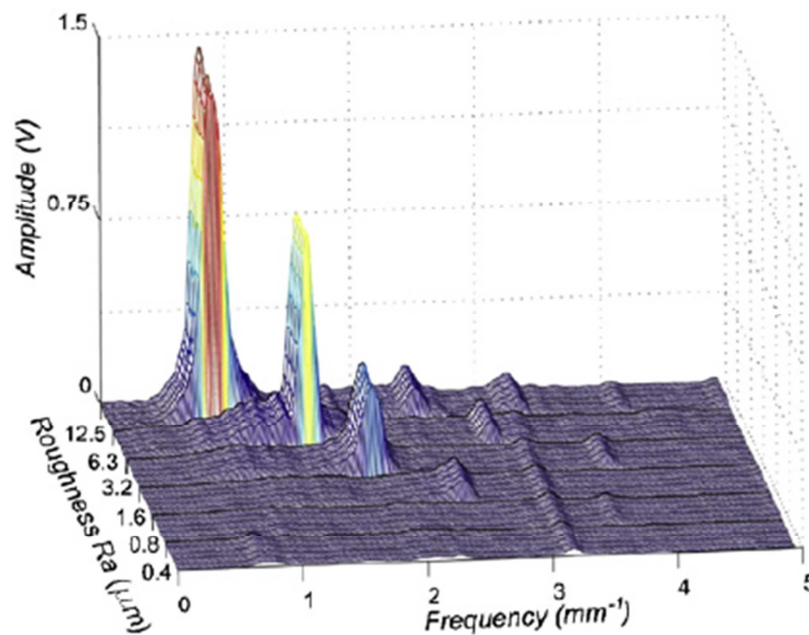


Figure 2-4: Dynamic response of a pneumatic sensor identifying surface roughness of milled surfaces [13].

While this relatively direct analysis is sufficient for milled or turned surfaces, the application of the same sensor to ground and lapped surfaces better demonstrates the depth of information captured by the dynamic response of the sensor. In the work of Koshy *et al.* [14], examining signals in the frequency domain from lapped and ground surfaces, each finished to $0.1 \mu\text{m Ra}$, the statistical analysis method of principal components analysis was successfully used to differentiate each surface and classify further surfaces.

The static and dynamic behaviour of a pneumatic sensor, as outlined by existing research, is promising in regards to monitoring the surface of a grinding wheel. Monitoring of dynamic pressure fluctuations provides the sensor with the

crucial ability to distinguish between a change in surface position and a change in surface topography, not previously available from the traditional application of pneumatic sensor employing nominal back pressure readings. However, the capabilities of a pneumatic sensor when applied to a grinding wheel surface remain uncertain, due to the significantly higher surface velocity and variable topography. The following section will build on the earlier discussion of grinding wheels, and provides some insight into the grinding wheel surface and the changes that take place during a grinding cycle.

2.2 The Grinding Wheel Surface

Before a pneumatic sensor can be applied to monitoring the surface of a grinding wheel, it is useful to have some understanding of the topographical structure and changes that can be expected from various dressing and grinding conditions. When discussing the grinding wheel surface, it is important to remember that the size, shape and spacing of each abrasive grain are probabilistic and that each surface grain is different in how it is initially dressed, how it cuts and how it wears.

2.2.1 Vitrified Grinding Wheels

The grinding cycle begins with the dressing of the wheel surface, and it is generally accepted that dressing is the most important factor in determining the condition and performance of a grinding wheel surface. As explained earlier, the

most common dressing method for vitrified wheels is the single point diamond dressing tool, which is used as in a turning operation to sharpen and open up the wheel surface. Other dressing methods exist, but are less common. Regardless of the method, the effect is the same, removing the worn surface to expose new grains or creating new cutting edges through grain fracture. In addition to wheel speed, which should be set to match the operating wheel speed, the dressed topography is typically controlled by selection of an appropriate crossfeed rate. The profile of the diamond dressing tool and the dressing depth also have some effect but are not as influential [15].

The crossfeed rate refers to the traversing rate of the dressing tool across the wheel surface, parallel to the axis of rotation, and is measured in distance per revolution. As in the comparable turning operation, low crossfeed rates result in a smoother surface and lower forces during the dressing operation. The terms coarse and fine dressing correspond to high and low crossfeed rates, and typically vary from half to one nominal grain diameter per wheel revolution [16]. Coarser dressing parameters produce a more open or aggressive wheel surface for bulk material removal while finer dressed wheels produce better surface finishes, but load more easily and correspond to limited material removal rates [17].

Once put into operation, the initial wear rate on a dressed wheel surface is typically very high, as shown in Fig. 2-5.

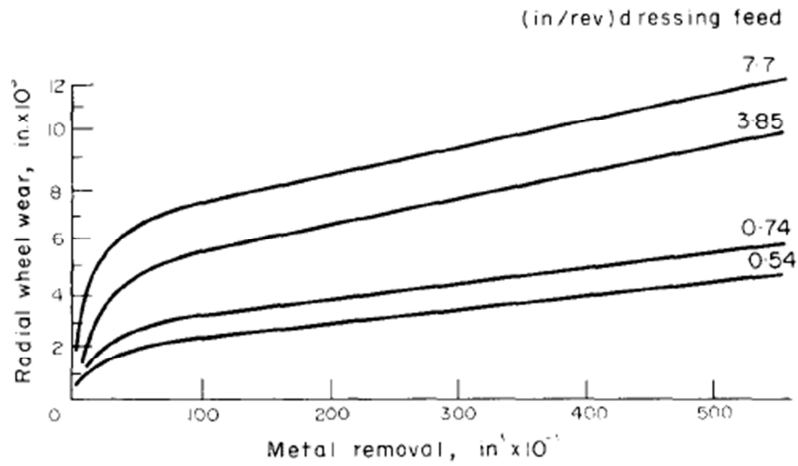


Figure 2-5: High initial wear for a range of crossfeed rates on a 60 grit vitrified wheel. [17]

In addition to this trend in wear, grinding forces rapidly climb to a peak and then descend [17,18,19]. Example results are shown in Fig. 2-6.

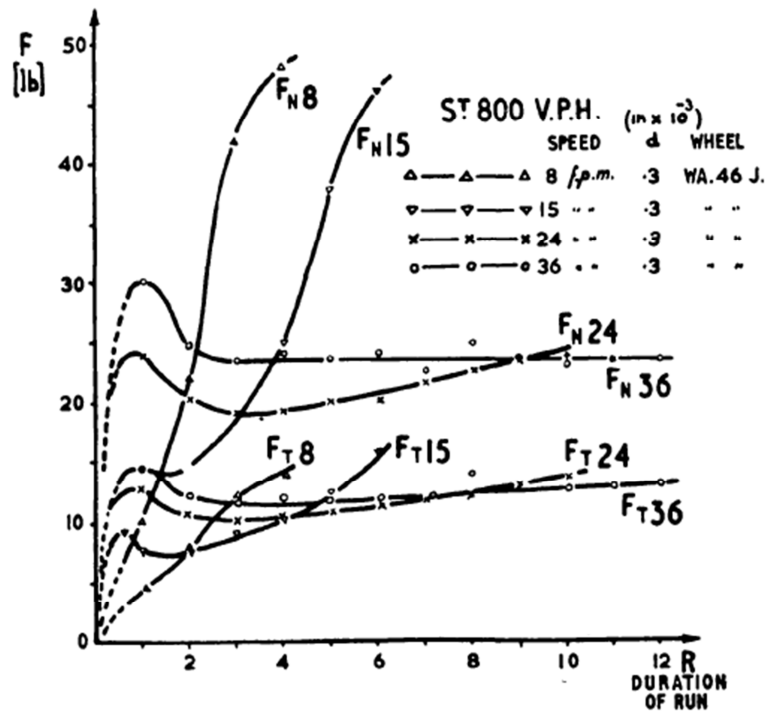


Figure 2-6: High initial grinding forces for a vitrified grinding wheel over a range of feed rates. [18]

Observations from researchers Davis and Grisbrook [17,18] have demonstrated these results and have studied the causes. Both researchers report that the wheel surface has many surface grains cut flush to the peripheral surface of the grinding wheel immediately after dressing. These flush cut areas provide no clearance and increase tangential and normal forces during grinding in the same manner as flank wear on conventional cutting tools. It is also reported that many larger flush areas are created by the bond material that surrounds and connects the abrasive grains being flush to the periphery of the grinding wheel, as shown in Fig. 2-7 [17], and by multiple grains in close proximity to each other [18]. In this way, the wheel may be considered to be semi-glazed just after dressing.

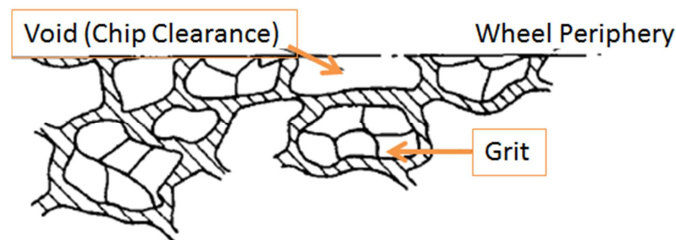


Figure 2-7: Illustration of semi glazed surface condition after dressing. Adapted from Davis [17]

According to Grisbrook [18], this initial state is quickly changed with successive grinding passes, and the bond material is broken away by the high initial grinding forces. With the loss of bond material, flush grains are sharpened as the edges are exposed and fracture. The surface is further opened up by the loss of grains without sufficient support, creating or enlarging pores and providing improved clearance for chips. As this initial wear or break-in process advances, the grinding forces decline by some degree and eventually reach a stable value

with a significantly reduced wear rate. For higher feed rates this is clearly seen in Fig. 2-6. An exception to this breaking-in process can occur when using exceedingly hard grinding wheels or low material removal rates, where the wheel surface is too strong or the grinding forces are too low. Fig. 2-6 illustrates this showing the forces for varying table feed rates. The forces generated by the lower feed rate do not peak, but climb steadily as the wheel surface becomes worn.

In assessment of crossfeed rate, Davis [17] reports that the semi-glazed effect is more pronounced for finer dressing parameters, with coarser parameters producing more fractured abrasive edges at the wheel periphery, but also greater forces during dressing. Many of the grains and bonds in a coarser dressed wheel surface are weakened as a result, and the initial wear rate is higher. In this way the dressing depth of cut also has some effect, but is not typically varied as a dressing parameter other than for spark-out passes.

The progression of wheel wear after the initial break-in is dependent upon the wheel makeup and dressing, as well as the workpiece material and the grinding parameters. As described above, the abrasive grains will dull and develop wear flats, reducing clearance and entraining chips. This leads to increasing grinding forces and the generation of heat. Self-sharpening occurs when the increased force causes grains to refracture or fall away to create or expose new abrasive edges and regenerate clearance. The wheel life is ended when repeated grain and bond fracture has eroded the wheel surface and dimensional accuracy is lost, or when the surface becomes glazed and the

workpiece is at risk of grinding burn. How a wheel wears and the rate at which it wears can be controlled to some extent by adjustment of process parameters, most significantly the wheel speed, feed rate and depth of cut. However, based on wheel, dressing, and operating conditions alone wheel wear is not entirely predictable, and it is a common experience for technically identical grinding wheels to have significantly different wheel life, even within the same batch.

2.2.2 Solid Bond Wheels

Abrasive grains of diamond and cubic boron nitride (CBN) are considered to be superabrasives, and are harder and tougher than conventional abrasives. With the exception of some very hard vitrified CBN wheels, superabrasives are almost always contained within a solid bond of metal or resin, which is stiffer and stronger than the conventional porous vitrified structure. The surface topography of a dressed solid bond grinding wheel is characterized by a relatively smooth bond surface with abrasive grains protruding from the surface.

In review of results collected by Koshy *et al.* [20] the protrusion height of the grains is dependent on the grain size and has an approximately equal distribution from near zero to a maximum protrusion height, as illustrated in Fig. 2-8. The wheel surface is mostly bond material, with protruding grains making up less than 30% of the surface area. The percentage of surface area represented by grains is dependent on the concentration of grains, which is given as percent

carats per cubic centimeter and ranges from 25 to 125. Fig. 2-9 shows the average area (%) due to exposed abrasives is mostly dependent on concentration.

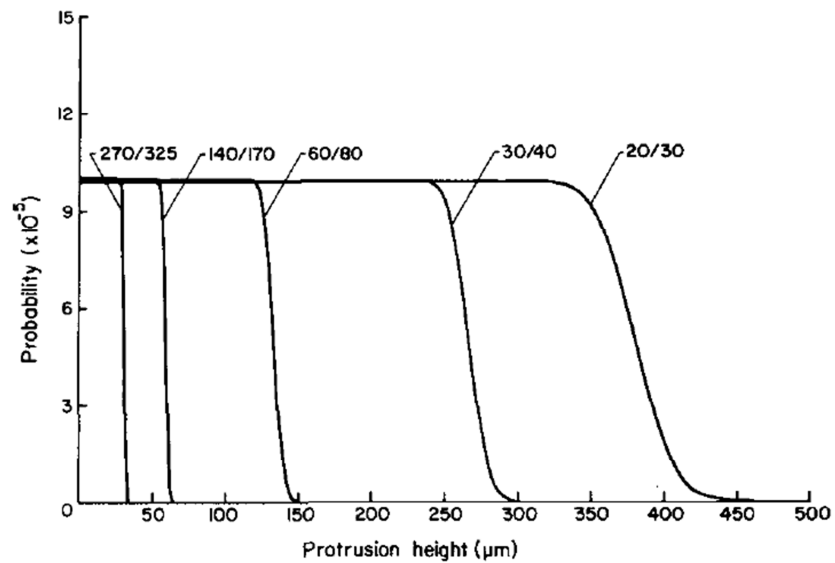


Figure 2-8: Distribution of grain protrusion heights for varying grit sizes [20].

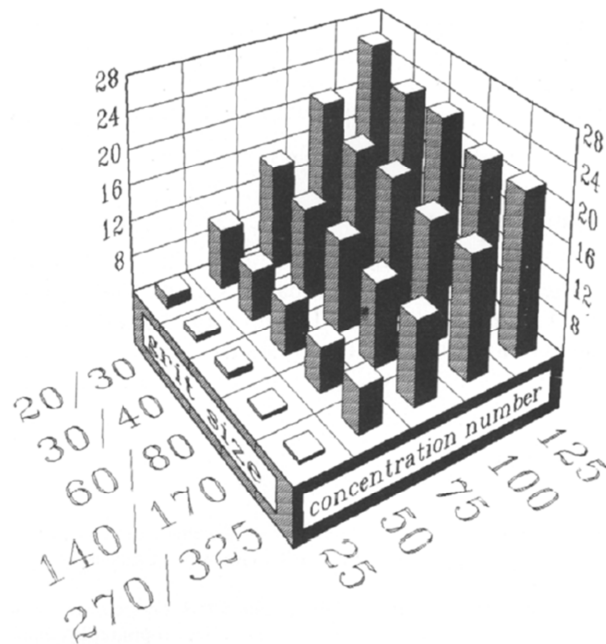


Figure 2-9: Percent of wheel surface area made up of exposed abrasive grains [20].

Unlike vitrified grinding wheels, the truing and dressing of solid bond type wheels is typically performed in two separate operations. Truing processes for these wheels remove bond material to correct runout, the wheel profile and release worn grains. Because of the presence of superabrasive grains the turning type process used for conventional abrasives is generally less common, as it can result in both the rapid wear of the dressing tool and unnecessary damage to the abrasive grains. More commonly, truing is accomplished by applying a hard, vitrified truing wheel, essentially a small grinding wheel composed of a friable abrasive, such as silicon carbide [15]. A rotary truing device, which can be brake controlled or set at an angle to the axis of rotation, feeds a truing wheel into and across the grinding wheel surface. This type of setup is shown in Fig. 2-10, with the truing wheel affixed to the table in a brake controlled truing device, driven only by the contact with the grinding wheel.

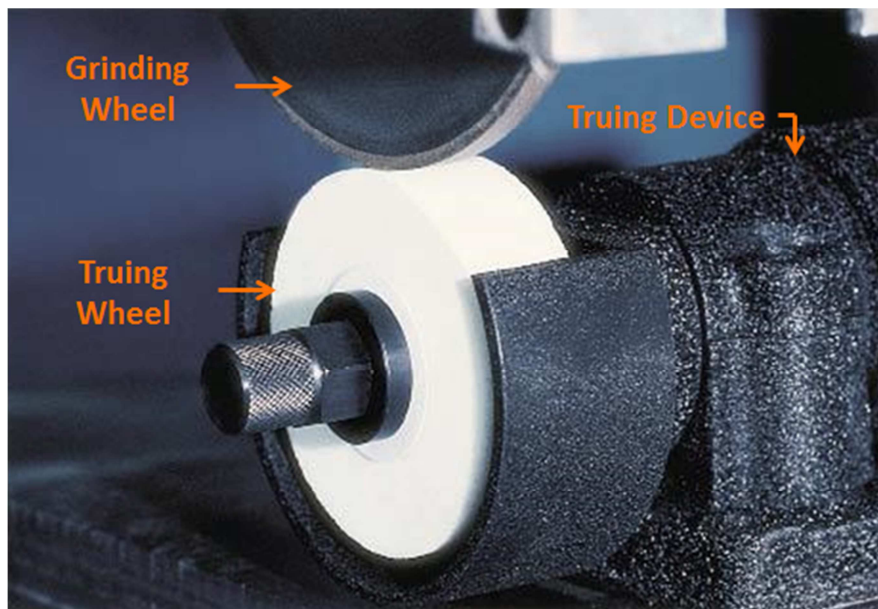


Figure 2-10: Brake Controlled Truing Device from Norton Abrasives [21].

The truing wheel's surface is crushed in the process and the debris created abrades the grinding wheel. Brake controlled or angled truing wheels create relative motion between the grinding wheel and the truing wheel to enhance the process. This is illustrated in Fig. 2-11.



Figure 2-11: Abrasive from the truing wheel erodes bond material [17].

The surface created by the truing process is generally smooth with many abrasive grains at the wheel surface or slightly protruding and the surface will often bear some shallow recesses left by grains that were released as a result of the abrasion of the surrounding bond material. The dressing process that follows is required to remove bond material from around each abrasive grain, many of which will be partially or completely obscured by bond material. Images of the wheel surface as trued and as dressed are shown in Fig. 2-12, and the relief created by the dressing process is evident. Dressing can be accomplished by applying a soft abrasive stick to the trued grinding wheel surface, capable of abrading the bond material but soft enough that protruding abrasive grains pass through unaffected [15]. When dressing a solid bond wheel the openness of a

wheel surface refers to the degree of grain protrusion or chip clearance created. A closed wheel surface is one where grains protrude less but are more securely held and supported by the bond layer.

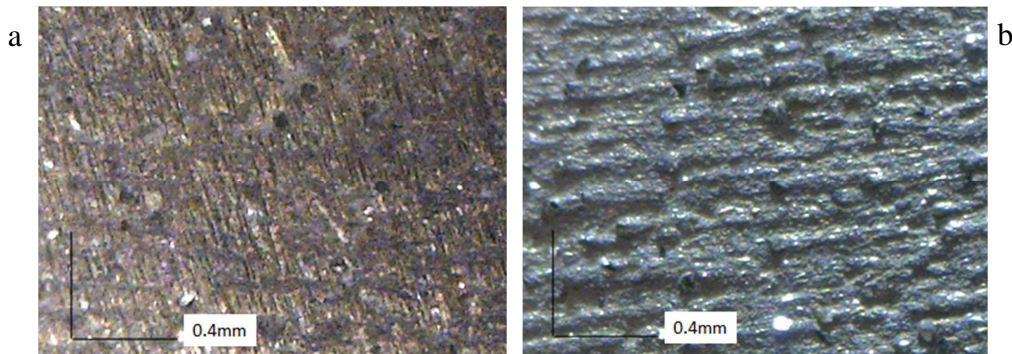


Figure 2-12: Magnified image of a 170 grit metal bond grinding wheel in (a) trued and (b) dressed condition.

The changing surface topography of a solid bond grinding wheel during the grinding process is attributed to four mechanisms; the development of wear flats, grain loss, grain fracture, and abrasion of bond material around grains. Based on research performed with solid bond diamond abrasive grinding wheels each of these mechanisms can be shown to exist for certain conditions.

As in conventional abrasives, a diamond grain will dull and develop a wear flat with continued use, Fig. 2-13. The development of this wear in diamond is accelerated when grinding low carbon ferrous metals, which have an affinity for carbon and dissolve the diamond with the aid of added heat and pressure. Such a grain generates more heat and grinding forces, and eventually either fractures or is dislodged from the wheel surface, leaving a recess [15,22].

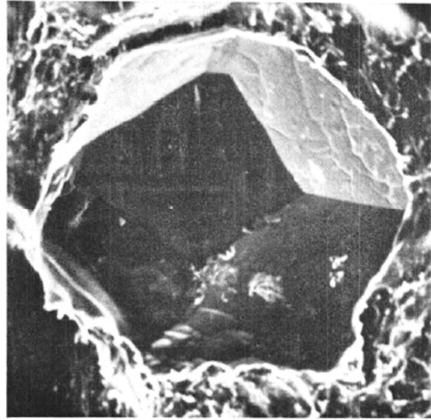


Figure 2-13: Typical wear flat developed on a diamond grain through grinding [22].

In addition to dull grains, grain fracture and grain release are known to occur to highly protruding gains, because they are not deeply set in the bond layer and therefore lack support. The effect is most prominent during initial grinding passes after dressing, and contributes to a high initial wear rate, as measured by reduction in wheel radius [17], similar to the one shown for vitrified wheels in Fig. 2-5.

For grains with lesser protrusion heights, where the chip clearance is insufficient, excess debris from cutting is forced into contact with the bond layer and abrades the material around the grain to create more chip clearance [17]. For more openly dressed wheels the peak force was significantly reduced, owing to greater chip clearance.

Attempts to monitor the surface condition of a grinding wheel with a pneumatic sensor have been made previously. The following section outlines the method and its limitations.

2.3 Existing Application of the Pneumatic Sensor to Grinding Wheels

The application of the pneumatic sensor to the monitoring of a solid bond grinding wheel surface has been previously pursued with limited success in the monitoring of dressing. Research work by Maksoud *et al.* [23] applies a pneumatic sensor to monitoring truing and dressing operations for 140/170 grit diamond abrasive grinding wheel with a resin bond. In their system, single measurement values of the back pressure are recorded by a system employing 1800 individual measurements per wheel rotation. Measurements are triggered using an optical switch and a slotted disk attached to the side of the grinding wheel. Sorted by location the individual measurements can indicate change in runout.

Fluctuations in the static pressure are reported to be the result of porosities and surface roughness, which alter the escape area between the nozzle and wheel surface. Assessment of wheel surface roughness for the dressing process was made by applying a high pass filter at 1 kHz, and calculating the signal RMS, which increased with the wheel surface roughness, reported as Ra . These results agree with recent publications, also employing RMS as an indicator of surface roughness [13].

New research suggests that improvements to the performance of the pneumatic sensor can be made for this application. In order to respond to small, rapid changes in the escape area between the sensor nozzle and the surface, both

increased dynamic sensitivity and decreased rise are time desirable. Results from other researchers [11,12,13] indicate these improvements can be made by minimizing the gap between the pneumatic sensor nozzle and the target surface. It is now recognized that an increase in the average back pressure enhances the dynamic response of the sensor.

In contrast, Maksoud *et al.* [23], position the sensor at a relatively large distance from the grinding wheel surface, at a distance of 3 mm, and employs the lowest of the supply pressures available, at 2 bar. In reference to Fig. 1-5 (pg. 10), the calibration curve provided by Maksoud *et al.* [23], Fig. 2-14, indicates that at a 3 mm distance the sensor is operating in the third region of the characteristic curve, where the sensitivity to changes in gap size severely reduced and the average back pressure is low.

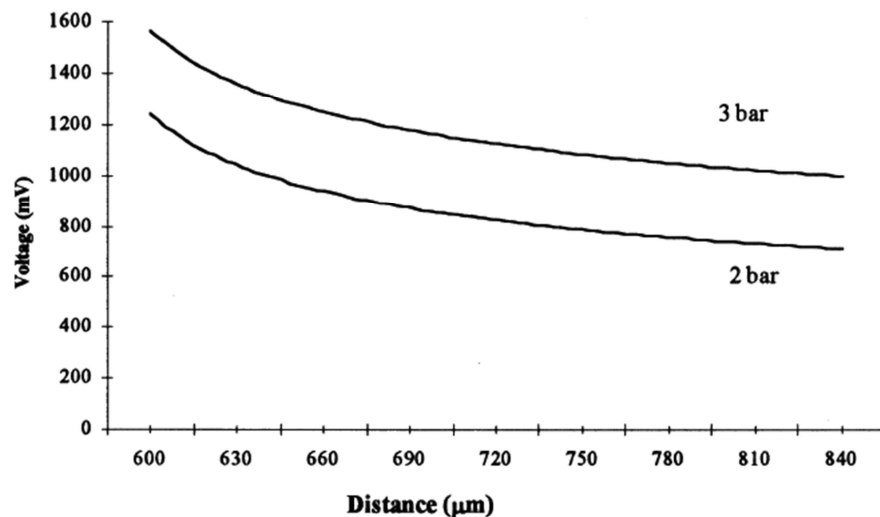


Figure 2-14: Calibration curve from Maksoud *et al.* [23]

In consideration of the grinding wheel grit size being only 140/170, fluctuations in the escape area by surface features can also be enhanced. By monitoring the surface from 3 mm away the influence of each surface grain on the total escape area is relatively small. A decrease in gap size would increase the influence of each grain on the escape area, and increase the resulting fluctuations in pressure.

The results of Maksoud *et al.* [23] are promising, and are achieved by methods that would result in a low sensitivity. Employing results from new research, the performance of the pneumatic sensor may be improved, and monitoring applications may be extended to include porous, vitrified grinding wheel and grinding wheel wear.

In monitoring the surface condition of a grinding wheel, the application of the pneumatic sensor is made difficult not only by the high surface velocities but also by the nondeterministic nature of the wheel surface and constantly changing topography. In this chapter existing literature for both the capabilities and behavior of a pneumatic sensor and grinding wheel topography have been reviewed. The remainder of this research work will outline the experimental work and development of a method to apply a pneumatic sensor to monitoring the surface condition of a grinding wheel.

3 Experimental Equipment and Setup

3.1 Monitoring Equipment

3.1.1 Hardware

A pneumatic sensor was constructed for this research, consisting of a nozzle, dynamic pressure transducer, gauge pressure transducer, control orifice and air supply fitting attached to a central body, Fig. 3-1. The sensor body contains a hollow cavity and a threaded mounting point in the base. A steel housing provides clearance for the connection of cables and air supply and can orientate and secure the sensor. If required the 'Y' shaped connector can be removed and the air supply mounted directly to the main sensor body.

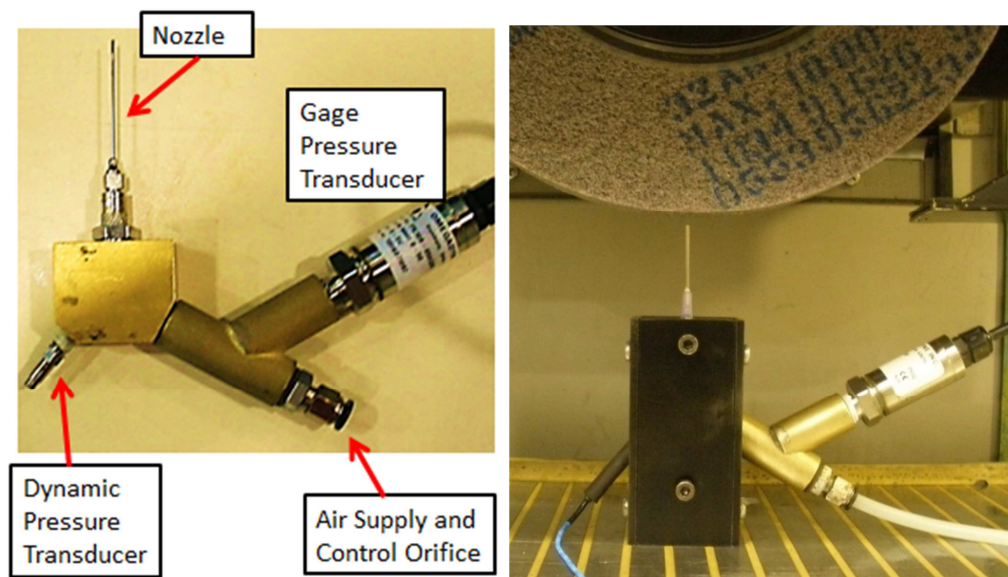


Figure 3-1: The pneumatic sensor used in this research.

The use of both dynamic and gauge pressure transducers allows one sensor to monitor the average back pressure, the gauge pressure transducer, while the second sensor could be dedicated to the measurement of the small pressure fluctuations expected from the grinding wheel topography. Additionally, because the sensitivity of a pneumatic sensor changes with the average back pressure, the gauge pressure transducer is an important element in keeping experimental results comparable, and in maintaining and monitoring testing conditions. Air is supplied to the pneumatic sensor at a constant pressure, controlled by a pressure regulator and a maximum pressure of 344.7 kPa could be provided. The specific transducers, regulator and gauge used in this research are given in table 3-1.

Table 3-1: Pressure Sensors and Regulators

Component	Make and Model
Pressure Regulator	Omega PRG101-60
Digital Pressure Gauge (Regulator)	Omega DPG1000B
Dynamic Pressure Transducer	PCB 112A22
Gauge Pressure Transducer	Omega PX309 – 050G5V

Nozzles are made by modifying hypodermic needles, which are inexpensive, easy to find in a range of sizes, and are the only wearing part in the pneumatic sensor monitoring system. Nozzles were changed as the development of the pneumatic sensor progressed, and selected to suit the target surface. In general a smaller nozzle diameter means that a passing surface feature would have a greater influence, impinging or relieving more of the escape area. This generates a greater pressure pulse and increasing the dynamic sensitivity of the pneumatic

sensor. However, smaller nozzles are limited in their useable measurement range, and cannot be used on more porous surfaces.

Control orifices also affect the useful range and dynamic response of the sensor, and were selected to suit each target surface and nozzle diameter. Each control orifice was chosen to make the pneumatic sensor as sensitive as possible to both dynamic fluctuations and changes in distance when positioned at the wheel surface. Referring to Fig. 1-5 (pg. 10), a control orifice is selected such that when positioned at the wheel surface the average back pressure of the sensor should correspond to the left hand edge of the second region of the characteristic curve. This provides both sensitivity to distance changes and a high average back pressure, which has been shown to enhance dynamic performance [11,12,13].

Control orifices are constructed in one of two ways, as shown in Fig. 3-2. Diameters larger than 0.5 mm are constructed from M8 bolts, which are drilled and tapped to accept an air fitting for the air supply. Control orifices with diameters smaller than 0.5 mm were constructed by rapid prototyping, producing an insert with the desired diameter. Inserts can be fitted into an adapter made from an M8 bolt with a seal. The assembly is screwed into the pneumatic sensor and the air supply is connected.



Figure 3-2: Control orifices.

3.1.2 Data Acquisition

The development of the pneumatic sensor included the development of the data collection method, including changes to the data collection rate and resolution. All data collection equipment used is outlined here as well as the general operation, including data acquisition cards and power supplies. Additional operating specifics for variations in data collection methods are clearly outlined for each experiment in their respective sections.

For all experiments, all sensors except the gauge pressure transducer and table dynamometer were powered by a Kistler Power Supply/Coupler Type 5134B. No filtering was applied by the power supply to any sensor, and no RMS functions were performed. The power supply was used to control gain to increase signal strength, and to improve signal resolution.

Sensors were connected by shielded cable to a National Instruments data acquisition card, or DAQ card. An NI 9215 BNC card was used for all sensors for proof of concept experiments as well as for experiments involving a series of textured disks mounted in a lathe, discussed below in section 3.4. Development of the sensor and applications on metal bond grinding wheels and vitrified grinding wheels used the NI 9215 BNC card for all sensors except the dynamic pressure transducer. For these tests the dynamic pressure transducer was sampled by an NI PCI-6115, allowing higher sampling frequency. Sampling frequency, or sampling rate, for the dynamic pressure transducer was 200 kS/s (kilo samples per second),

unless otherwise stated. Table 3-2 shows the range, resolution and maximum sample rate for each of these DAQ's.

Table 3-2: Data Acquisition Cards

Model	Voltage Range	Resolution	Sampling Frequency
NI 9215BNC	+/- 10V	16 bit	100 kS/s Maximum
NI PCI-6115	Variable: All tests +/-10V	12 bit	10 MS/s Maximum

3.2 Software

3.2.1 Data collection

To interface with the data collection hardware and NI DAQ cards, the National Instruments developed program, LabVIEW was used to create a flexible program for monitoring and recording. The raw signal from any sensor can be sampled, and displayed in real time, along with the frequency domain signal, RMS and other signal qualities. This allows for monitoring of the gage pressure transducer for the average back pressure, an important variable for consistent testing conditions. Additionally, the signal from the dynamic pressure transducer signal was monitored during data collection, ensuring common difficulties such as saturation of the sensor were avoided.

3.2.2 Data processing

Of the two transducer signals, only the dynamic pressure transducer required any significant processing. The raw signal was processed using programs

written and operated in MatLab. Programs written specifically for this research were used to apply frequency transforms, high pass filtering, calculation of RMS, and visualizations of spectrograms and plotting of data. When investigating the frequency domain response of the sensor to changes to the complex surface of a grinding wheel a more sophisticated analysis tool was required.

Multivariate Analysis (MVA) was performed with ProSensus MultiVariate Software 11.08. Frequency domain signals from the dynamic pressure transducer are input as data sets of frequencies and voltage amplitudes, and modeled by Principal Component Analysis, or PCA. In this method each frequency is considered an independent variable, with a value given by the voltage amplitude. The program identifies the dominant trends in the data sets and what variables are most strongly associated with those trends. In this way the dimensionality of the data is reduced, from thousands of separate frequencies to just a few independent components. When identifying the response of the sensor to changes in surface condition, a group of data sets is generated for each condition and entered into one PCA model. The data sets are not designated or labelled as belonging to a particular surface condition during the analysis and building of the model. That is to say in the PCA model, successful modeling is dependent upon the variation within a surface condition group being smaller than the variations from one group to the next.

3.3 Machine Tool Setup

3.3.1 Grinding Machine

Experiments were conducted on a Blohm Planomat 408 CNC grinding machine, located in the Machining Systems Laboratory, McMaster University (Fig. 3-3). The machine is capable of profile and surface grinding, and provides for a range of standard truing and dressing tools. Motion in three linear axis can be fully automated or controlled manually, and position is indicated with a resolution of 0.00001 inches. Changes in wheel diameter due to dressing or wheel wear can be automatically tracked and used to correct wheel speed and maintain grinding conditions.



Figure 3-3: Blohm Planomat 408 CNC grinding machine at McMaster University.

When required for an experiment, surface grinding was used to generate wear on the surface of the grinding wheel. Workpieces were preground in place, and the wheel surface was redressed before the start of each experiment. Grinding parameters were set depending on the experiment and intended surface condition, and could be varied in depth of cut, table feed and wheel speed. Workpiece materials were tool steel, specifically HSS was employed for both conventional and diamond abrasive grinding wheels, with the exception initial proof of concept testing which used 1040 steel.

3.3.2 Grinding wheels

Experiments involved both conventional vitrified grinding wheels and metal bond grinding wheels. The vitrified wheels were 32A46-GV40P and 32A60-HVBE. The former is more porous or open in structure with a coarse grain. This wheel was principally used during proof of concept experiments. The latter is a finer grit wheel with a porous structure.

For this research a single point diamond dressing tool is used for both truing and dressing operations on vitrified grinding wheels. The dressing tool used was an Amplex T6UA, 1 carat weight diamond, set in a holder (Desmond DH-15) at 15 degrees and affixed to the grinding machine table. The dressing depth of cut per pass is approximately 18 μm , while the cross feed rate is variable, depending on the experiment. The majority of grinding wheel experiments used a coarse dressing of one or nearly one nominal grain diameter crossfeed per wheel

revolution, or about 0.25 mm/rev for a size 60 grit wheel. Total depth cut is approximately 125 μm , or the process may be repeated until the wheel surface is restored.

The metal bond wheel is a diamond abrasive wheel, 1A1 8X0.5X5, 170 75 1/8, being nominally 8 inches in diameter and 1/2 inch wide, with a grit size of 170, and concentration of 75. Truing and dressing were performed separately for this wheel. The wheel was trued using a Norton Brake Controlled Truing Device, operated as recommended by the manufacturer. The truing wheel was a vitrified aluminum oxide wheel, Norton 38A80-M8VBE, and inclined by 10 degrees to the rotational axis of the grinding wheel to enhance the relative motion between the truing and grinding wheels. The grinding wheel used in this research had an abrasive layer 1/8 inches thick, allowing for multiple truing and dressing cycles.

Dressing was performed by a dressing stick. A Norton 37C150-KV silica carbide dressing stick, best suited to the 170 grit wheel, was mounted in the grinding machine and fed into the grinding wheel at 100 mm/min.

3.3.3 Additional Equipment

Grinding wheels were balanced using Grinding Electronics BMT100 from Micro Präzision Marx (MPM). Following the manufacturer's operating procedure, grinding wheels were mounted, trued at low speed and an initial balancing was performed. Grinding wheels were then retrued and balanced again at operating speed.

Coolant was delivered by a shoe type nozzle as standard equipment with the Blohm Planomat, with a maximum volume flow rate of 250 l/min. In addition to conventional use during grinding, the effect of coolant on the operation of the sensor is tested by applying coolant to the grinding wheel surface ahead of the sensor nozzle to flood the surface.

3.3.4 Positioning the Pneumatic Sensor

The position of the sensor relative to the grinding wheel is set in reference to the initial wheel surface. The nozzle should be kept perpendicular to the grinding wheel surface for monitoring. With the sensor mounted on the grinding machine table, the nozzle is vertical and directed upward, and should be located at the bottom dead center of the grinding wheel. For reference, the grinding wheel is moved in the horizontal axial direction (Z axis) and vertical direction (Y axis), while the table motion provides the final horizontal axis (X axis). Repeatability requires that the position in all three axis be set and consistent.

The wheel is positioned in the Y axis direction by touching off, or very lightly grinding, on the tip of the pneumatic sensor nozzle, setting a zero for the stand-off distance. Once the sensor nozzle tip is brought close to the approximate bottom dead center of the grinding wheel the wheel height is slowly reduced by a series of grinding passes until touch off occurs. The initial positioning of the nozzle tip may be aided by monitoring the internal average gauge pressure. In cases where the nozzle position and stand-off distance has been set once already

for a given wheel and surface condition, a known internal pressure may be approached to bring the wheel surface within 10 to 20 μm of the nozzle tip. Variability in the wheel surface as a result of changes such as dressing cross feed rate or wheel wear can influence the average internal gauge pressure at touch off, making touch off process a requirement at the start of each experiment.

Nozzles, which consist of a range of hypodermic needles with the ends blunted and ground flat, may develop a burr as a result of the touch off of the grinding wheel. These burrs are removed from the inside and outside of the nozzle by the light application of a countersink and fine abrasive stick, Fig 3-4.

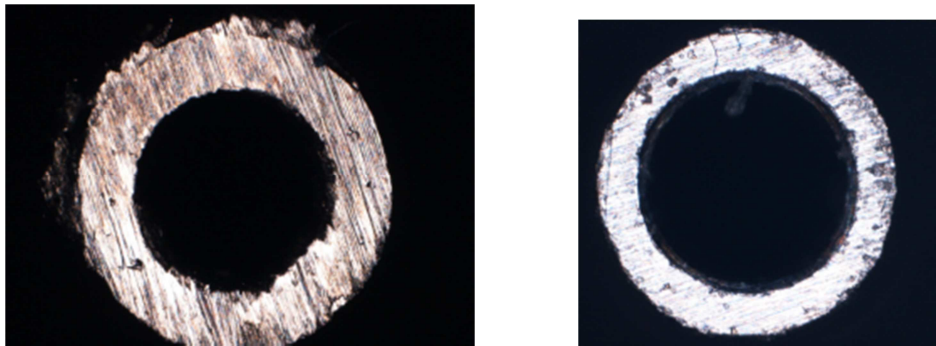


Figure 3-4: Removal of significant burrs from the nozzle tip.

The X axis position is set after establishing the Y axis and clearing any burrs from the nozzle tip. The wheel surface is raised by a small distance from the nozzle tip, 5.08 μm , to ensure no further contact is made between the nozzle and the wheel. To set the X axis and locate the bottom dead center of the wheel, the X axis traversed from one side of the wheel center to the other. As the position is incrementally shifted, the average internal gauge pressure is monitored, with the

highest pressure corresponding to the nearest point on the wheel and bottom dead center. In any other sensor orientation this step would be carried out by traversing the sensor on an axis tangential to the wheel, locating the nearest point and setting the nozzle perpendicular to the wheel surface.

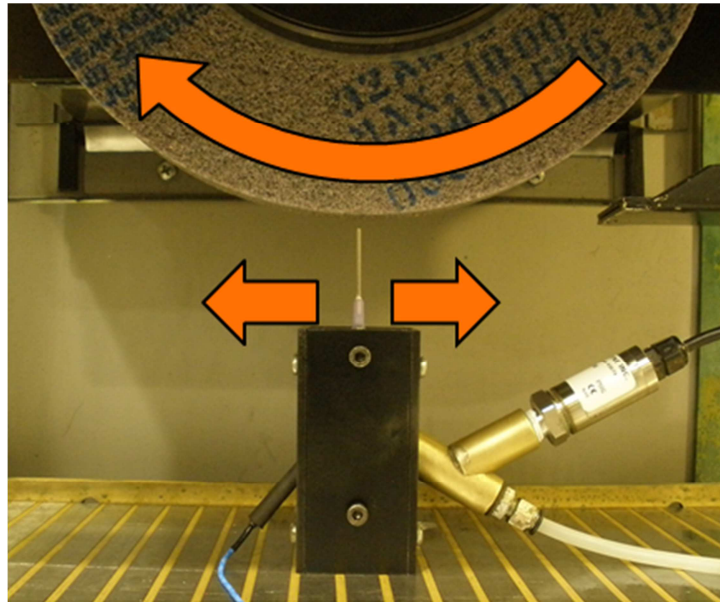


Figure 3-5: Setting bottom dead center.

The Z axis or wheel axial direction is initially set manually by visual alignment, and relocated by the machine coordinate system. In most experiments multiple measurements were taken at each of several axial locations on the wheel surface. However, unless specifically investigated, measurements were not taken with the sensor positioned near the edge of the grinding wheel or edge of the worn area, so as to maintain consistent measurement conditions.

3.3.5 Additional Sensors

In addition to the pressure transducers, some experiments involved additional sensors. The following is an outline of the equipment and general setup.

3.3.5.1 Accelerometer

An accelerometer was used to monitor against any vibrations that may create fluctuations in the stand-off distance and compromise experimental results. A PCB 607A11 accelerometer was used, with a frequency range of 0.5-10 kHz, measuring up to 50 g, and a broadband resolution of 350 μg . This sensor was connected to the Kistler power supply/coupler type 5134B, and the NI 9215 BNC DAQ card. In the grinding machine the accelerometer was attached magnetically to the pneumatic sensor housing or to the main grinding wheel bearing, Fig. 3-6.



Figure 3-6: Accelerometer positioning.

3.3.5.2 *Three-Component Dynamometer*

A Kistler 9255B quartz three-component dynamometer was used for the measurement of normal forces during grinding. The dynamometer is powered by a Kistler Dual-Mode Amplified Type 5010. Forces were measured continuously immediately before, during and after a grinding pass, with all three axes measured. The dynamometer was oriented with one axis vertical and the second axis parallel to the table feed axis. Measurements from the dynamometer were used to observe relative changes in grinding forces with the progression of wear.

3.4 Lathe

Several experiments were carried out on a CNC Lathe (Fig. 3-7). The lathe is an Okuma Crown L1060, fitted with a hydraulic three jaw chuck, and capable of automated or fine manual control. Use of a lathe allowed experiments investigating the static and dynamic behaviour and response of the pneumatic sensor to specific conditions or excitations to be conducted and carefully controlled.



Figure 3-7: Okuma Lathe at McMaster University.

The pneumatic sensor was applied to known or deterministic surfaces on rotating disks in a variety of experiments, investigating the effects of changes to the target surface or to the setup of the sensor. The majority of experiments conducted on the lathe with control surfaces were on an aluminum disk, 20 cm in diameter and 4.5cm in width, mounted on a shaft and provided a maximum surface velocity of 35 m/s, Fig. 3-8. This aluminum disk was turned smooth and concentric, and surface run out could be increased or reduced using a series of metal shims placed between the end of the aluminum shaft and the live center of the tail stock.

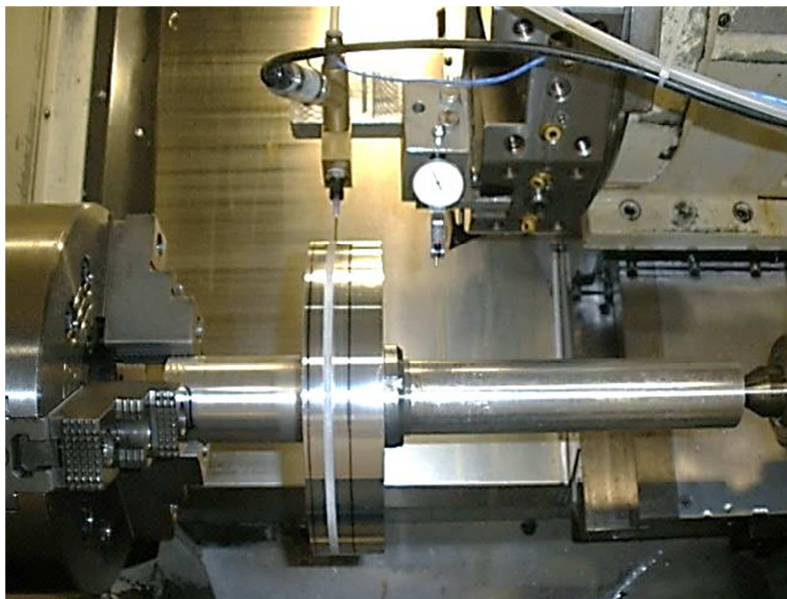
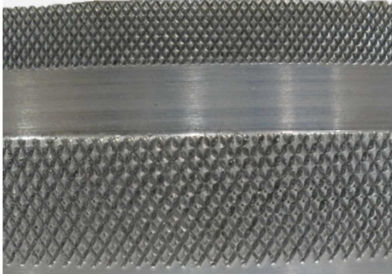


Figure 3-8: Shaft mounted aluminum disk test surface.

Various surface finishes and textures were imparted to the aluminum disk, including knurls or various types and sizes, multi start threads, smooth

turned surfaces. Unlike the surface of a grinding wheel the surface of the disk could be controlled, applying known or measurable and consistent textures means that the response of the pneumatic sensor could be compared with a known input. While some investigations were made using straight cut knurls, multi-start threads and plain, smooth surfaces, the majority of tests were conducted on diamond knurl surfaces. Because of their size, fine and medium diamond knurls were used as analogous to a porous grinding wheel surface, and tests were conducted at surface and rotational velocities typical of grinding. Surface samples from a knurled disk were examined by optical microscope to determine length, width and depth, as shown in table 3-3 and Fig. 3-9. Diamond knurls could also be adjusted in orientation, and their height could be changed by reducing the imparted depth, or by partially turning the surface after knurling. The geometry of the coarse, straight knurl is also given in table 3-3. These knurls formed triangular ridges across the disk surface and were always parallel to the axis of rotation.

Table 3-3: Knurl geometry

 <p>Figure 3-9: Sample of Diamond Knurled Surface</p>	Nominal Dimensions	
	Fine Diamond Knurl	
	Length	0.85 mm
	Width	1.25 mm
	Depth	0.35 mm
	Medium Diamond Knurl	
	Length	1.33 mm
	Width	2.00 mm
	Depth	0.50 mm
	Coarse Straight Knurl	
	Length	1.50 mm
	Depth	0.60 mm

3.4.1 Pneumatic Sensor Mounting

In order to secure the pneumatic sensor in the lathe, a mounting bracket that could be clamped in the existing tool holder was created. The sensor, positioned with the nozzle normal to the surface, was fastened securely by a bolt. Also mounted on the bracket is a dial gauge for taking measurements of surface run out, Fig. 3-10.

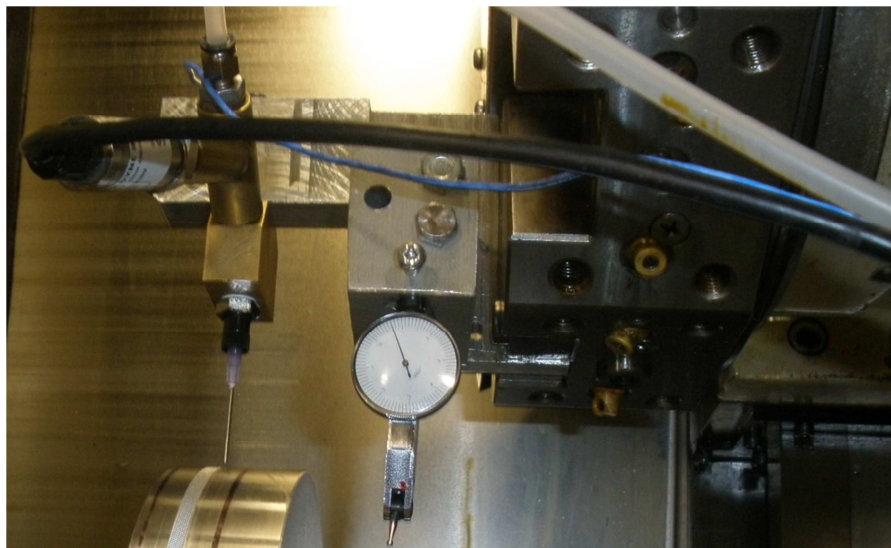


Figure 3-10: Pneumatic sensor mounting in lathe based experiments.

3.4.2 Accelerometer

As in the grinding experiments the accelerometer was applied to the lathe to detect any vibration that may influence the pneumatic sensor. The sensor was

mounted magnetically to the main spindle bearing. Mounting to the sensor was not necessary as an initial test showed the tool holder is well isolated from vibration.

3.4.3 Coolant

When required for experimental conditions, coolant was delivered to the opposing side of the aluminum disk by an extension of the coolant system in the lathe. Experimentally this setup was used to test the effect of the presence of a fluid layer on the disk surface on the pneumatic sensor. The disk surface could also be rapidly cleared of coolant by an air jet directed at the bottom of the disk, between the coolant nozzle and the sensor, Fig.3-11.

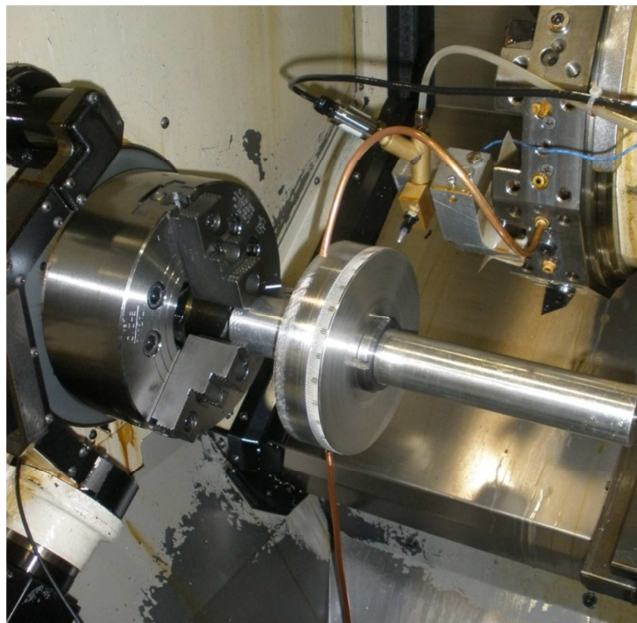


Figure 3-11: Indirect coolant application and cleaning in lathe based experiments.

3.5 Data Collection Method

As part of the monitoring process, the specific setup of the pneumatic sensor, data collection method and operation of associated equipment and software evolved constantly through this research work. The progression of the data collection method during experiments is therefore detailed in the following chapter with the corresponding experimental results that support each step in the sensor's development, beginning with the initial setup and proof of concept.

In the monitoring of the wheel surface the pneumatic sensor is applied to multiple axial locations across the wheel surface, and at multiple stand-off distances for each location. Depending on the application 6 to 8 axial locations are used, and 3 to 5 equally spaced stand-off distances span the useful distance range of the sensor. The specific application determines the physical setup and operation of the pneumatic sensor, including the selection of control orifice and nozzle diameters, supply pressure and the stand-off distance range. Table 3-4 gives the setups used for monitoring each grinding wheel used in this research. As explained in section 3.1.1, differences in nozzle and control orifice diameter are due to the differences in the target grinding wheel grit size, surface roughness and porosity.

Table 3-4: Sensor setup according to grinding wheel.

	Vitrified: 32A60-HVBE	Diamond: D170-75M1/8
Nozzle Diameter	1.194 mm	0.603 mm
Control Orifice Diameter	0.95 mm	0.42 mm
Supply Pressure	275.8 kPa	275.8 kPa
Distance range	5 – 200 μ m	5 – 50 μ m

To prevent unintentional alterations of the nozzle tip, a zero stand-off distance is not used. Stand-off distances are set relative to the original wheel surface, such as the dressed wheel surface for wear monitoring. Stand-off distances are fixed for the duration of the experiment and are not adjusted for the recession of the wheel surface from wear, Fig. 3-12.

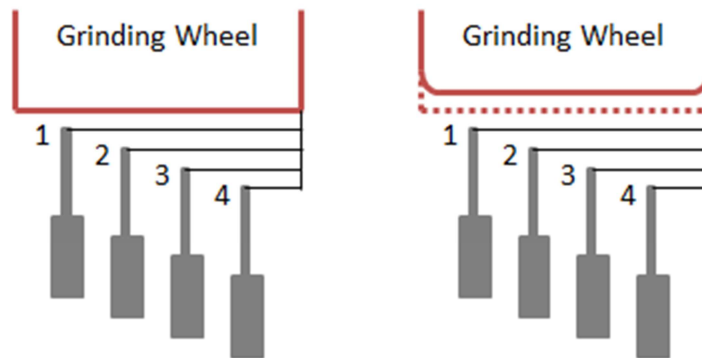


Figure 3-12: Illustration of fixed stand-off distance reference.

A measurement with the pneumatic sensor consists of recording the relative position and distance, average back pressure and collecting a continuous sample of the dynamic pressure transducer signal. A 0.5 second sample is collected at 200 kS/s using the NI PCI 6115 DAQ card. As stated earlier, measurements are made inside the grinding machine work space with the wheel at operating speed. Sets of measurements are taken at set intervals, monitoring changes to the surface condition. Each set is processed and graphed to indicate the average recession of the wheel surface and change in high frequency fluctuations in the dynamic signal.

With the experimental equipment and setup well understood, the following chapter details the development of pneumatic sensor and monitoring method. With no previous pneumatic sensor research demonstrating sufficient dynamic capabilities for monitoring grinding wheels this current work seeks to determine if a pneumatic sensor can be applied to monitoring the surface condition of a grinding wheel.

4 Experimental Results and Discussion

4.1 Proof of concept

The first step in the development of the pneumatic sensor for the monitoring of a grinding wheel surface was to conduct proof of concept testing, investigating if it is possible for the sensor to differentiate between a dressed grinding wheel surface and a worn grinding wheel surface. An initial setup of a data collection system and the sensor was made and altered iteratively. The development of the pneumatic sensor began by determining if the sensor was influenced by the passing surface of the grinding wheel, if this influence produced measureable output from the sensor, and if a change in the wheel surface would be reflected by a change in the sensor output.

4.1.1 Initial Experimental Setup

Initial proof of concept experiments were conducted on a vitrified grinding wheel, 32AR46-GV40P, using a surface speed of 20.3 m/s, at approximately 1300 RPM. The grinding wheel was dressed at a cross feed rate of 0.195 mm/rev, at a depth of 18 μm per pass. Unless otherwise stated, all measurements were taken with the wheel at operating speed.

Data collection with this initial setup was by an NI-9215 with BNC DAQ, with USB connection. Data collection rates were initially 50 kS/s for establishing nozzle and control orifice diameters. For analysis of changes to the grinding

wheel surface, it was approximated that 15 kS/s was a sufficient data sampling rate, with a total of 50 000 samples taken per measurement, for reasons that will be discussed below.

Setting the initial setup of the pneumatic sensor involved varying the nozzle diameter, the control orifice diameter, and the air supply pressure. The effect of changing each of these parameters on the sensitivity, and distance range from the surface was guided a theoretical model [24], which is based on an ideal surface, a smooth and flat plate.

A theoretical model, based on published literature was limited to a maximum supply pressure, P_s , of 207 kPa due to the compressibility of air. So the model remained applicable the supply pressure was similarly limited in the initial experiments. According to theory and Eq. 4-1 [24] a greater air supply pressure will result in higher sensitivity at any given distance X_i for a fixed nozzle and control orifice diameter, Fig. 4-1. The curve is referred to in this research as the Back Pressure Curve, and established experimentally by taking measurements from the gauge pressure transducer at varying and non-sequential stand-off distances. Measurements are 4 seconds in length and averaged.

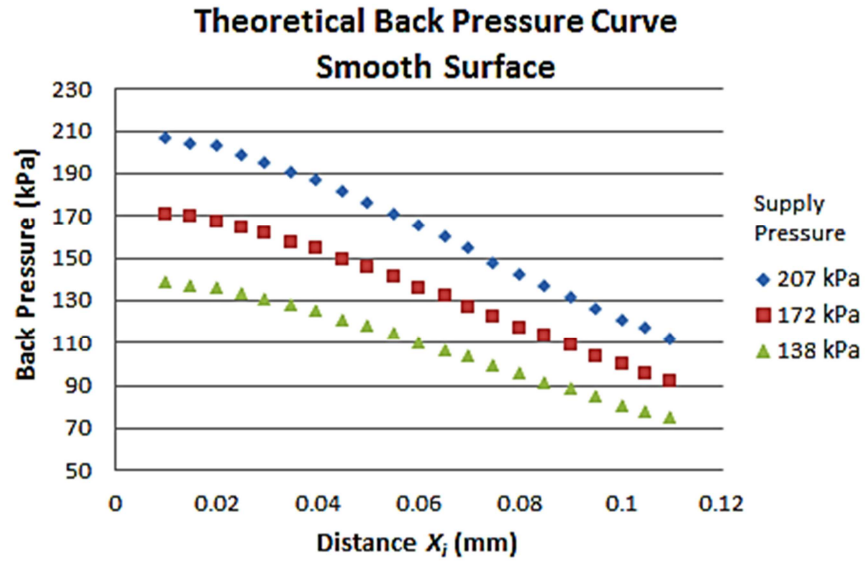


Figure 4-1: Distance and Back Pressure: Theoretical relationship.

$$P_b = \frac{P_s}{1 + 16 \left(\frac{d_n^2 X_i^2}{d_s^4} \right)} \quad \text{Equation 4-1}$$

An initial setup with a 0.84 mm control orifice and nozzle diameter provided a measureable dynamic signal and distance sensitivity. The sensitivity in this case refers to the change in the average back pressure P_b , the internal pressure of the sensor, for a change in the stand-off distance, or SOD. A back pressure curve was experimentally established for this setup, but using the surface of the vitrified grinding wheel in place of the smooth surface assumed by the theoretical model, Fig. 4-2. The term stand-off distance refers to the distance from the nozzle to the outermost surface of the grinding wheel, and is used in Fig. 4-2 in place of the theoretical value X_i because of the rough and porous nature of the

wheel surface. This distance is set while the grinding wheel is rotating, and is controlled and known through the axis of the CNC machine, as explained in section 3.3.4.

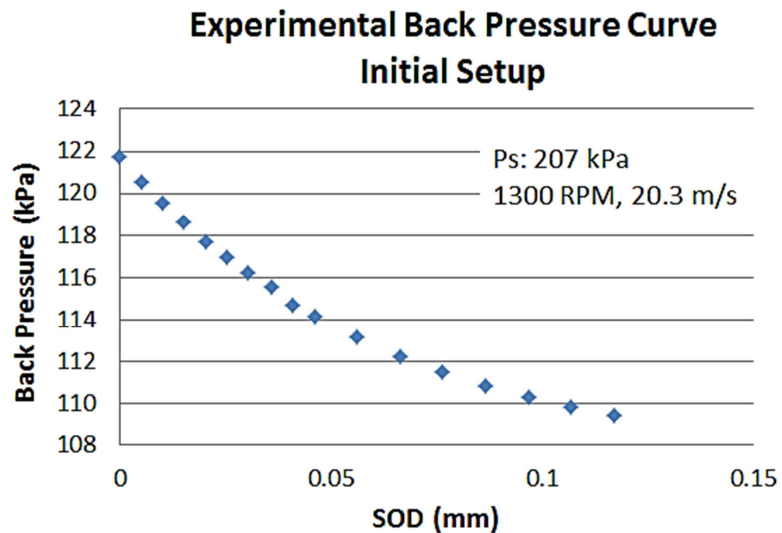


Figure 4-2: Back pressure curve for initial sensor setup with vitrified grinding wheel.

4.1.2 Special Considerations

4.1.2.1 Effective Stand-Off Distance

While determining the initial setup for the pneumatic sensor, an important limit imposed by the nature of the vitrified grinding wheel construction was highlighted by the back pressure curve. Given the roughness of a grinding wheel surface, when the tip of the sensor nozzle has a zero stand-off distance from the outer grains, the back pressure will be significantly below the supply pressure. Fig. 4-2 illustrates this, in consideration that the supply pressure is 207 kPa. In

contrast, the conventional use of a pneumatic sensor in measurement of displacement is against a relatively smooth and flat surface and a near zero stand-off distance would result in near equality of supply and back pressures. The effect of surface roughness as well as curvature was tested by Wager, who found the effects were similar and quantified the increase in escape area as an equivalent distance from a flat plate [10]. The porosity of a vitrified grinding wheel further contributes to the discrepancy as air able to escape into and even through pores and spaces between the grains and bonding structure that make up the grinding wheel surface. The end result is that the actual back pressure and sensitivity experienced by the pneumatic sensor at a given stand-off distance from the wheel surface will correspond to a greater stand-off distance, based on a flat, smooth target surface. This effective stand-off distance is a consideration when establishing the diameters of the nozzle and control orifice. While setups where the control orifice is much smaller in diameter than the nozzle have the greatest sensitivity, they are only useful over a short stand-off distance range, and cannot operate at the greater effective stand-off distances that result from the rough and porous surface of the grinding wheel.

4.1.2.2 Edge Effect

An early test using the initial pneumatic sensor setup and vitrified grinding wheel showed a decrease in the average back pressure occurred when in close proximity to the wheel edge. The experiment recorded the average back pressure values while varying the distance between the edge of the sensor nozzle and the

edge of the grinding wheel, for three stand-off distances. The results are shown in Fig. 4-3, graphing the location of the sensor and the average back pressure, indicated in volts.

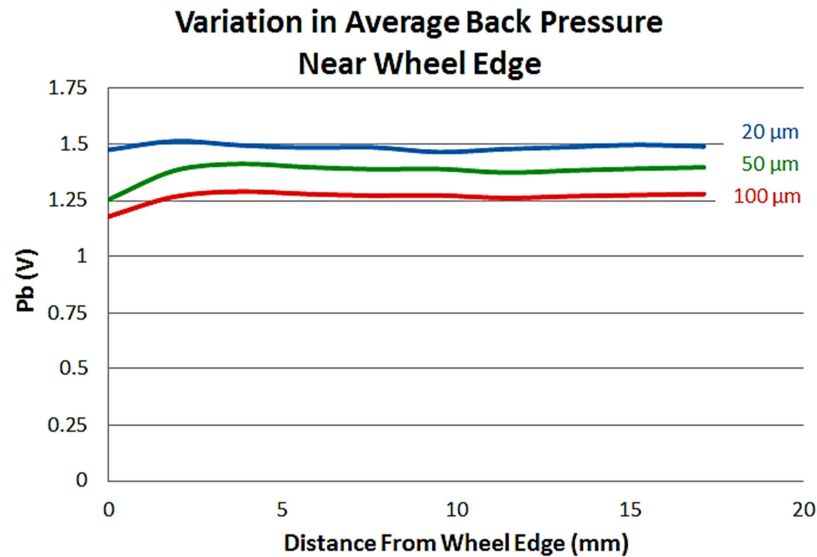


Figure 4-3: Edge effects.

The effect on the back pressure is minimal for the smallest SOD, but for larger values the decrease is significant, with the 50 μm P_b value dropping to the inboard value of the 100 μm SOD. While it is not clear why a decrease in the P_b occurs, the effect is isolated to the area near the wheel edge. During experiments and testing of the pneumatic sensor and the development of the monitoring method, the taking of measurements near the edge of the grinding wheel or worn surface was avoided.

4.1.3 Initial Detection

Using the initial experimental setup of the sensor the sensor was able to produce a fluctuating internal pressure in response to the wheel surface, which could be measured by the dynamic pressure transducer. The raw signal taken from the dynamic pressure transducer while testing on a 32A46-GV40P vitrified grinding wheel rotating at 1300 RPM, with a surface speed of 20.3 m/s is shown in Fig. 4-4(a). The signal is amplified by a gain of x1, with amplitude of about 150 mV, corresponding to a dynamic pressure fluctuation of little over +/- 10 kPa. With a resolution of 0.305 μ V, the signal amplitude is well described even without amplification.

For comparison, the time domain signal taken for the same conditions but without wheel rotation is shown in Fig. 4-4 (b), with amplitude of less than 5 mV.

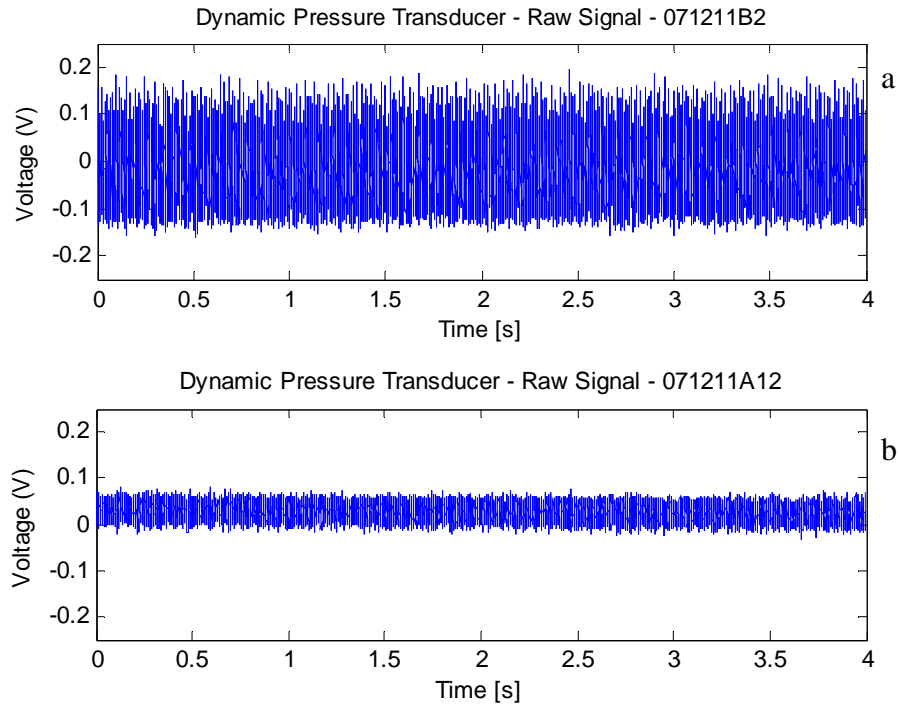


Figure 4-4: Raw pressure transducer signal with rotating wheel surface (a) and without (b).

The presence of high frequency pressure fluctuations in Fig. 4-4(a) is confirmed by applying a Fast Fourier Transform (FFT) to the raw signal, and looking at the frequency domain. Fig. 4-5 shows voltage amplitudes across a frequency range up to 25 kHz. Significant and measureable voltage amplitudes can be observed at frequencies that are hundreds to a thousand times the 21.6 Hz rotational frequency of the wheel, or more. These high frequencies are a good indication that the sensor is responding to features of the grinding wheel surface.

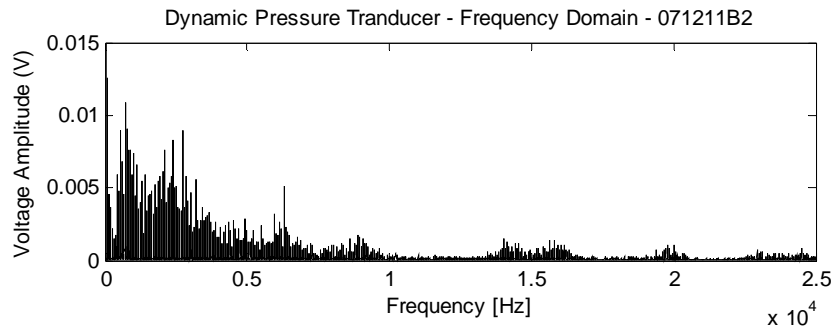


Figure 4-5: Frequency domain of the dynamic response to the moving wheel surface.

Similarly the frequency domain of Fig. 4-4(b) can be plotted for comparison, Fig. 4-6. Significant difference in the voltage amplitude is visible across all higher frequencies.

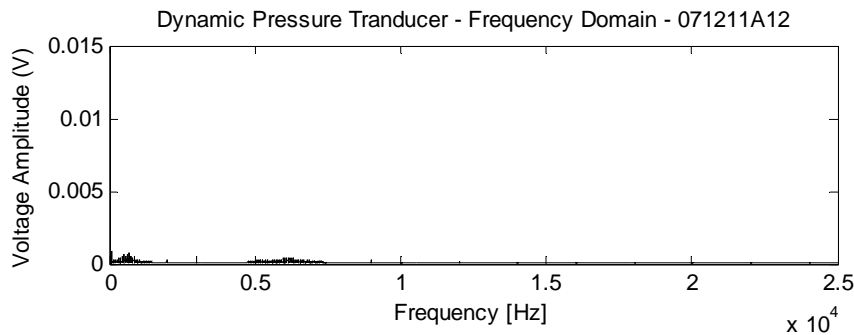


Figure 4-6: Frequency domain of dynamic signal without a moving wheel surface.

4.1.4 Incremental Wear & MVA Modeling

Multivariate Analysis, or MVA, was used to assist in determining if changes to the surface of a vitrified grinding wheel would be reflected in the measured output of the pneumatic sensor, and specifically in the signal from the

dynamic pressure transducer. Discussed in section 3.2.2 (pg. 37), MVA is a statistical analysis tool with methods that are well suited to handling large data sets, finding dominant trends and in identifying and removing noise or random variations from the data.

Measurement of the wheel surface at operating speeds were taken with the initial sensor setup and a collection rate of just 15 kS/s, for changing surface conditions and input into a MVA modeling program. The sampling rate was reduced from the 50 kS/s in the interest of practicality, specifically the computational load associated with the large amounts of data generated by higher sample rates. The lower sample rate was chosen as a rate that would capture the majority of the energetic frequencies contained within dynamic pressure transducer signal. Fig. 4-5 is an example the output signal from the dynamic pressure transducer sampled at 50 kS/s, for a vitrified grinding wheel with a surface speed of 20.3 m/s. The amplitude of frequencies above 7500 Hz are significantly smaller than those below, leading to the selection of 15 kS/s.

For proof of concept test the sensor took measurements of four wheel conditions, with the wheel coarsely dressed and then incrementally worn, as illustrated in Fig. 4-7, for a 32A46-GV40P vitrified wheel. Wheel surface speed was maintained at 20.3 m/s while the pneumatic sensor was applied to the wheel surface, with the coolant turned off.

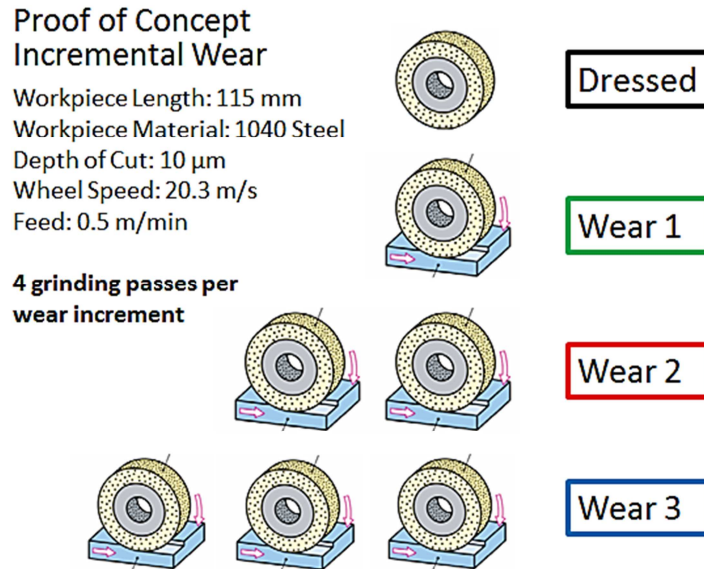


Figure 4-7: Incremental wear for proof of concept.

For the PCA model, ten measurements were taken for each surface. Three measurements from each set of ten were selected randomly and withheld from the analysis for verification. The model was then constructed based on the remaining twenty eight measurements. In this model each frequency and corresponding amplitude are entered as a variable and value.

The initial model contained 32 764 frequencies from 0 to 7500 Hz at equally spaced intervals. From this original data set the model was unable to clearly differentiate between measurements from different surface conditions. To improve the model the typical preprocessing of converting variables to a unit vector and mean centering was omitted. Additionally, the size of the data set was reduced using a process called variable pruning to remove noisy or insignificant variables from the model. Noisy or insignificant variables are identified as those

that are not associated with any of the trends in the data or otherwise do not contribute to the model, such as those with zero values. Data sets can be further refined by specifying a minimum degree of significance or association between variables and dominant trends. This process reduced the number of frequencies being considered to just sixty, and the resulting model was able to differentiate between measurements taken from each of the four surface conditions. The success of the model is particularly highlighted by the fact that the groups of measurements have actually been placed in order of increasing wear. The measurements of the dressed surface are at the bottom, with each measurement set above belonging to an increasingly worn surface, Fig. 4-8.

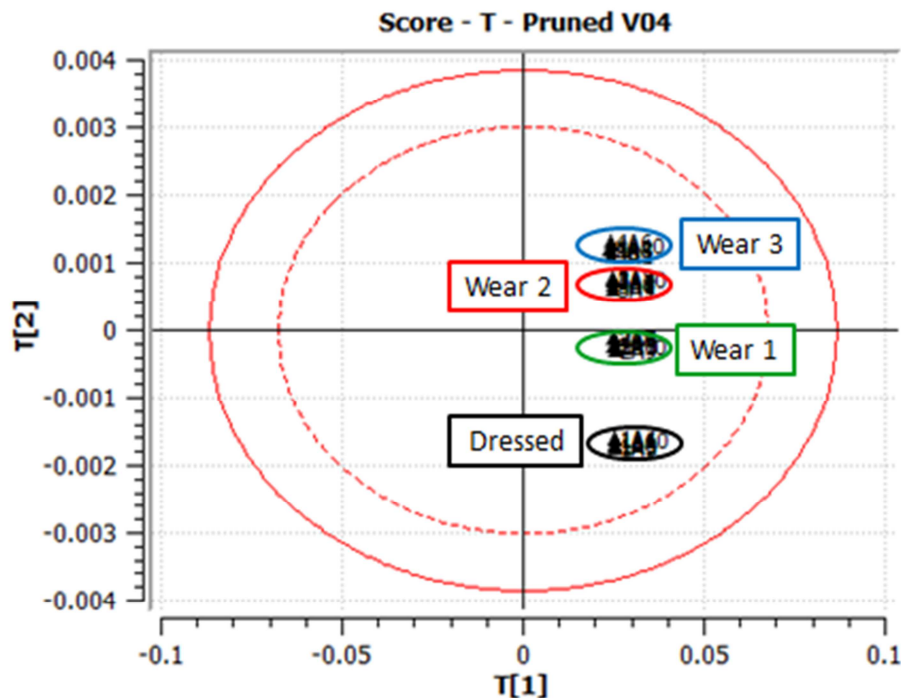


Figure 4-8: Score plot of PCA model for incremental wear.

While the PCA program does cross-validate the model generated, it is diligent to validate the model by applying it to data sets that were not included during the construction of the model. The twelve measurements originally withheld were used to test model, and applied in what is referred to as a prediction set. The model was able to correctly differentiate between measurements taken for each surface condition. The figure shown below is the score plot of the pruned data, with the prediction set data displayed over the original model as the green data points.

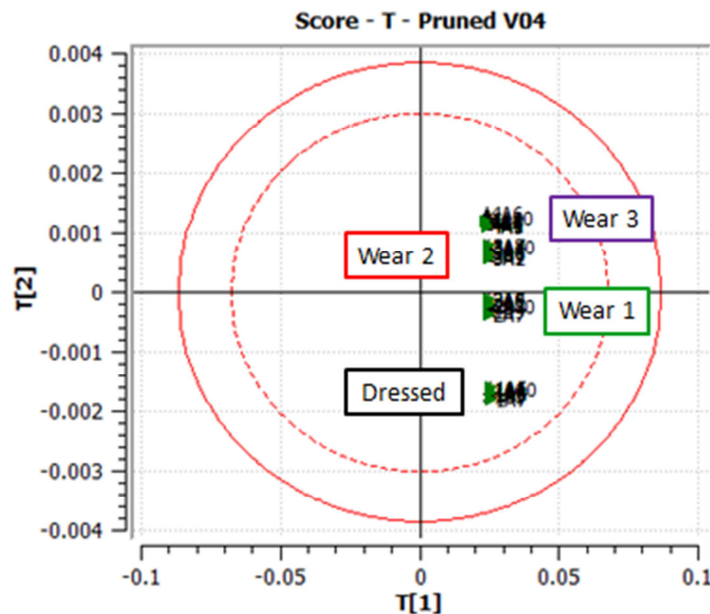


Figure 4-9: Score plot of verified PCA model.

This result is very encouraging and indicates that the change in surface condition can be reflected in changes to the signal generated by the dynamic pressure transducer. Unfortunately the results of this model are not universally applicable. When the measurements of the wheel surface were repeated for each

wheel condition to create a new data set a successful PCA model was created and again it could differentiate by surface condition. However, the model for the new data set is different from the original. While both data sets identify frequencies from across the entire 7500 Hz range, different frequencies are significant in each model. Highlighting these differences, when the original PCA model is applied to the new data set, the new measurements do not fit the model. The result can be seen in Fig. 4-10, with the new measurements not in order of increasing wear and not associated with the surface condition groups from the original data. Specifically this shows that when the wheel wear test was repeated, the wear caused a different set of frequencies to change.

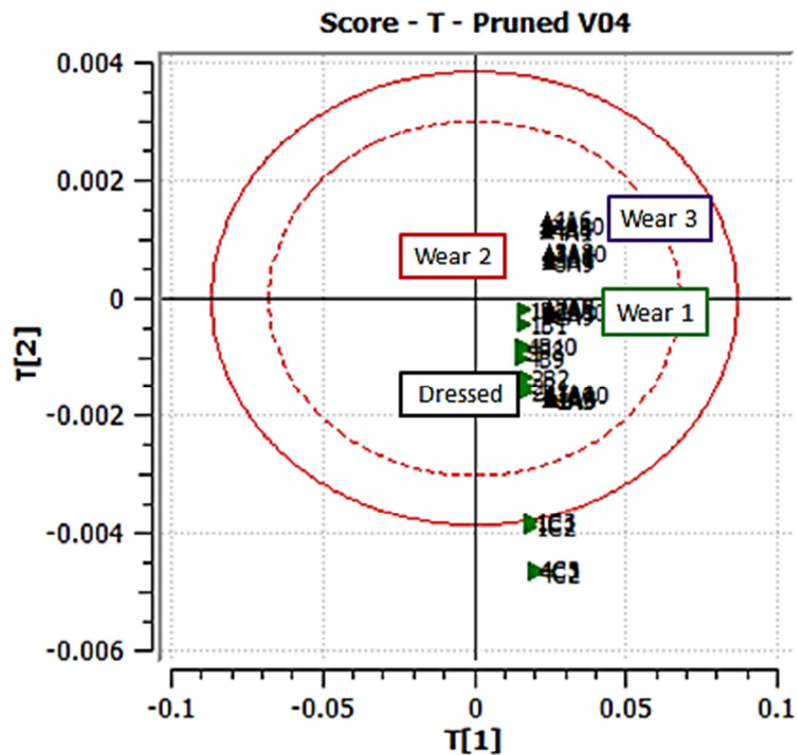


Figure 4-10: A unique PCA model is created by each data set.

4.2 Characterizing Surface to Sensor Relationships

While the results of the MVA models are promising, it can only be concluded that a systematic change in the dynamic pressure transducer signal occurred as the wheel was worn. Exactly what caused the signal to change, or the association with the wheel wear is not yet identified. It is of interest to return to the original question of the relationship between the surface of the grinding wheel and pneumatic sensor. To describe and demonstrate this relationship an investigation is made into the sensor's response to changes in the grinding wheel surface and operating conditions.

The small size of features of a grinding wheel surface, the abrasive grits and open pores, combine with the surface velocity typical in grinding require the sensor respond at high frequency in order to measure the surface. A series of experiments was used to establish that the pneumatic sensor is capable of responding to a passing surface at high frequency and at high surface velocities, and to establish the limit of the frequency range for the pneumatic sensor.

4.2.1 Axial Sensitivity and Frequency Spacing

The nondeterministic structure of a grinding wheel means that each section of the surface is inherently unique and different to any other section, even for the same dressed condition on the same wheel. A simple test is able to show that the response of the pneumatic sensor, particularly as measured by the dynamic pressure transducer, is likewise unique for each section of the wheel.

By means of shifting the axial position of the pneumatic sensor measurements of two different sections of the grinding wheel surface may be taken. Using the initial setup previously described, measurements of the wheel surface were taken, sampling the dynamic pressure transducer at just 50 kS/s, allowing the calculation of frequencies up to 25 kHz. Examining this frequency range it is possible to test the ability of the sensor to respond to differences in the wheel surface at 20.3 m/s. The graphs in Fig. 4-11 show the frequency domain of the raw signal, taken at two axial positions. While the two signals show some similarities, importantly the amplitudes of the excited frequencies are unique to each surface.

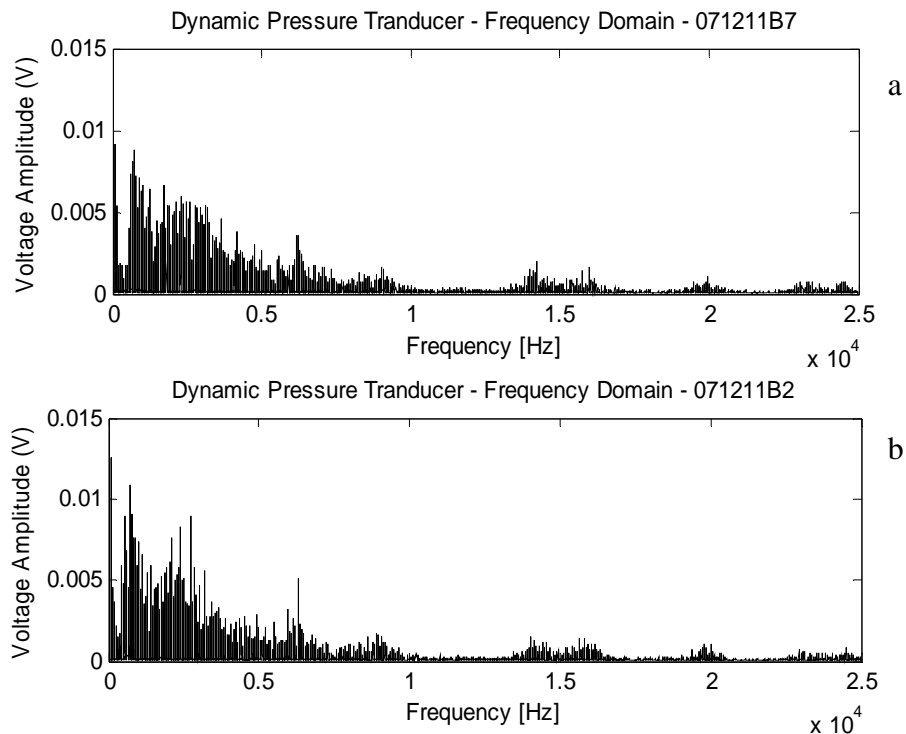


Figure 4-11: Dynamic signal from a grinding wheel surface at two axial locations.

Further evidence of the sensor responding to the surface is given by showing that the frequencies being excited are regularly spaced, and multiples of the rotational frequency of the grinding wheel. Looking at the signal in Fig. 4-11(b) as an example, for that experiment the wheel rotated at 1222 RPM, with a diameter of approximately 317 mm. The rotational frequency is clearly visible in Fig. 4-12, as well as low frequency harmonics at equal spacing for 0 to 250 Hz. The same spacing of frequency spikes can be seen from 24250 to 24500 Hz, and elsewhere on the frequency spectrum.

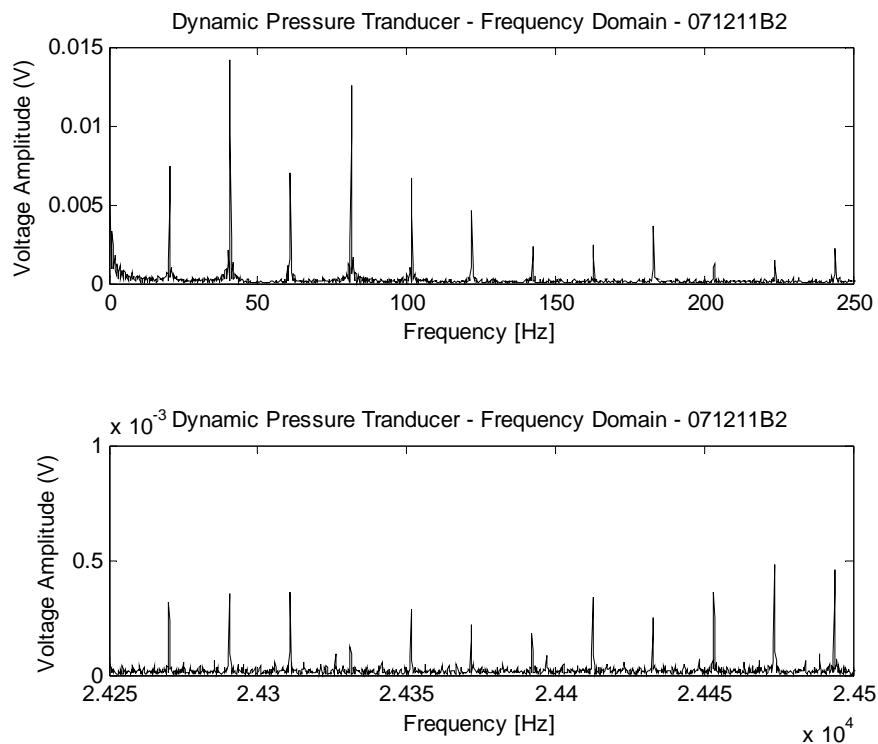


Figure 4-12: Equal spacing of frequencies generated by the wheel surface.

It stands to reason that this consistent spacing of frequencies is the result of the sensor being repeatedly exposed to one or more surface features for each rotation of the wheel. The frequencies generated are correspondingly at one or more times the rotational frequency. Applying this knowledge to the model in section 4.1.4 (pg. 64), the frequencies identified by the PCA model also corresponded to consistently spaced frequency spikes.

Sensitivity to axial position and the spacing the frequency signals indicates that the sensor's response is dependent upon the surface, and shows that pressure fluctuations of high frequency are generated and measureable. However, in detecting a grinding wheel it is not clear if these high frequency signals are dependent upon a high frequency feature, such as pores and grains, or are generated as harmonics of a lower frequency. Further experiments are needed to judge the frequency response range of the sensor.

4.2.2 Deterministic Surfaces

To test the ability of the sensor to respond to high frequency features and push the limits of the sensor's frequency range, the sensor was applied to a knurled surface. Being a deterministic surface of known geometry, the knurled surface provided the opportunity to test the sensor and verify the signal. The knurl sizes tests were of similar size to pores and large abrasive grits common to coarse vitrified grinding wheels. The sensor response for a given, controlled surface can be contrasted against the response for smooth surface of the aluminum disk, for a

varying surface velocity, or a new surface geometry. For the fine diamond knurl, which had a nominal pitch of 0.85 mm, the sensor output was verified by comparing the output signal to a predicted signal from a geometrically based model. The geometry of a sample surface was measured by an optical microscope, accurate to 10 μm .

Applying the pneumatic sensor to a disk with a fine diamond knurl disk at a surface velocity of 20 m/s, produces the dynamic signal shown in Fig. 4-13(a). For these tests the dynamic pressure transducer signal was amplified by a gain of 50 before the DAQ, improving resolution. The portion of the frequency domain signal corresponding to the knurled surface is more clearly seen when compared to a smooth surface, also with a surface velocity of 20 m/s shown in Fig. 4-13(b).

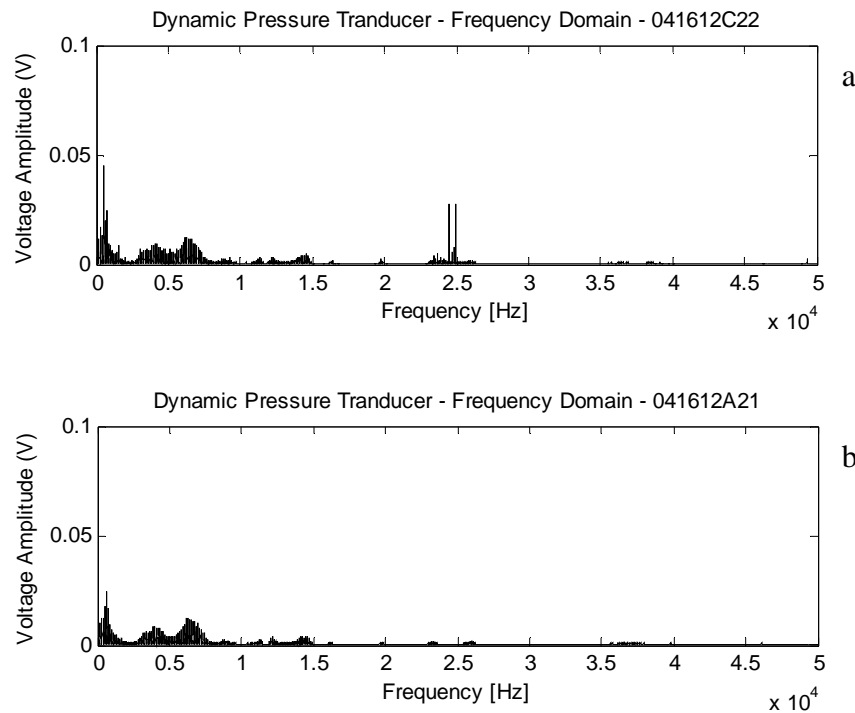


Figure 4-13: Knurled (a) and smooth (b) surface frequency domain plot.

The difference between the two graphs is the two high frequency signals at approximately 24 434 and 24 919 kHz, as well as a significant peak at 485 Hz. Initially only one high frequency peak was expected, and an explanation needed to be found for both the second high frequency peak and the lower, 485 Hz peak.

It was noted that both high frequency peaks are slightly higher than the expected value of 23 529 Hz, given the surface speed of 20 m/s and a nominal length of 0.85 mm per knurl. Furthermore, close investigation of the disk surface it was noted that the knurls are not perfectly straight, but are at a slight angle and form a helical spiral around the disk, as shown in Fig. 4-14.

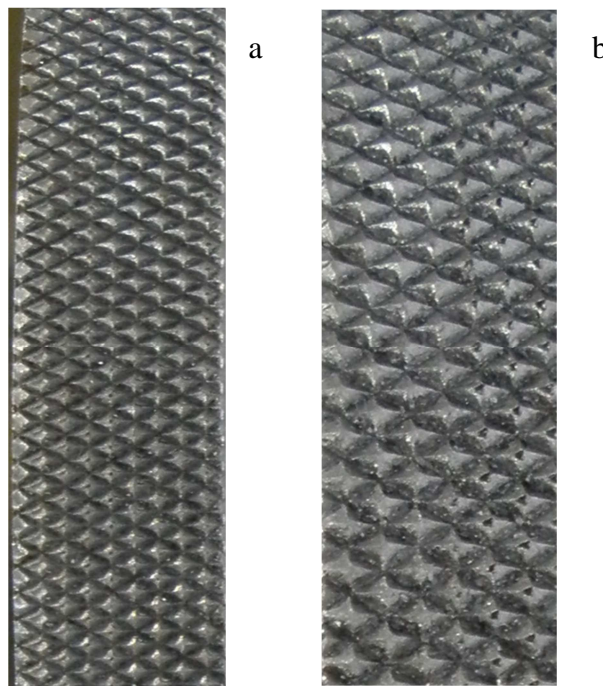


Figure 4-14: Helices formed by knurls in fine (a) and medium (b) diamond knurls.

This helix causes the pneumatic sensor to cross multiple columns of knurls as the disk rotates. In the example above, the knurls formed 14 columns of the

surface of the disk, creating 14 helices. With a rotational frequency of approximately 34.7 Hz in the example, the frequency peak of 485 Hz reflects the presence of the helix. The angle of the knurls also explains the presents of two high frequency peaks. These peaks are created as the result of the helix angle and circular geometry of the nozzle. When the nozzle is crossing into a column of knurls, the first knurl in the column will be detected as it passes at the edge of the nozzle area. With a helix, each successive knurl will pass closer to the center of the nozzle. This will increase the perceived frequency of the knurls because the circular shape of the nozzle causes a knurl passing at center to be detected earlier than one passes at the edge. Once the center of the nozzle is reached, each successive knurl will pass closer to the far edge of the nozzle, and in a similar fashion, decrease the corresponding frequency. For this reason the high frequency peaks are separated by 485 Hz.

In regards to the measured frequencies being higher than expected, the exact length of a fine diamond knurl in the circumferential direction of the wheel was variable from the nominal value of 0.85 mm, and could range from 0.81 to 0.86 mm in measured samples. Being produced by a pair of diagonal knurl wheels, the diamonds produces can be of slightly unequal side length in addition to being set at an angle to the surface velocity direction. For this reason the exact frequencies of the two high frequency signals were not always consistent from one knurled surface to the next, even if the same fine diamond knurling tool was used to produce both surfaces.

The frequencies shown for a smooth surface in Fig. 4-13(b) are not the result of surface features, but rather the result of the air flow through the internal volume of the sensor. This is demonstrated in Fig. 4-15(a), where the surface has been removed, and the sensor is directed into open space. The pattern of the frequencies and amplitudes generated are similar to the smooth wheel case. Inside the sensor, air flows through several changes in geometry, including changes in diameter, threaded attachment points and ‘Y’ connections where the dynamic and gauge pressure transducers are connected. These internal features were considered as a possible cause of the frequencies generated by a smooth wheel surface.

The effect of the internal geometry was investigated by removing the ‘Y’ joint that connects the air supply and the gauge pressure transducer to the body of the pneumatic sensor, shown in Fig. 3-1, (pg. 32). The gauge pressure transducer was excluded, and the control orifice and air supply were connected directly to the main body. The new dynamic signal for a flat surface is shown in Fig. 4-15(b), and the frequencies generated are visibly different from those of Fig. 4-15 (a).

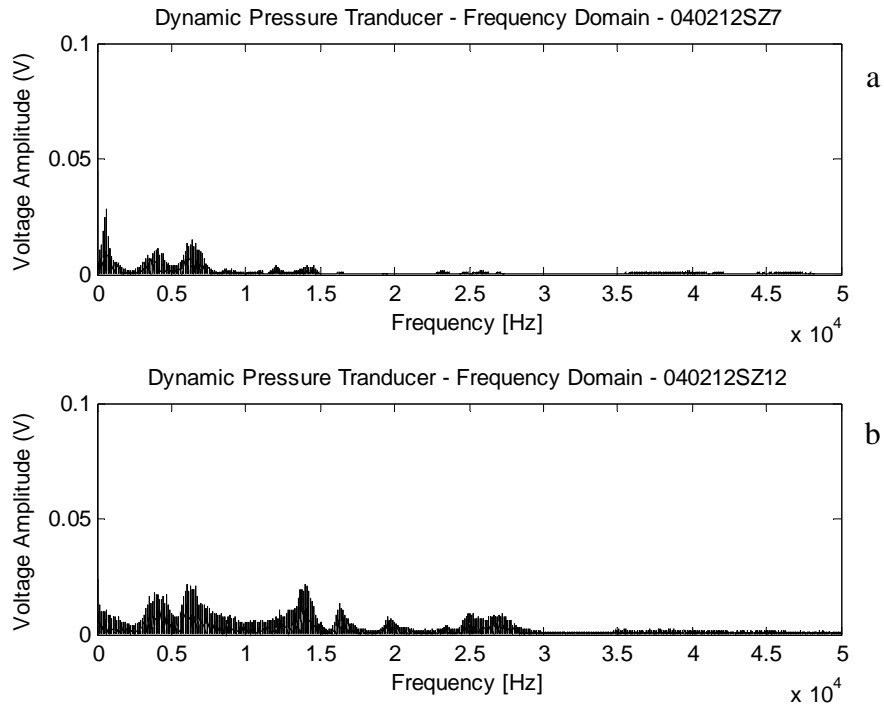


Figure 4-15: Varying the internal geometry and volume of the pneumatic sensor.

Confirmation that the high frequency signals from Fig. 4-13(a) are the result of the knurled surface can be provided by changing the surface velocity or by further changing the geometry of the surface. Fig. 4-16, shows the signal from the dynamic pressure transducer for the fine diamond knurl at 30 m/s, with a rotational frequency of 52 Hz. The two high frequency peaks are now at 36 650 and 37 378 Hz, although at the higher frequency the amplitude of the signal is reduced. The low frequency peak is at 727.8 Hz, and again corresponds to the helical formation of the knurls in 14 columns.

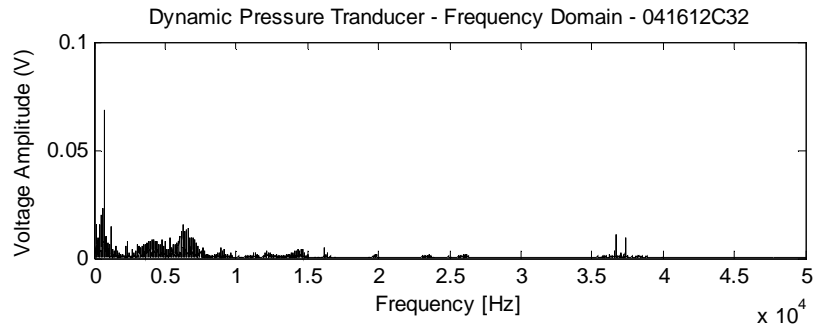


Figure 4-16: Frequency of knurls shifts with increasing surface velocity

Changing the geometry of the target surface, Fig. 4-17 shows the signal generated by the measurement of a coarse, straight knurl with a surface speed of 20 m/s. the frequency generated is 13 070 Hz, which is close to the expected value of 13 333 Hz for a nominal knurl length of 1.5 mm. This further confirms the high frequency signal from Fig. 4-13(a) is in response to the fine diamond knurling on the disk surface.

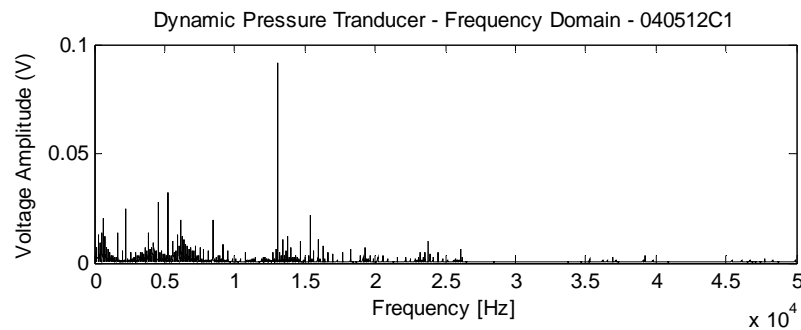


Figure 4-17: Frequency domain of straight, coarse knurl surface.

Further investigating the ability of the pneumatic sensor to correctly respond to the surface of the disk, the effect of the helix of the knurls was

investigated by varying the helix angle, and effectively changing the number of helices generated. Although the helix could not be entirely eliminated, two experiments show the effect of the change clearly. In Fig 4-18(a) and Fig. 4-18(b) the helix angle is varied to produce 13 and 17 helices respectively. At a surface speed of 20 m/s and a rotational frequency of approximately 34.8 Hz, each knurl set generated two high frequency peaks. Specifically, in Fig. 4-18(a), for 13 helices peaks are generated at 24 387 and 24 839 Hz, separated by 452 Hz. In Fig. 4-18(b), 17 helices generated peaks at 24 283 and 24 874 Hz, which are separated by 591 Hz. Comparison of the two frequency domain plots shows the increased separation of the frequency peaks.

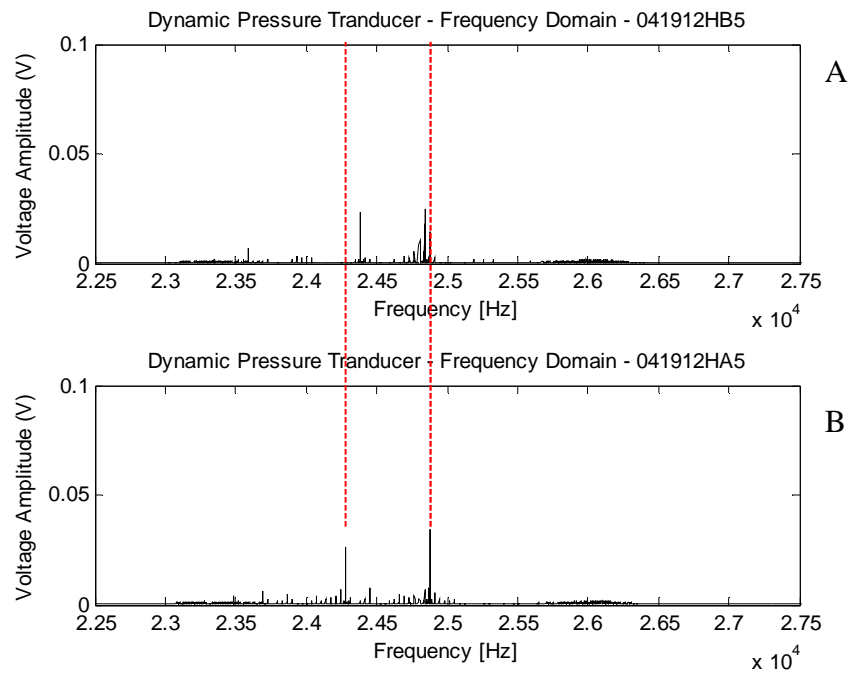


Figure 4-18: Separation of frequency peaks due to knurling helices.

In order to isolate and verify the lower frequency generated by the helices formed by the knurls, a sample surface was prepared on an aluminum disk with 7 helices in the form of a 7 start thread, shown in the figure below. The thread has a pitch of 0.5 mm. The threaded section is wide enough to accommodate the entire width of the nozzle at approximately 3 times the outer nozzle diameter in width (Fig. 4-19).

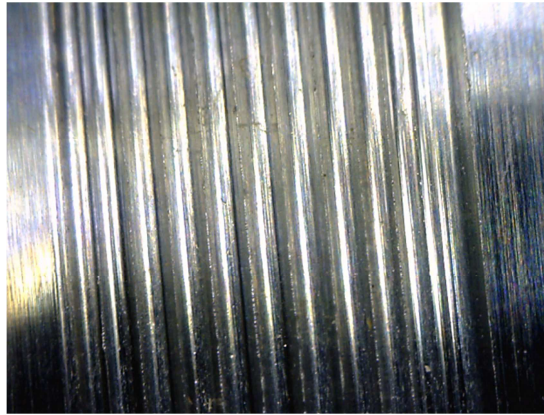


Figure 4-19: 7-start thread in disk surface.

The threaded surface was measured by the sensor at 20 and 30 m/s surface velocity, corresponding to a rotational frequency of 34.8 Hz and 52.2 Hz respectively. With seven starts it is expected that a frequency of 243.6 Hz and 365.4 Hz will also be generated. Looking at the full frequency spectrum for the 20 m/s test in Fig. 4-20(a) the high frequencies observed in Fig. 4-13(a) are gone. The other signal amplitudes at higher frequencies have already been shown to be dependent on interior geometry of the sensor, and not on the disk surface, as in

Fig. 4-13(b). The knurl surface signal in Fig. 4-13(a) does show the low frequency peak, which is reproduced by the treads and highlighted in Fig. 4-20(a).

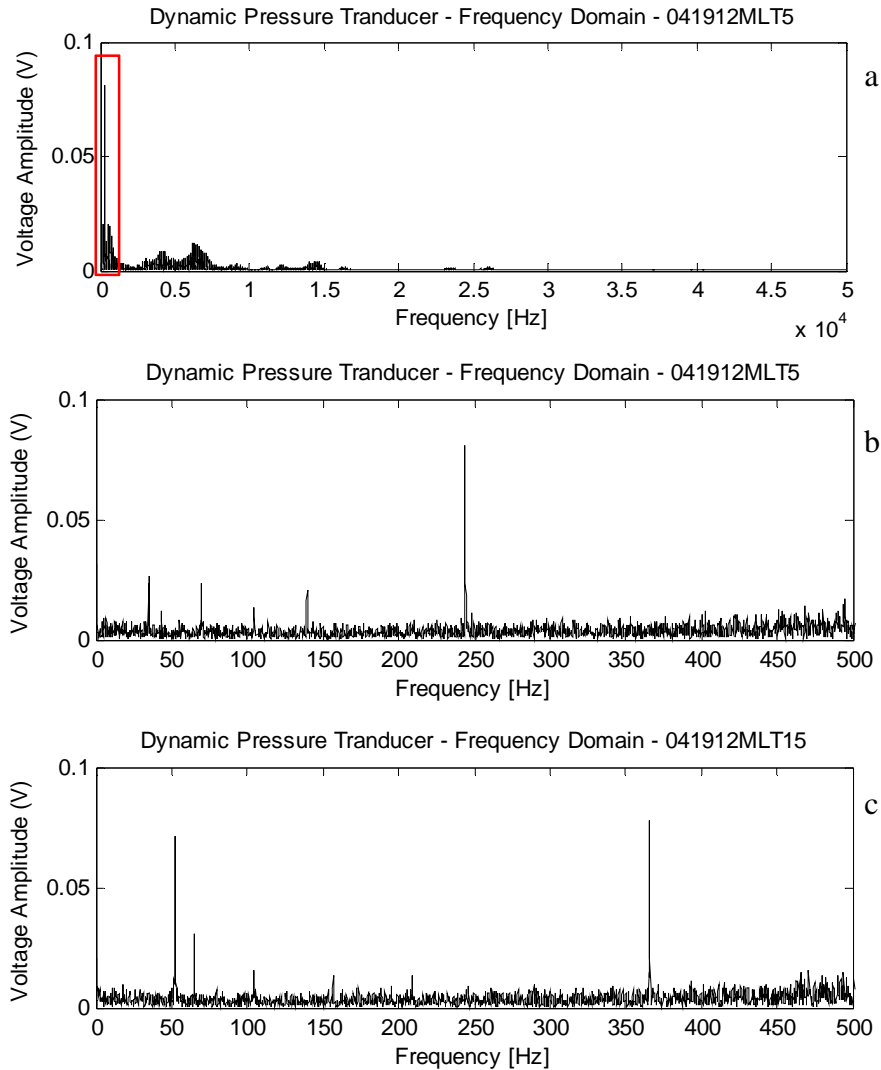


Figure 4-20: Frequencies generated by multi-start thread for 20 m/s (a, b) and 30 m/s (c).

Looking at the first 500 Hz of the spectra from Fig. 4-20(a), the frequency peaks seen in Fig.4-20(b) and Fig. 4-20(c) for the threads at each speed are present near their expected values. They are 243.9 and 365.8 Hz for 20 and 30 m/s

respectively. The frequency graphs also show peaks for the rotational frequency in each case as well as harmonics, which are the result of run out that could not be entirely eliminated from the experiment.

Having investigated the response of the pneumatic sensor to different knurl sizes and types, the height of the knurls was varied specifically to test the depth response of the sensor. Experimentally, a fine diamond knurl was trimmed by means of a turning operation, removing approximately 0.1 mm from the original 0.33 mm height of the knurls (Fig. 4-21). The resulting frequency domain signal, shown in Fig. 4-22, clearly shows the high frequency signals of the trimmer surface in blue are reduced in comparison to the full knurl in red for surface velocities of 20 m/s.

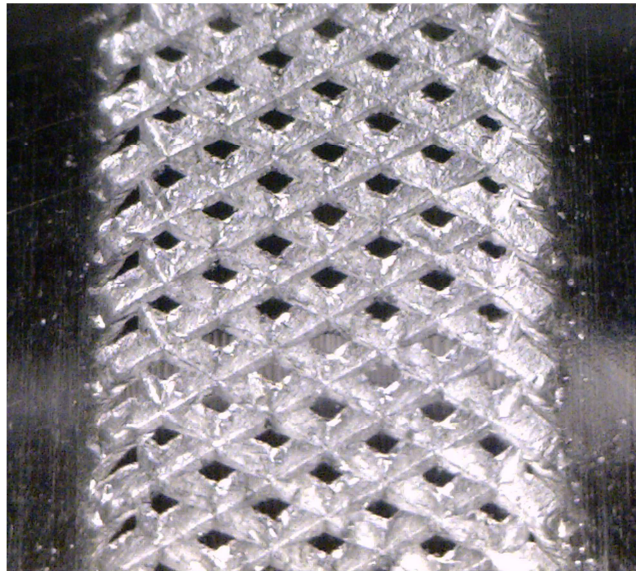


Figure 4-21: Trimmed knurls

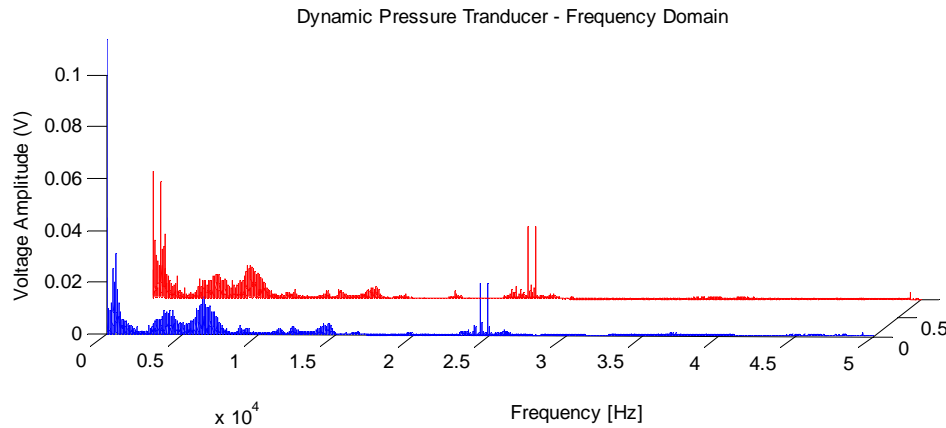


Figure 4-22: Amplitude of frequency response is reduced by trimming knurls

The ability of the sensor to reflect a change in surface height as a change in signal amplitude shows that the height of protrusion or depth of recession for an abrasive grain or pore could be accounted for by the sensor. Along with the influence of spatial distribution of grains and pores reflected by which frequencies are excited, these simplified surface experimental results are promising.

4.2.3 Knurl Surface Modeling

The signal generated by the pneumatic sensor in response to the fine diamond knurl was confirmed and verified by a geometric model. The knurled surface can be measured and therefore is of approximately known geometry, although some variations may exist. A geometry based model provides insight into the double high frequency peaks in the frequency domain, such as those seen in Fig. 4-13(a), as well as the effect of the helix formed by the angled path of the knurls.

To construct the model, a sample of the surface geometry was created with 10 μm resolution, using the nominal knurl dimension given in Table 3-3 (pg. 47). To allow a small sample of the surface to be looped, the boundary conditions at the initial and end values for each row and column were made equal. The surface sample is shown in Fig. 4-23 for illustration.

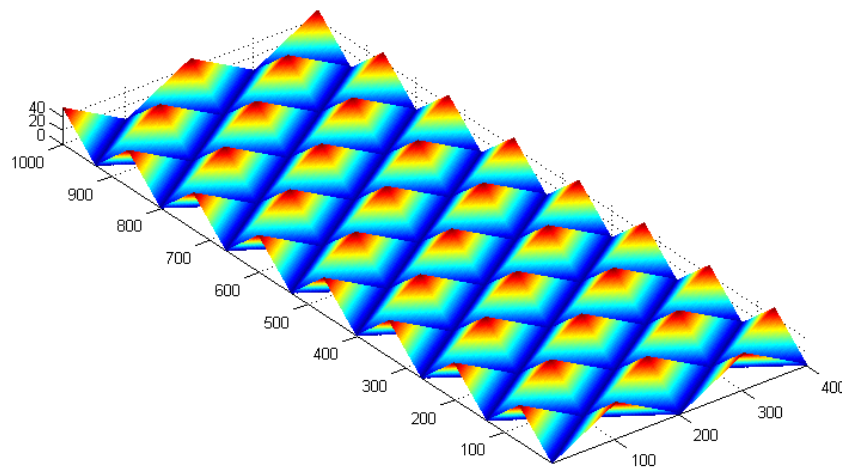


Figure 4-23: Model of knurled surface.

To simulate the geometry experienced by the sensor nozzle as it passes over, a circle of the same inner diameter as the nozzle is projected over the model surface at a set stand-off distance, and the area between the circle's perimeter and the surface is calculated. As discussed in section 1.4, the pneumatic sensor outputs an internal pressure that is dependent upon the area through which the air flow is restricted. When the nozzle is close to a surface the area between the nozzle perimeter and the surface is less than the cross sectional area of the nozzle. At such a distance the internal pressure of the sensor is dependent upon the distance

to the surface and any features that may change the escape area. Any feature in the surface that is above or below the mean surface will impinge or relieve the flow of air, resulting in a pressure fluctuation. This area is calculated at a rate that correctly matches the surface speed of 20 m/s and the data collection rate of 100 kS/s for the dynamic pressure transducer. Fig. 4-24 shows the projected vertical area of the knurled surface at the perimeter of the nozzle circle for three increments.

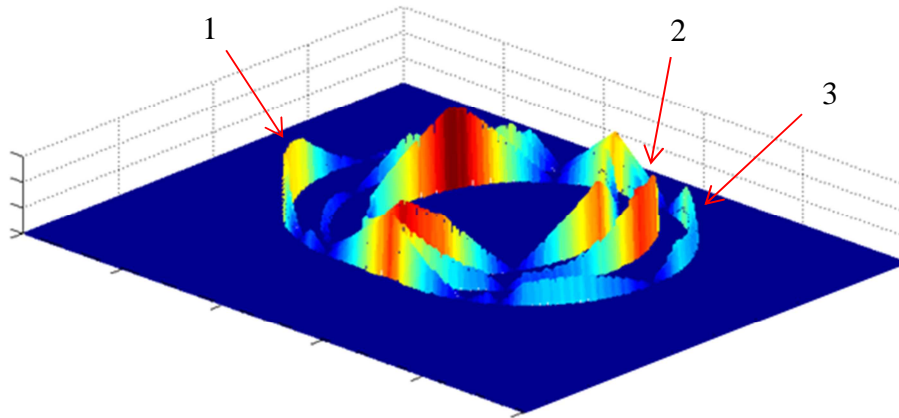


Figure 4-24: Knurl model of the escape area, 3 increments.

Increasing the number of increments the plot of the surface at the perimeter of the nozzle more clearly shows the topography of the knurled surface. Fig. 4-25 shows 40 increments of the nozzle over the model surface, and also models the effect of the helices by traversing from one column of knurls to the next.

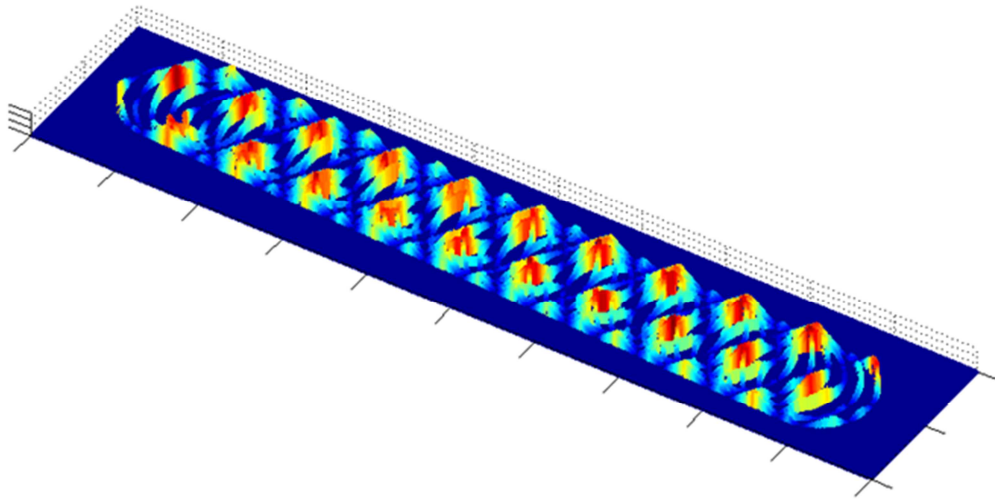


Figure 4-25: model of knurled surface at nozzle perimeter, 40 increments, with helix.

To develop an approximation of the dynamic pressure transducer signal, the area is calculated for twenty thousand increments. The area calculated is recorded in the time domain and then transformed to a frequency domain plot for comparison to the experimental results from the dynamic pressure transducer. Running the model with a similar surface geometry and helix angle to the fine diamond knurl disk surfaces tested in section 4.2.2, generates a signal that is comparable to the dynamic pressure transducer signal taken during those experimental tests. The model of the fine knurl surface with 14 helices employed a rotational frequency of 35.1 Hz, at a surface speed of 20 m/s. The resulting frequency domain signal shown in Fig. 4-26 exhibits many similarities to the dynamic pressure transducer signal shown in Fig. 4-13(a). Notably, in Fig. 4-26 a low frequency peak at 491 Hz occurs, as do two high frequency peaks at 23 684 and 24 175 Hz. As in the experimental results, the separation between these two

peaks matches both the low frequency peak and the product of the rotational frequency and number of helices. The similarities between the experimental results and those of the geometric model demonstrate that experimental signal is the result of surface geometry.

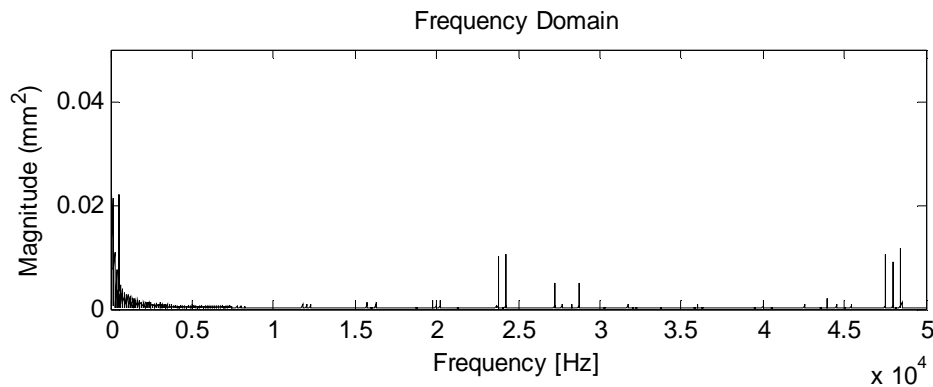


Figure 4-26: Frequency response to fine knurl at 20 m/s predicted by model.

The model also predicts three higher frequency signal peaks in Fig. 4-26, at 47 368, 47 859, and 48 350 Hz. The first and third of the peaks are harmonics, being twice the value of the 23 684 and 24 175 Hz peaks. The middle of the three is the result of the nozzle diameter being close to the width of the diamond knurls, and detecting the staggered peaks of two columns. This geometry is visible in Fig. 4-25, where the nozzle passes over two columns of knurl peaks, shown in red. These peaks are not present in the experimental signal, suggesting that sensitivity at that frequency range is less.

The effect of the helix can be shown in the model by removing it from the simulation. This is shown in Fig. 4-27, and results in a single high frequency

signal at 23 999 Hz, and a harmonic. Notably there is no twin peak near 24 kHz, and the low frequency peak, such as the 491 Hz peak in Fig. 4-26, is not present.

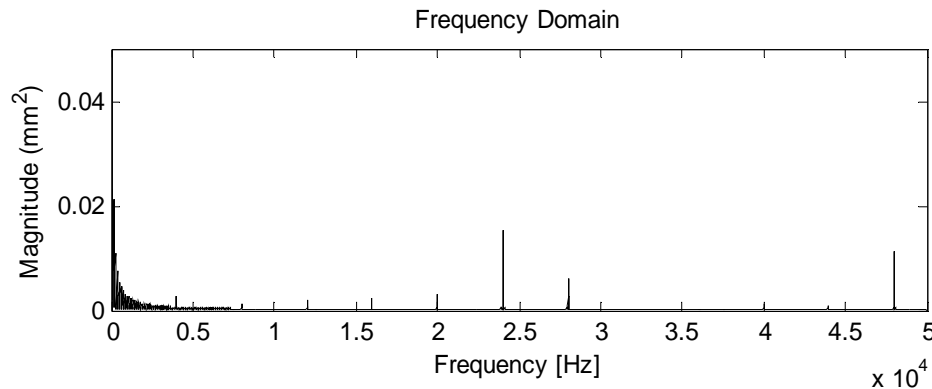


Figure 4-27: Frequency response predicted by model with no helix.

While it was not possible to remove the helix for experimental testing, varying the degree of the helix was possible, and replicated in the model. Agreement is found between the experimental results in Fig. 4-18 and the simulation for the effect of changing the angle of the knurls and thus the number of helices formed. Simulations were made of a 10 helices case and 20 helices case, for a surface velocity of 20 m/s and rotational frequency of 35.1 Hz, and are shown in Fig. 4-28.

Comparing the graphs, it can be easily seen that increasing the number of helices increase the value of the low frequency peak from 352 to 702, and increases the separation between the two peaks. This result is similar to the effect observed in Fig. 4-18.

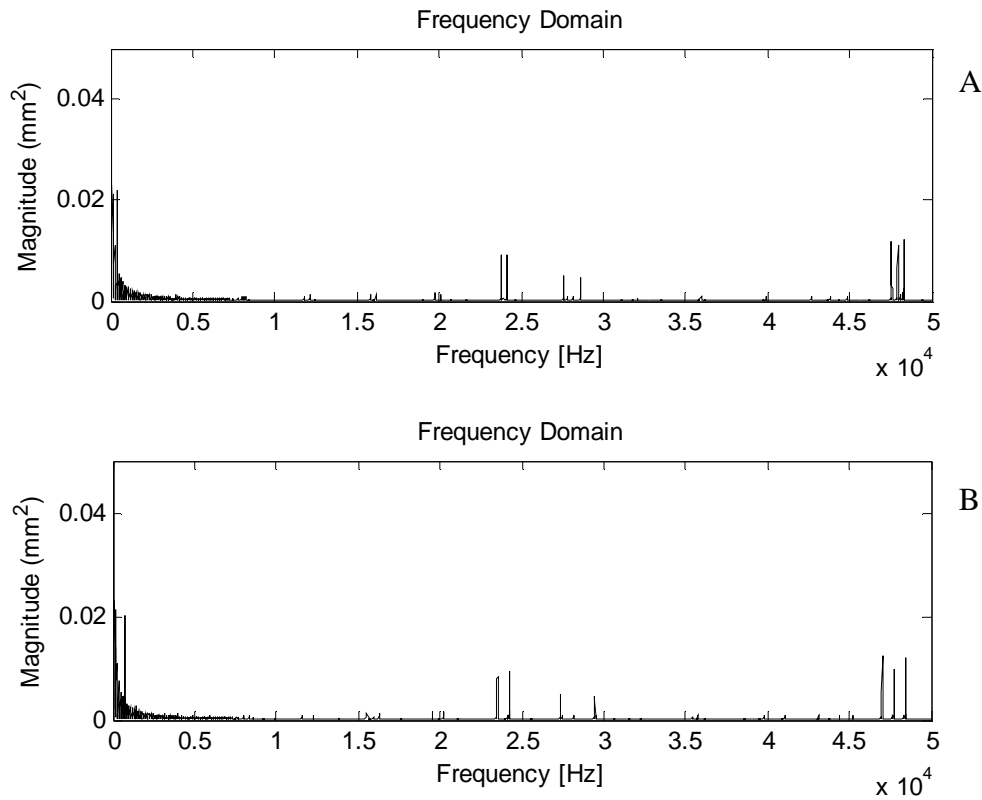


Figure 4-28: Simulated effect of helices for 10 (a) and 20 (b) helices per rotation.

Results from the geometric model agree with the experiments in section 4.2.2 and support the conclusion that the dynamic pressure transducer signal taken from the pneumatic sensor is representative of the target surface.

4.2.3.1 Influence of Nozzle Diameter by Simulation

It is difficult to isolate the effect of nozzle diameter alone by experimental means because the nozzle diameter influences the relationship between the stand-off distance and average internal pressure. By simulation however, it is possible to see how diameter of the nozzle changes the signal generated. For experiments and the simulation results discussed above used a nozzle with a diameter of 1.194 mm,

or needle gauge of 16. Changing that diameter does not change the frequencies generated, but does alter the amplitude. By example, if the nozzle diameter from the 10 helix example above is changed to 0.8 mm, close to the pitch of the fine diamond knurls, then the signal amplitude is increased, Fig. 4-29. This is logical as the changes to the area through which the air may escape will be more extreme as a result of nearly matching the surface pitch.

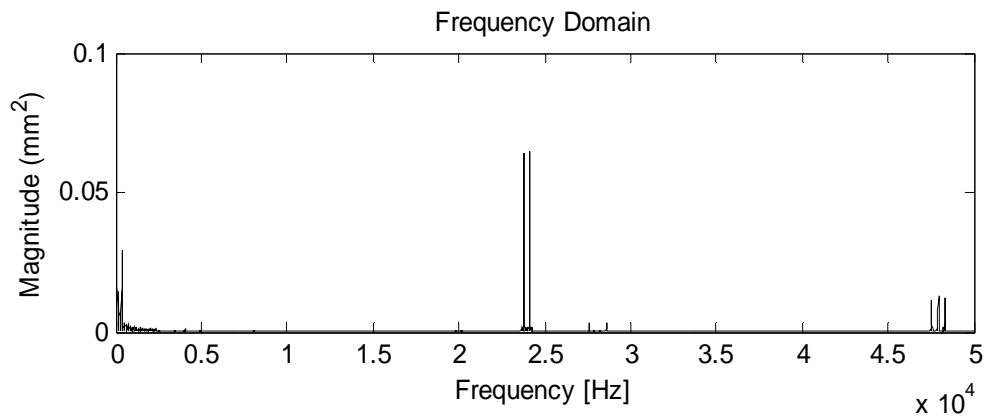


Figure 4-29: Simulation of varying nozzle diameter.

The conclusion to be made from the simulation is that the nozzle diameter can have significant influence on the amplitude of the signal generated, but the specific frequencies generated will be dependent upon the geometry of the features of the wheel surface.

4.2.4 Detecting Nondeterministic Surfaces

Having demonstrated that the pneumatic sensor is capable of operating at high frequencies past 37 kHz, the application of the sensor to a nondeterministic

surface required further increasing the measurable frequency range. Experimenting with the metal bond diamond abrasive wheel presented the possibility that the small grains of the 170/140 grit wheel could generate much higher frequencies, in addition to being harder to detect. Applying the pneumatic sensor to the surface of the metal bond diamond abrasive wheel produced a signal that demonstrated a relationship between the wheel surface and the output signal.

To identify the frequencies in the signal from the pneumatic sensor that were in response to the surface of the grinding wheel, the signal from the grinding wheel, in Fig.4-30(a), was first compared to a signal taken from a trimmed fine diamond knurl surface with the same operating conditions, Fig. 4-30(b). Both of these signals were taken with surface velocities of 30 m/s.

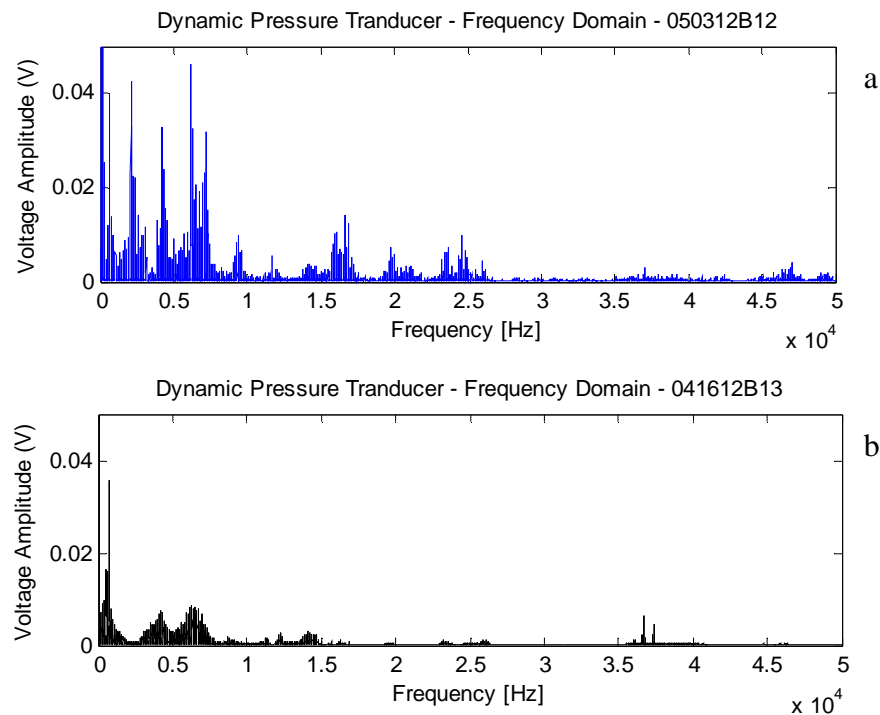


Figure 4-30: Frequency response to (a) metal bond grinding wheel and (b) trimmed knurls

For this comparison the knurled surface produces a frequency domain signal that is typical of the experimental knurl results, in section 4.2.2. In contrast the signal produced by the grinding wheel surface show frequency peaks across the measured frequency range. These frequency peaks are not common to the noise observed from the knurled surface signal. A closer view of the frequencies generated by the grinding wheel surface is shown in Fig. 4-31. From this graph it is possible to see that the grinding wheel surface produces individual frequency peaks. Similar to the results observed in Fig. 4-12, the frequency peaks are separated by the base rotational frequency of the grinding wheel.

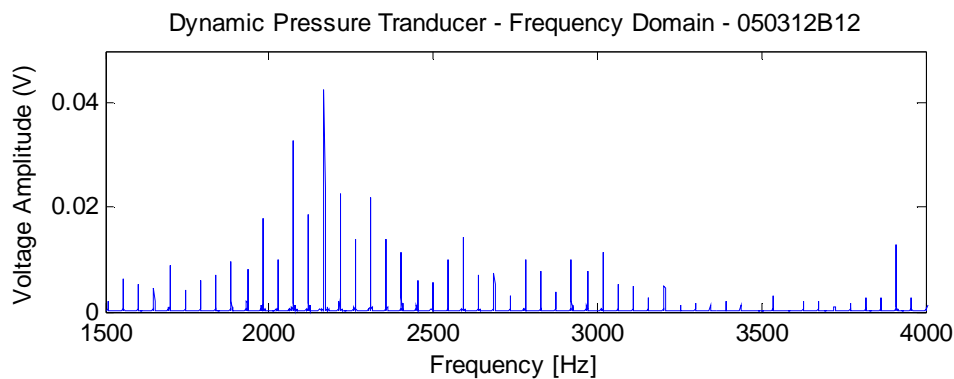


Figure 4-31: Separation of frequency peaks in metal bond grinding wheel

To enhance the performance of the pneumatic sensor the setup of the sensor was changed to the one listed in table 3-4. Most importantly, reducing the nozzle diameter to 0.603 mm made the sensor more responsive to small grain size of the metal bond, diamond abrasive wheel. With the new setup the dynamic frequency range of the sensor was observed to increase, and it became possible to observe separated, individual frequency peaks at much higher frequencies. A

sample of the resulting frequency domain signal is shown in Fig. 4-32, for the frequency range of 80 kHz to 82.5 kHz. Although the amplitude of the signals is much lower, the frequencies generated are still distinct and at regular intervals.

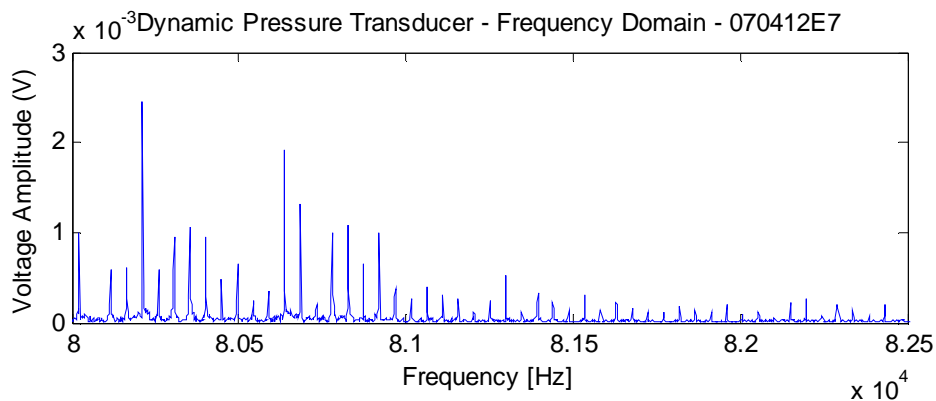


Figure 4-32: Signal separation at high frequency.

To determine the useful measureable frequency range the data collection sampling was increased to 2 MS/s, or 2 million samples per second, allowing a broad frequency range of up to 1 MHz to be viewed and assessed. The figure below shows an example signal in the frequency domain. Only the first 200 kHz are shown.

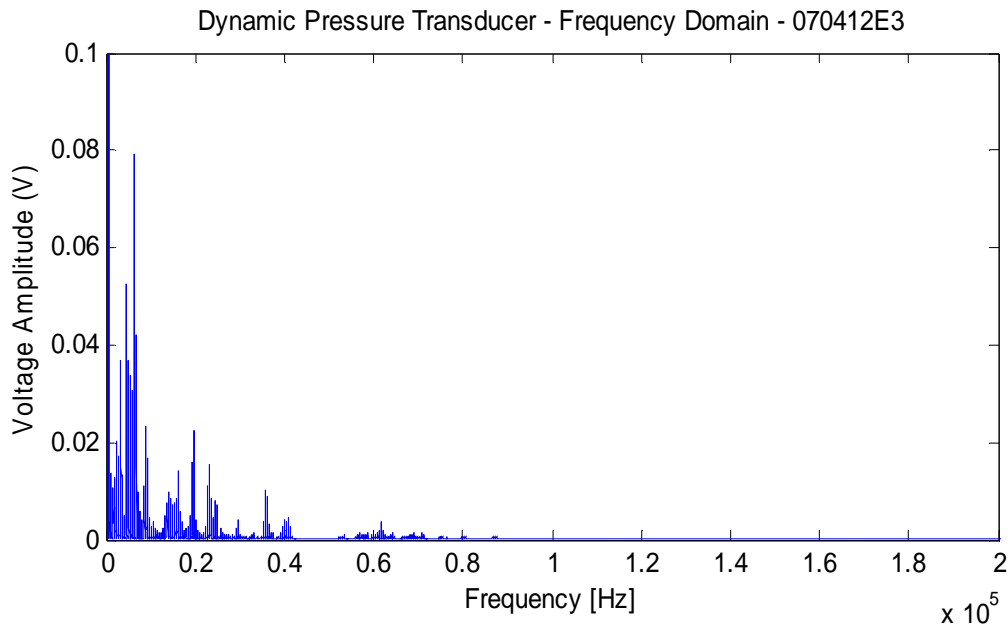


Figure 4-33: High sample rate signal in the frequency domain

The signals collected from experiments with high sample rates were able to produce frequencies as high as 100 kHz. This set the data collection rate for tests conducted on nondeterministic surfaces at 200 kS/s. This is the rate used for the development of application on both metal bond and vitrified bond grinding wheels.

The response of the sensor to a change in surface geometry at high frequency was also investigated for the metal bond diamond abrasive grinding wheel. To this end the sensor was applied to the grinding wheel under identical conditions, except for a change in the surface condition. The grinding wheel was trued and dressed using the method described in section 2.2.2 (pg. 25). The sensor was applied to the wheel surface for trued, Fig. 4-34(a) and dressed, Fig. 4-34(b),

wheel conditions. These experiments were conducted without coolant and at a surface velocity of 30 m/s. The nozzle position was fixed at a distance of 5 μm from the trued wheel surface.

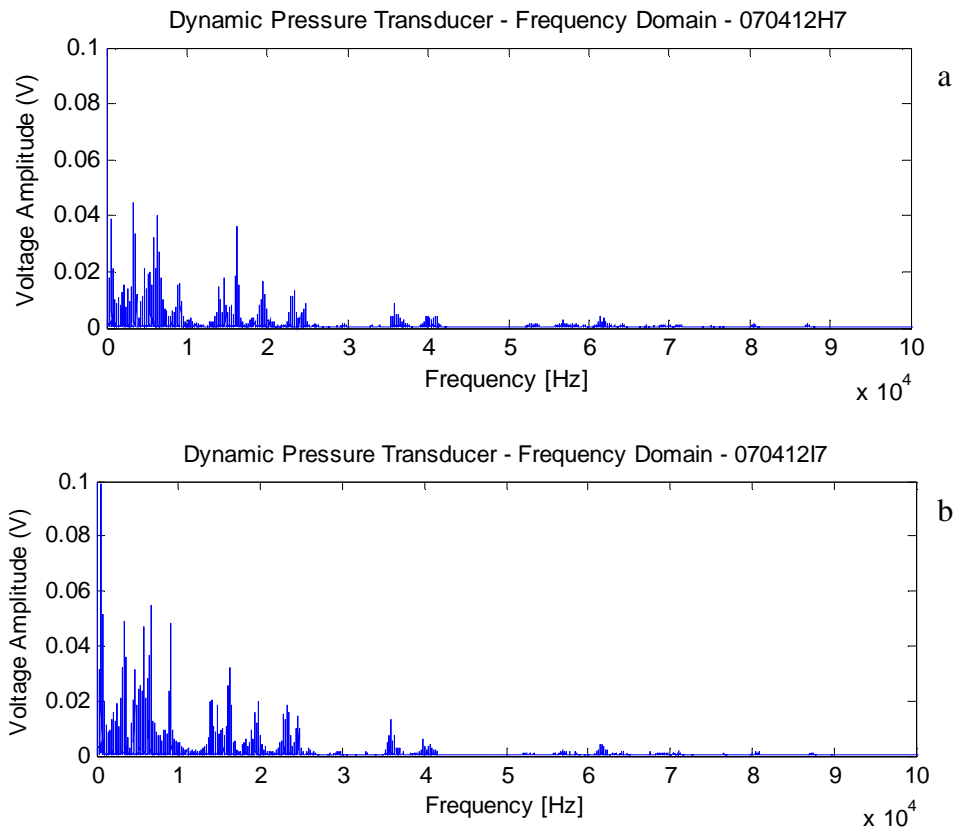


Figure 4-34: Response to trued (a) dressed (b) surface condition

Comparing the trued and dressed surface signals shows a significant increase in the amplitude of most frequencies for the increase in roughness caused by dressing. Closer examination of the two frequency domain plots showed that this is true for both the strongest frequencies visible in these figures, but also for frequencies with smaller amplitudes.

For these tests the SOD was not compensated, and the reduction in average P_b caused by dressing would have reduced the amplitude of the dynamic response of the sensor. In spite of this decrease in dynamic performance, the change in surface roughness visibly affects the dynamic pressure transducer signal across the frequency range. This is a promising result, and suggests that it may be possible to monitor changes in wheel surface topography.

4.2.5 Stand-off Distance and Dynamic Signal Amplitude

How close does the sensor need to be to the surface to monitor it, and how does a change in the distance effect the dynamic signal? The stand-off distance, SOD, is an important variable in determining the performance of the pneumatic sensor, influencing both the geometry of the escape area and average back pressure. As previously established by other researchers, as the average back pressure increases the dynamic response also increases. It is shown in this section that this is true for the rapid dynamic pressure fluctuations caused by grinding wheels.

The SOD also changes the extent of air flow impingement caused by passing surface features and topography, and thus the intensity of the corresponding pressure fluctuation. When the SOD is relatively large, fluctuations in escape area caused by passing surface features make up a lesser percent of the total escape area. When the SOD is reduced the fluctuation in area from surface features makes up a greater portion of the escape area, and generates greater

dynamic pressure signal amplitude. This section details the investigation of this relationship at high frequencies and establishes a method for determining the maximum SOD for surface monitoring.

The net effect of increasing SOD on the amplitude of the dynamic pressure transducer signal can be observed in a simple test. Applied to a vitrified grinding wheel, 32A46-GV40P, the dynamic pressure transducer signal was recorded for three SOD values. The tests employed a constant supply pressure and a surface velocity of 20.3 m/s.

The resulting time domain plots of the raw dynamic signals, Fig. 4-35 show that increasing the distance between the wheel surface and the nozzle tip reduces the signal amplitude.

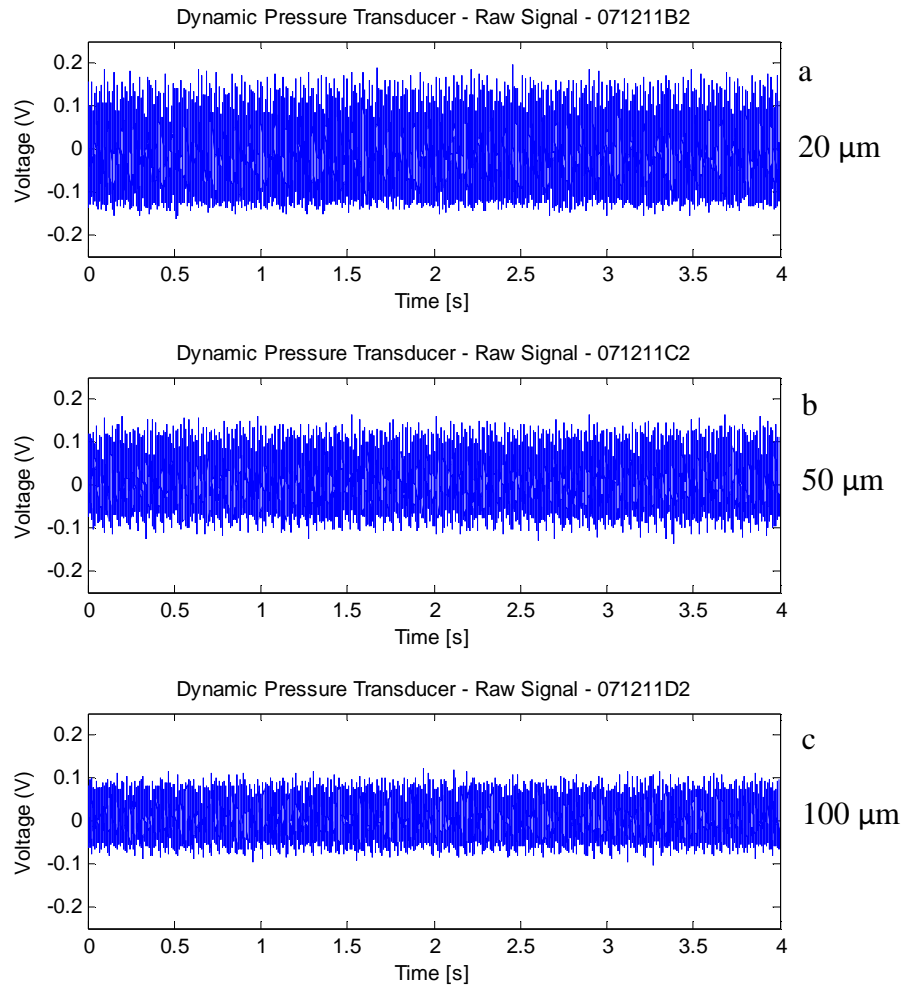


Figure 4-35: Raw dynamic signal for varying SOD

It is clear from these results that distance greatly influences the dynamic performance of the sensor. These results however, are caused by both decreasing average back pressure and the decreased influence of surface features on the escape area caused by a larger average gap size. A simple investigation can be made to verify that both of these effects are influential and should be considered in the operation of the pneumatic sensor. It is convenient to return to the knurled

surface and aluminum disk for these tests. Using a controlled surface to generate a dynamic signal that is now well understood, from section 4.2.2, the effect of changing a single variable is easy to observe.

4.2.5.1 Increasing Stand-off Distance

To investigate the change in the sensor's high frequency response to increasing the SOD with operating conditions otherwise held constant, experiments were conducted on a coarse, straight knurled surface. Stand-off distances of 20, 40 and 50 μm were investigated and example signals in the frequency domain are shown below in Fig. 4-36. At a surface speed of 20 m/s the knurls produce a frequency of approximately 13 070 Hz.

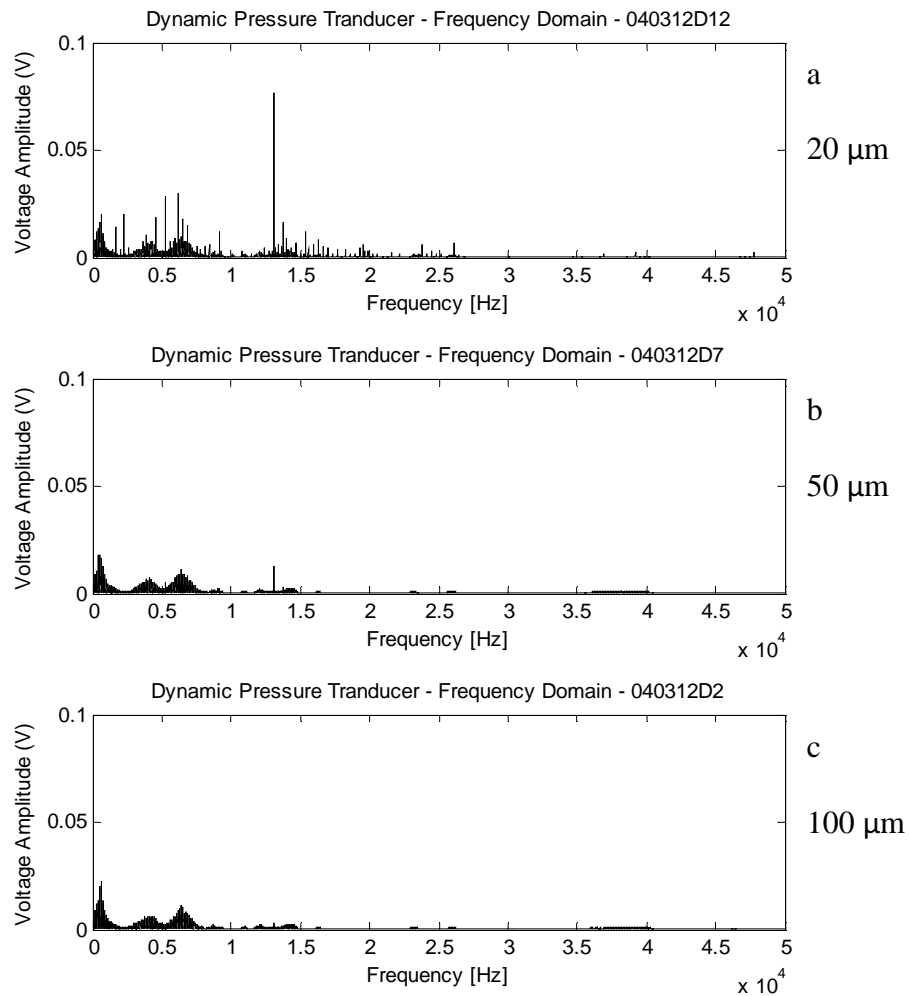


Figure 4-36: Increasing SOD on coarse, straight knurled surface.

The signal amplitude at 20 μm is strong, but doubling the SOD to 40 μm severely reduces the signal strength. Increasing the SOD by just another 10 μm , the high knurl frequency amplitude is nearly eliminated from the signal. Simply put, as the distance between the nozzle and knurled surface increases, the fluctuation in escape area caused by passing knurls make up and smaller percent of the total escape area, and thus create smaller fluctuations in pressure.

Particularly interesting about the result of this experiment is that the air flow is restricted by the surface for all distances. This leads to the conclusion that although the surface may be within the measurement range of the sensor for displacement measurements, the dynamic pressure fluctuations are not guaranteed to be sufficient for monitoring purposes.

4.2.5.2 Internal Pressure Effect

It is already established that the stand-off distance influences the average back pressure and the geometry of the escape area, and it is important to acknowledge that the average back pressure can independently influence the dynamic performance of the sensor. A rise in average back pressures will increase the sensitivity of the sensor to dynamic pressure fluctuations [11]. To demonstrate this experimentally the sensor was applied again to a coarse, straight knurled surface and measurements were taken at multiple supply pressures. By varying the supply pressure this time the average back pressure could be increased without altering the SOD. These tests, conducted at 30 m/s and at an SOD of 25 μm , clearly show the increase in pressure resulting in increased amplitude of the high frequency signal generated by the knurls, Fig. 4-37.

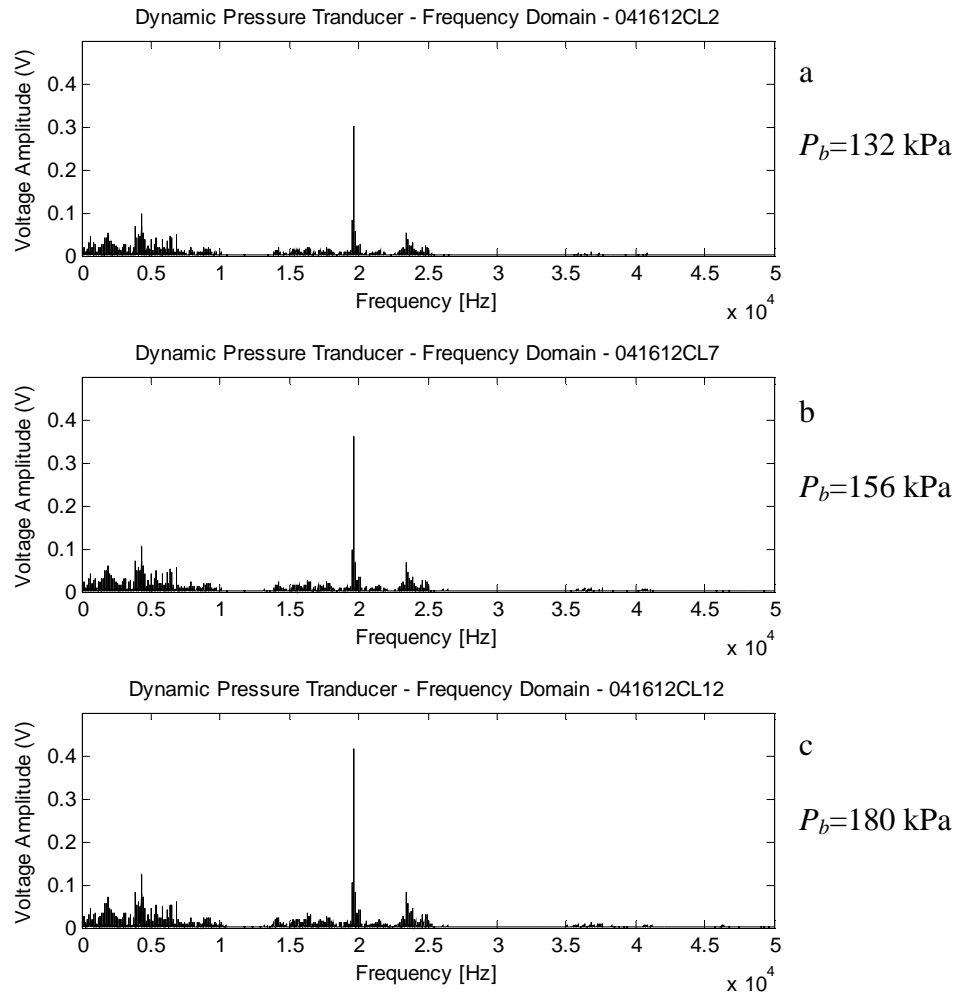


Figure 4-37: Increases in average back pressure on straight, coarse knurl.

Following the results shown in Fig. 4-36 and Fig. 4-37, it is logical that both the average back pressure and the average distance from the target surface should be maintained when using the sensor to detect changes in surface topography. To accomplish this it is necessary to adjust the SOD from one surface to the next so that a constant average back pressure may be maintained. In reference to the concept of effective stand-off distance introduced in section

4.1.2.1 (pg. 56), the SOD is a simple measurement from the nozzle tip to the outer most edge of the wheel surface, and it not representative of the real average gap size. This is illustrated in Fig. 4-38, in which a nozzle is positioned at the same distance from the average surface height, but due to surface roughness has two different SOD values.

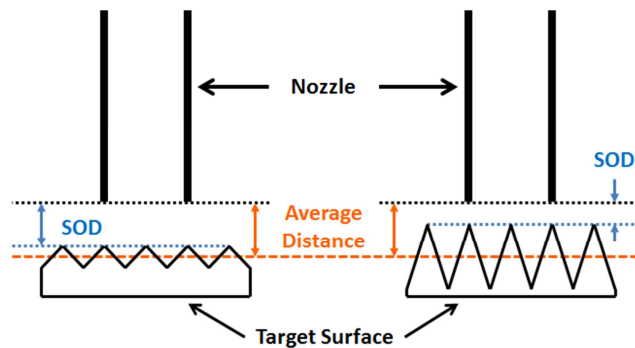


Figure 4-38: Stand-off distance and actual average distance

Maintaining an average distance enables a fair comparison of surface features to be made, based on the degree of air flow impingement and resulting pressure fluctuation created by each feature. If it can be assumed that average distance and effective stand-off distance are equivalent, then adjusting the nozzle position to maintain a constant average back pressure will also ensure a constant average distance.

4.2.6 Maximum Stand-off Distance

To establish the maximum SOD for application to grinding wheels with both solid and porous bond structures, a test of signal amplitude assessed at what

distance the dynamic pressure signal was influenced primarily by the surface of the wheel. As the nondeterministic surface produces dynamic pressure frequencies across a broad range, root mean square, or RMS, is used to quantify the signal amplitude. The sensor was applied at several SOD values, and the raw signals are put through a high pass filter, set at 1000 Hz, to remove signal energy associated with wheel waviness or run out. The test was repeated at 6 axial locations and the average values are shown in Fig. 4-39 along with the standard deviation.

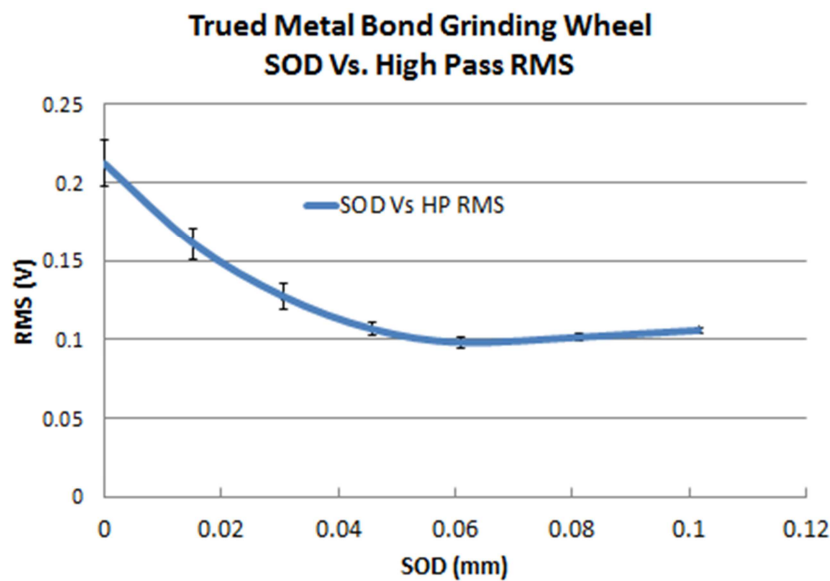


Figure 4-39: Finding maximum SOD for a metal bond grinding wheel.

For this experiment the wheel speed was 20 m/s and 42 measurements were taken in total. From this graph it can be seen that around 50 μm the high frequency signal stops responding to changes in the stand-off distance, and illogically begins to increase.

To explore what could be influencing the sensor the experiment was repeated once more but with a surface speed of zero. Figure 4-40 shows the change in high pass RMS is comparatively minor for small SOD values but increases with increasing SOD. This is likely resulting from increased air velocity in the sensor producing dynamic pressure fluctuations such as those seen in Fig. 4-14. The result matches well to the increasing RMS values observed in high surface velocity case in Fig. 4-39 for SOD values above 50 μm .

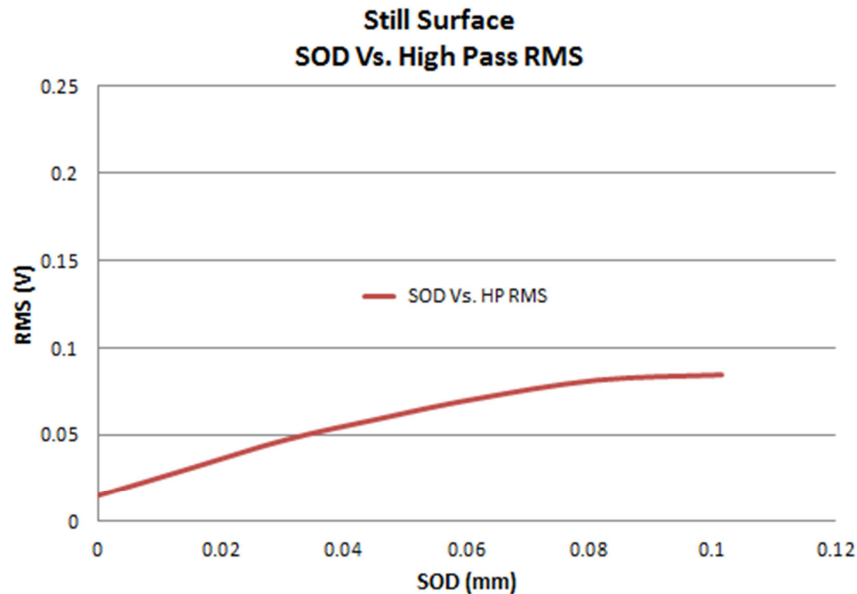


Figure 4-40: High pass RMS response to stand-off distance for zero surface velocity.

The same process can be applied to the vitrified grinding wheel surface. For the coarse dressed 32A60-HVBE wheel the response of the sensor declines considerably with respect to changes in SOD as it approaches 200 μm . The appreciable increase in maximum distance is the result of a change in the setup of the sensor, as shown in table 3-4, including the use of a larger nozzle diameter.

The larger nozzle diameter was required for the vitrified wheel due to the porous nature of the wheel surface, as explained in section 4.1.2.1, (pg. 56).

4.2.7 Frequency Dependent Sensitivity

It has been observed for the pneumatic sensor used in this research that for some frequency ranges or spectra, the signal is consistently amplified. These amplified spectra produce groups of strong frequency peaks that do not shift in frequency when the velocity of the wheel is changed, Fig. 4-41. The signals are taken from a metal bond diamond abrasive wheel with a dressed surface. The top signal is taken at 20 m/s and the bottom signal, shown inverted, is taken at 30 m/s. The fact that groups of signals do not increase in frequency by 50% indicates that the amplification is an attribute of the sensor, and not of the surface. This is not to say that the signal is not related to the surface, as has already been demonstrated, but that the sensor's dynamic sensitivity is frequency dependent.

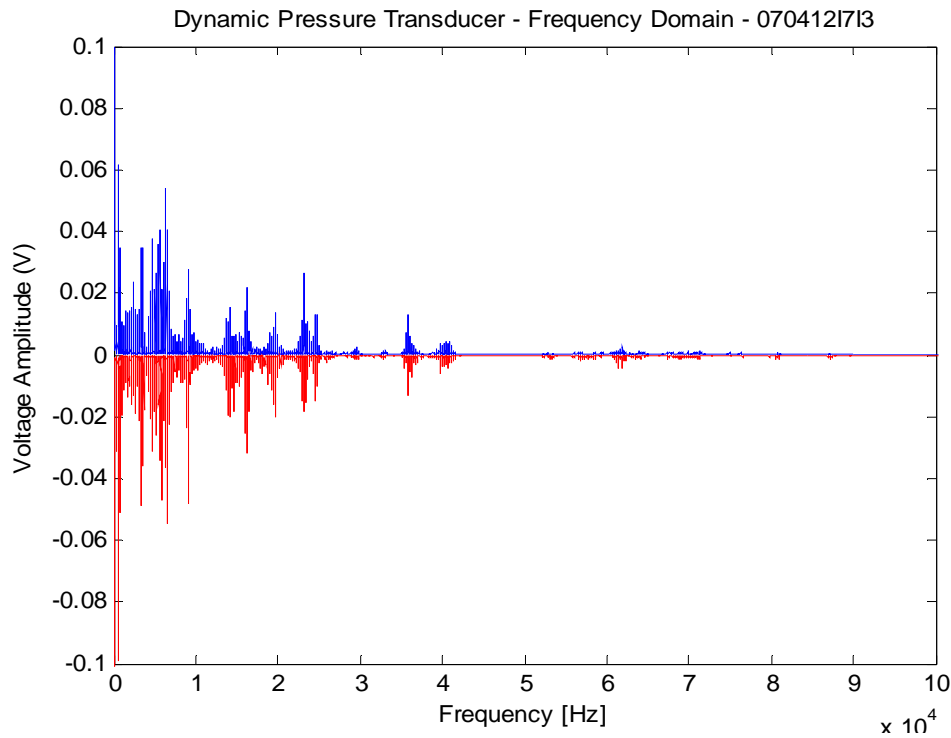


Figure 4-41: Frequency domain signal for 20 and 30 m/s, vitrified wheel.

The frequency dependent sensitivity can be better observed by increasing the surface velocity and focusing on groups of signal peaks within a frequency range. In Fig. 4-42 on the next page, signals from measurements taken from the same wheel at 20, 20.4 and 20.8 m/s are shown in the frequency range of 1500 to 4000 Hz. The frequency range of 3200 to 3600 Hz is amplified, while 1500 to 1900 Hz and 3700 to 4000 Hz are suppressed. With this in mind it becomes easy to track groups of signals as they shift across the frequency range with each 2% increase in surface velocity.

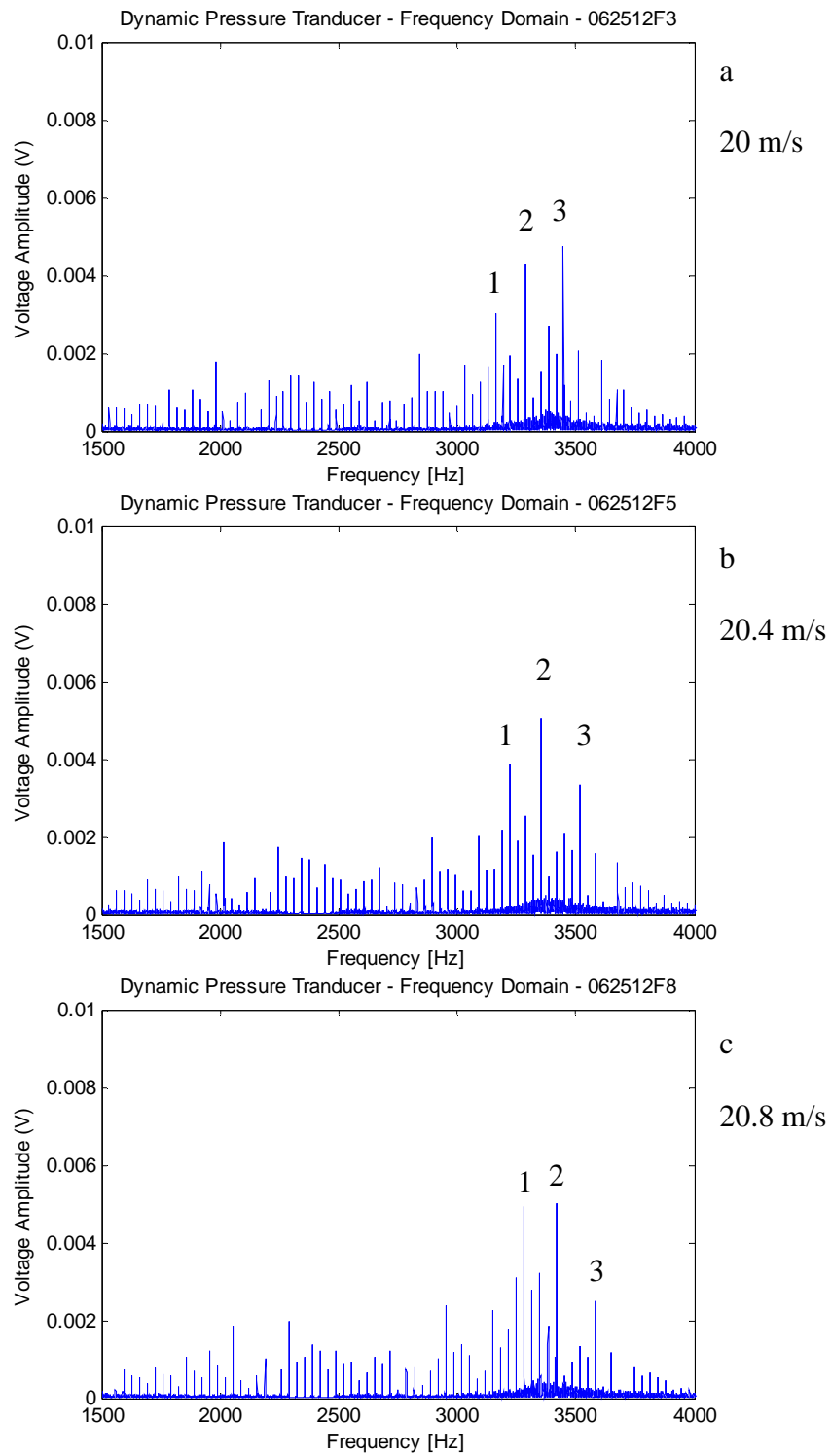


Figure 4-42: Frequency peaks shifting in response to increasing surface velocity

Each increase in velocity of 2% results in a corresponding increase in the frequency of any given peak. By example, three prominent peaks are numbered in each graph in Fig. 4-42. The shifting of peaks on the frequency axis also further demonstrates the ability of the sensor to respond to changes in the surface of the grinding wheel. While more difficult to show, this shifting is also visible at higher frequencies.

It is difficult to assess what effect differing sensitivity across the frequency range of the sensor will have. Frequency dependent sensitivity would be an important consideration if the pneumatic sensor response to changes to the wheel surface were restricted to a specific frequency range. However, as previously shown in Fig. 4-34, the dressing of the diamond abrasive grinding wheel caused an increase in signal amplitude across a broad frequency range.

Further investigation was made with the use of MVA models to determine how the dynamic pressure signal changed with changing surface conditions. An MVA model was created for tests conducted on trued and dressed surfaces for a metal bond diamond abrasive wheel. A PCA model successfully differentiated between the dressed and trued surfaces, as well as measurements taken with no surface velocity, marked 'N' in Fig. 4-43. Using the method of variable pruning described in section 4.1.4, where by variables least associated with any dominant trend are removed from the model, 90% of the frequencies were removed. The top 10% of frequencies remaining are plotted in Fig. 4-44, with the variable importance indicated in the vertical axis.

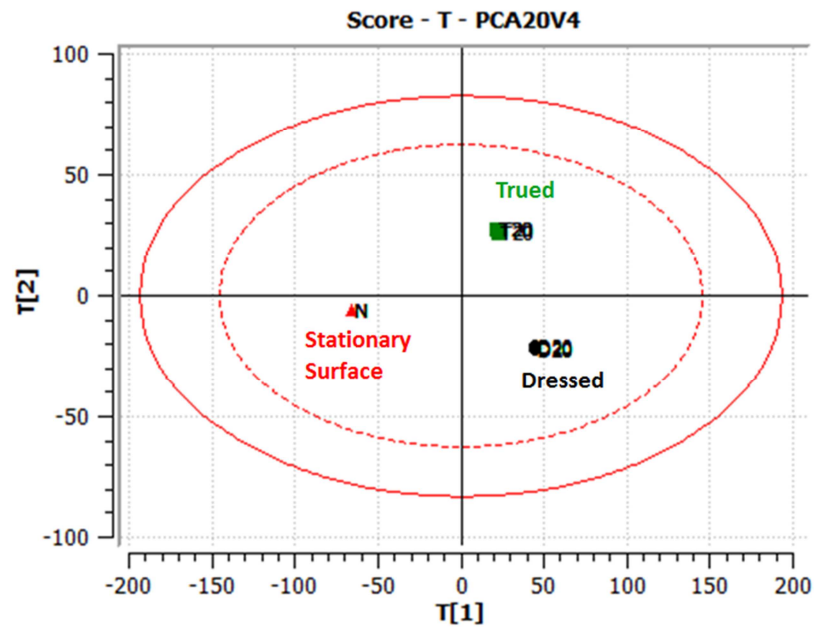


Figure 4-43: PCA score plot of trued and dressed metal bond wheel.

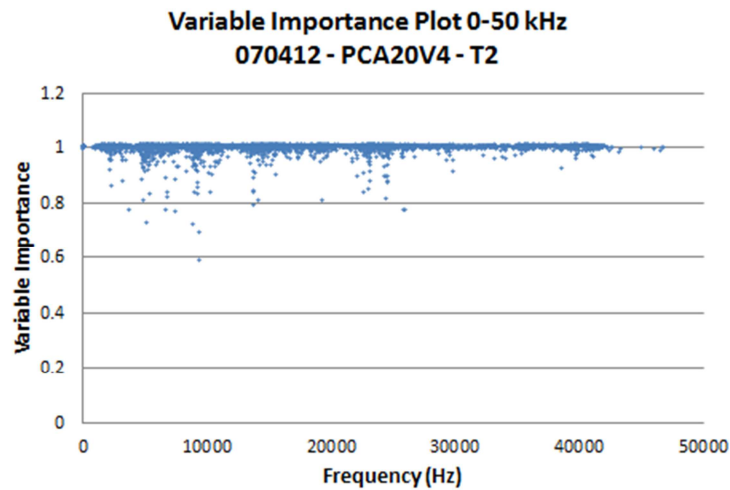


Figure 4-44: Variable importance plot of trued to dressed PCA model.

The variable importance plot is shown for T2, or the score plot axis with most greatly distinguishes the dressed surface from the trued surface. The distribution of important variables from the model indicates that no one frequency

band or range is more strongly related to the change in surface condition than any other. The even distribution is not surprising given the probabilistic spacing of grains the wheel surface can excite many frequencies as it passes under the nozzle.

4.3 Quantifying the Dynamic Pressure Transducer Signal

Root-Mean-Square or RMS is chosen as a method to quantify the signal from the dynamic pressure transducer because it is a simple way to indicate the energy in the dynamic signal. To specifically target smaller wheel features, such as pores and grains, a high pass filter is applied to the raw signal at 1 kHz. The filter is to remove the effects of wheel eccentricity or form errors from the dynamic signal, isolating only the effects of changes to surface roughness.

It is known from the results of sections 4.2.1 through 4.2.4, and specifically Fig. 4-42, that the dynamic pressure transducer signal is dependent on the wheel surface. Additionally, the comparison of a trued and dressed metal bond wheel in Fig. 4-34 (pg. 93) clearly indicates that the individual frequencies that make up the dynamic pressure transducer signal increase on average when the surface roughness increases. Statistical analysis of the dynamic signals generated by changing wheel surface conditions, shown in Fig. 4-44 and in section 4.1.4 supports the conclusion that changes in the wheel surface condition influence individual frequency peaks across the entire high frequency range of the sensor. It is therefore proposed that monitoring changes in the surface roughness of a

grinding wheel can be accomplished by monitoring the overall change in frequency peak amplitudes. In this way a high pass filtered RMS value is a convenient indicator of changing surface roughness.

4.3.1 Use of High Pass RMS

An initial experiment was conducted to explore the use of high pass RMS for monitoring changes to surface roughness. The sensor was applied continuously to the surface of a metal bond diamond abrasive wheel while it was being dressed with a dressing stick. The experiment begins with the wheel surface as trued, which is relatively smooth compared to the dressed surface. The resulting high pass filtered RMS signal is shown with respect to time in Fig. 4-45, clearly indicates that the high pass RMS value increases as the wheel surface is made rougher by the dressing process.

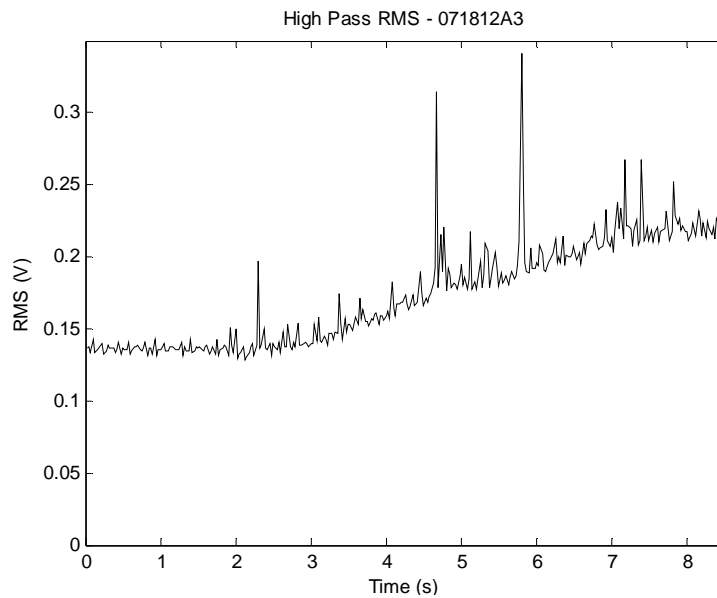


Figure 4-45: Continuous monitoring of dressing of a metal bond grinding wheel.

This experiment was conducted with the sensor position fixed and no compensation was made for the decrease in average back pressure as the surface of the metal bond receded. Despite this decrease in dynamic sensitivity, the pneumatic sensor still clearly detects the increase in surface roughness. It should be noted that the dressing process does not begin until approximately 2 seconds into the recorded sample, and that in this test the dressing process consumed approximately 15 mm of dressing stick.

4.3.2 RMS Repeatability

The repeatability of high pass RMS values was explored experimentally by taking dynamic pressure transducer signals from the surface of a metal bond diamond abrasive grinding wheel. For a given section of the grinding wheel surface the raw signal shows minimal variation. The spectrogram in Fig. 4-46, taken from a metal bond wheel with a dressed surface at 20 m/s at approximately 1900 RPM, shows little variation.

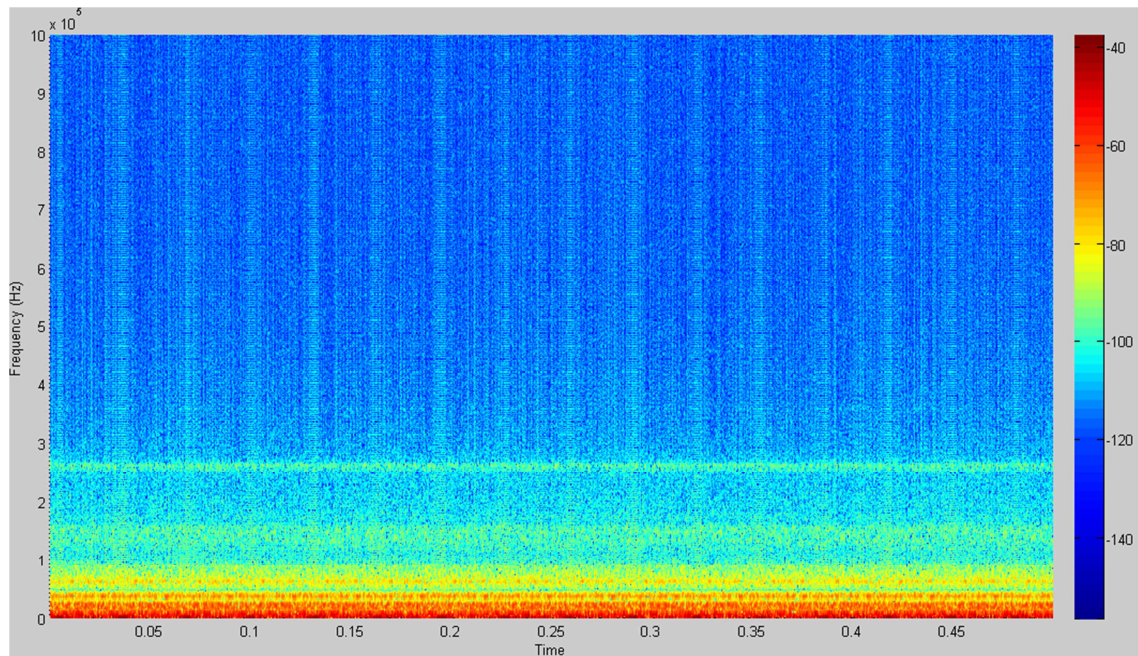


Figure 4-46: Spectrogram of the raw dynamic pressure transducer signal.

For this research the RMS can be calculated after the signal has been filtered and using the entire 0.5 second sample length as the window size. Repeatability of RMS values can be increased if the sample does not include a partial wheel rotation. However, with proper truing and dressing this effect is minimal, and for this research a consistent sample length was employed.

Demonstrating the repeatability of measurements, signals were collected five times from the same axial location, SOD and wheel surface condition, in order to assess the variation from one sample to the next. The experiment was conducted for three different axial locations, and for trued and dressed surface conditions and for surface velocities of 20 and 30 m/s, for a total of 60 collected signals. Surface velocities of 20 and 30 m/s, each half second signal collected

measured approximately 15.7 and 23.6 revolutions of the grinding wheel respectively. No triggering was used to determine when to initiate the signal collection.

The experiment shows that the variability in the measured values was negligible when compared to the average measurement value. Average High pass RMS values are shown in Fig. 4-47 for each measurement location. Values varied most greatly by surface condition, ranging from 144 to 201 mV, then by axial location and finally surface velocity. For any single combination of the wheel condition, position and surface velocity, the standard deviation of the high pass RMS was no more than 0.2% of the measured value. The maximum deviation from the average value for any one set of high pass RMS measurements was about 0.3% of the measured value. The influence of velocity on repeatability was minimal, although measurement taken at 20 m/s did show a slight improvement over those taken at 30 m/s.

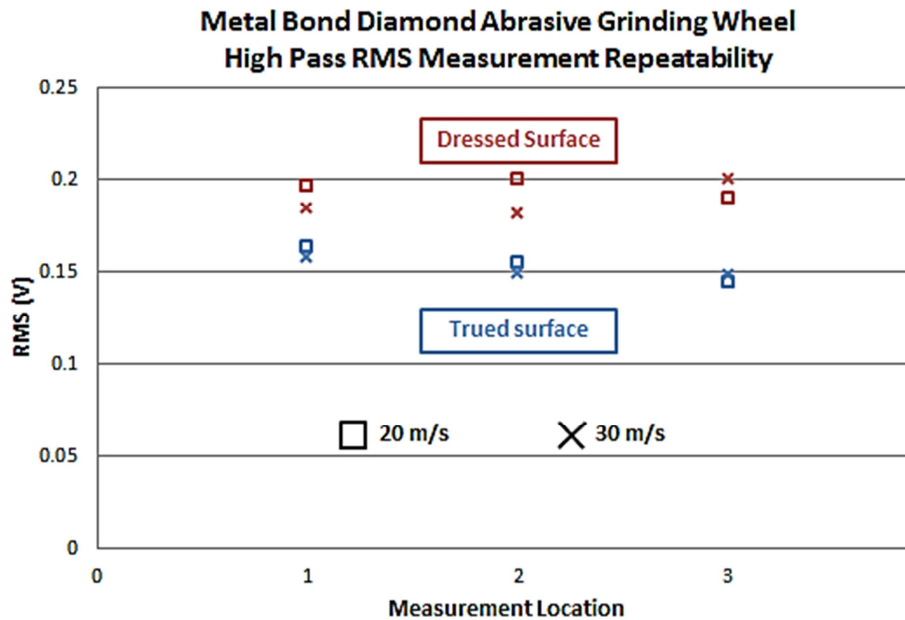


Figure 4-47: Axial variation of high pass RMS values.

The variation in high pass RMS from one axial location to another demonstrates that the high pass RMS value is dependent on what section of the wheel surface is being examined, even though the entire surface is at approximately uniform condition. This variation in high pass RMS by axial location was accompanied by small variations in average back pressure.

4.3.3 Setting the Back Pressure Range

In establishing a practical method to apply a pneumatic sensor to monitoring the condition of a grinding wheel, a range of SOD values must be established for each grinding wheel and sensor setup so that meaningful measurements may be taken. In this research grinding wheels with very different

constructions were measured by the sensor though different nozzle and control orifice diameters, each suited to produce the strongest dynamic pressure signal for that grinding wheel. As already discussed in 4.2.6 there is an SOD value for each case where the high pass RMS no longer responds to a change in SOD, and therefore is no longer responding to the wheel surface. The maximum SOD for meaningful measurements is approximately 50 μm and 200 μm for the metal bond and vitrified grinding wheels respectively. For this research maximum SOD values, set from the initial wheel surface, were 30 μm and 150 μm respectively. However, typically distance is indirectly measured, and calculated from the directly measured average back pressure, P_b . For this reason high pass RMS values should be compared by average back pressure, which is also a superior indication of the sensor's condition and dynamic response. The back pressure range of the sensor was measured in a similar manner to the maximum SOD, and is shown in Fig. 4-48. It should be noted that the average back pressure is reported in volts, and nominally converts to pressure at 68.9 kPa/V.

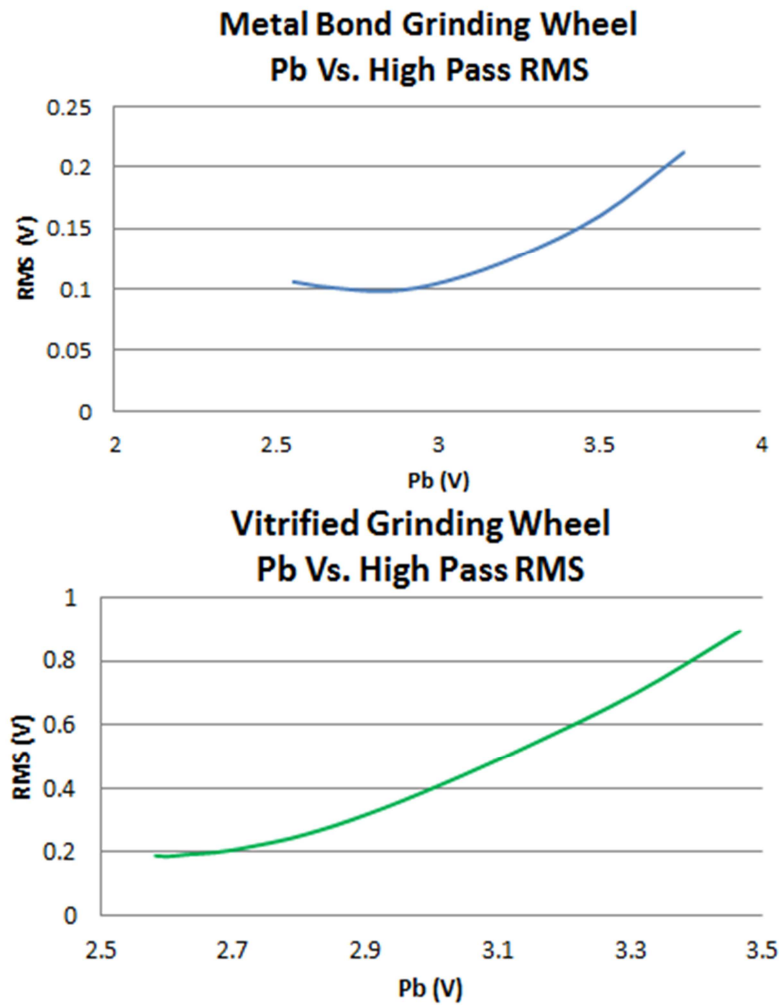


Figure 4-48: Finding the average back pressure range.

4.3.4 Principle of Dual Transducer Monitoring

Changes to the surface condition of a grinding wheel present new challenges for maintaining sensitivity. When examining the surface of a grinding wheel, the surface roughness, porosity, and distance between the surface of the wheel and nozzle determine the average back pressure. It is also established that a

decrease in the average back pressure would decrease the dynamic and static sensitivity of the sensor.

Changes to the porosity of the surface of a grinding wheel result in changes to the average back pressure, although the outer diameter of the wheel may not change significantly. The increase in surface porosity will increase the escape area and the average back pressure will decrease. With the average surface further from the nozzle and the average back pressure reduced, the dynamic performance of the sensor is compromised, and measurement conditions are no longer consistent. The ability to maintain dynamic sensitivity in such a case by decreasing the stand-off distance is limited by the wheel surface, which will abrade the nozzle, and by the resolution of the sensor positioning system. Similarly dressing metal bond wheels causes the majority of the surface area to recede while the protruding grains remain at the same height, making compensation of the average back pressure impossible. As a result, a new method is needed to accommodate changes in the grinding wheel surface and provide comparable measurements.

A new measurement method was devised, in which the nozzle is positioned at multiple axial locations and multiple SOD values. For each position the average back pressure and dynamic signal are recorded. The resulting measurements for a given surface condition provide a range of average back pressures, with corresponding dynamic pressure signals. With multiple axial measurement locations for each surface condition, values of the average back pressure and

dynamic high pass RMS can be average for each stand-off distance, and graphed as shown in Fig. 4-49, as a Pb-RMS curve. The initial wheel surface is taken as reference for all SOD values, and is held as a constant as the surface condition changes and recedes. This is illustrated in Fig. 3-12, (pg. 51).

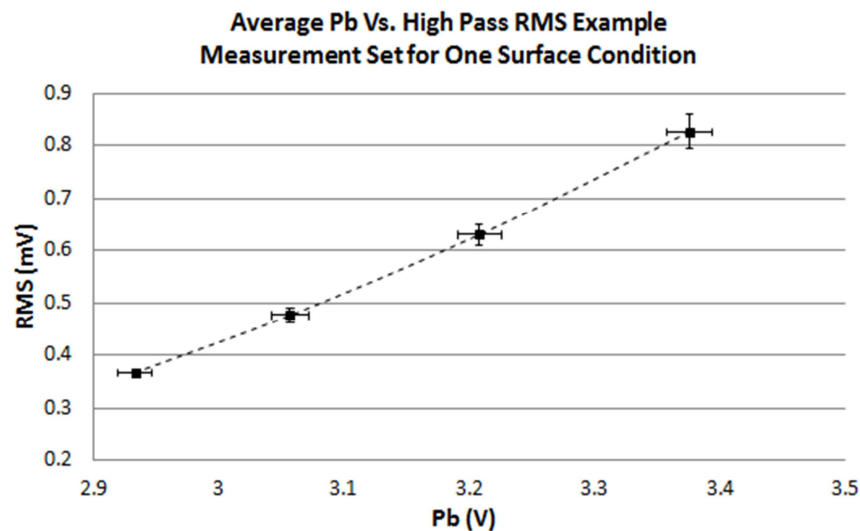


Figure 4-49: Plotting of gauge and dynamic measurements, Pb-RMS curve.

In addition to providing comparable dynamic sensitivity, this method can provide an indication of the recession of the wheel surface during wheel wear or dressing. Previous research has shown that changes in surface roughness have only a minimal influence on the average back pressure [10], while the effect of gap size is consistent at the grinding wheel speeds tested. In a simple test the pneumatic sensor was applied to the surface of the metal bond grinding wheel for both trued and dressed surface conditions, using the trued surface as reference the nozzle positions. Measurements of the average back pressure taken at multiple stand-off distances are plotted in Fig. 4-50 for trued and dressed surfaces. With

the reference point for all nozzle positions fixed, the dressed surface generates a lower average back pressure, due to the wheel surface receding during dressing. Aligning the dressed measurements to those from the trued surface highlights this recession, as the distance to the wheel surface is the only difference.

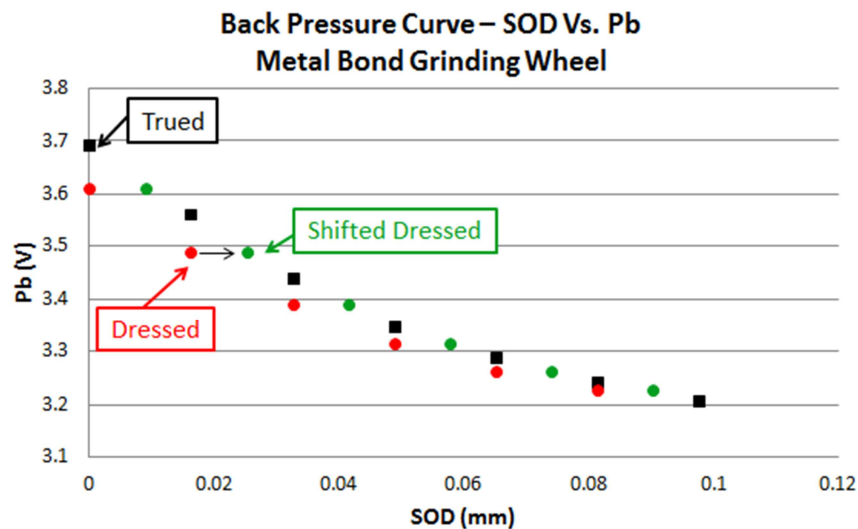


Figure 4-50: Trued and dressed back pressure curves.

4.4 Dressing

Applying the pneumatic sensor to monitor the dressing process provides an opportunity to investigate the response of the sensor to wheel surfaces that change in a known manner, as well as develop a useful application. In the case of the metal bond diamond abrasive wheel the dressing process begins with a trued surface, which is incrementally dressed with an abrasive stick to better expose the sharp abrasive grains. The ability of the sensor to respond to the increments in

grain protrusion from the wheel surface demonstrates that the sensor is capable of responding to small changes in geometry.

When dressing a vitrified grinding wheel the roughness of the wheel surface, often referred to as openness or aggressiveness of the wheel surface, is influenced by the cross feed rate of the dressing tool. Using higher cross feed rates for dressing creates a more open wheel surface, which is coarser and suited to aggressive cutting and high material removal rates. A low cross feed rate results in a more closed wheel surface for fine surface finishes on workpieces. The pneumatic sensor is applied here to differentiate between grinding wheel surfaces dressed with different cross feed rates.

4.4.1 Metal Bond Wheel

The dressing of the metal bond diamond abrasive wheel allows the abrasive grains at the surface to protrude cleanly from the surface and creating room for chips by wearing away some of the metal bond material. It is useful to monitor this process because it is possible to under or over expose the diamond grains. Under exposure occurs when the abrading of the bond layer is stopped too soon, either by using too fine a dressing stick or prematurely ending the dressing operation. Typically over exposure is much more common and occurs when optimally exposed grains are unable to prevent further abrasion of the bond layer. In such a case continued dressing is wasteful and functionally becomes a truing operation.

To investigate the response of the sensor to the changing surface conditions for dressing the metal bonded diamond abrasive wheel, the grinding wheel was spun to a surface velocity of 20 m/s trued and then dressed incrementally with a dressing stick. The dressing stick was fed into the wheel surface at a rate of 100 mm/min. Measurements of the surface were taken with the sensor for the trued surface and after feeding 1, 2, and 4 cm of dressing stick into the wheel surface. For each surface condition the sensor was applied to 6 different axial locations, and at 3 distances from the original wheel surface. For a given surface condition the average measurements from each of the three distances are used to form a curve. Fig. 4-51 shows the average back pressure versus the high pass RMS values for each of the four surface conditions, which are labeled as trued or by the length of dressing stick consumed by the process. The curves, referred to in this research as Pb-RMS curves, are shown with standard deviation at each distance

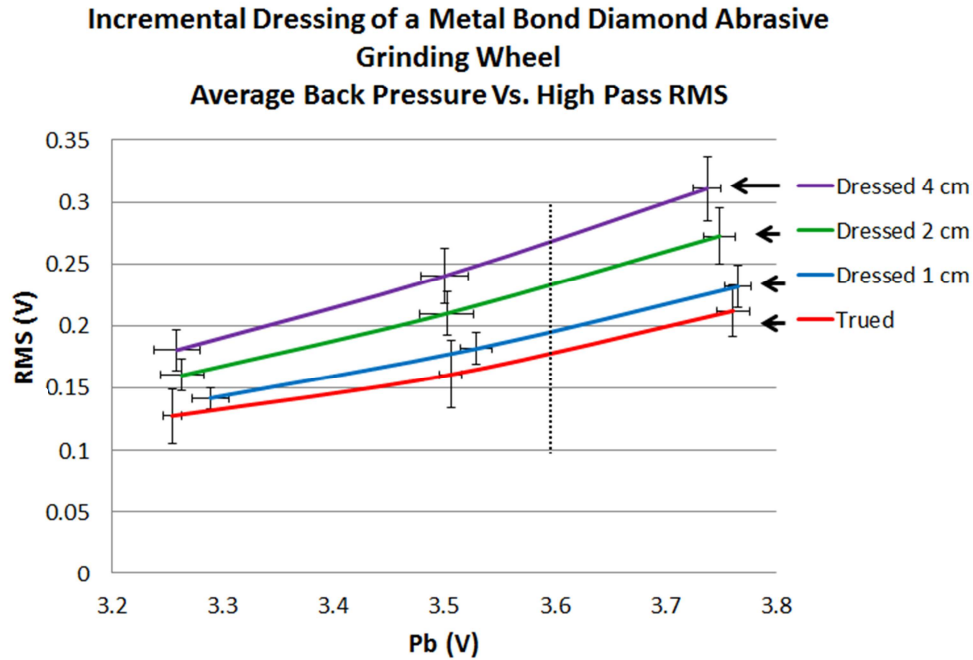


Figure 4-51: Pb-RMS curve for incremental dressing of a metal bond grinding wheel.

In this application the relative change in surface roughness may be monitored by observing the increase in the high pass RMS value. Using a constant value for the average back pressure a fair comparison of the high pass RMS can be made. For example, in Fig. 4-51 a vertical dotted line intersects each Pb-RMS curve, yielding interpolated values of high pass RMS for each surface condition at a constant average back pressure, and thus at equal sensitivity. In this test the response of the pneumatic sensor shows a significant increase in high pass RMS. The incremental dressing creates an increasingly rougher wheel surface, which is reflected in the resulting measurements of high pass RMS. This response relates well to the exposure of gains and abrading of the bond layer.

Visible on Fig. 4-51, the average Pb value increases initially for the first dressing increment. Because it is a dressing operation it is only possible for the wheel surface to recede as it becomes rougher. It cannot gain material. It is likely that this is due to the change in surface roughness. Observations of air flow restriction made by Wager [10], for much higher surface speeds, near 70 m/s, showed that the degree of air flow restriction was enhanced by increasing surface roughness and speed, and by increasingly smaller nozzles. In the monitoring of the metal bond diamond abrasive wheel a small, 0.603 mm nozzle is used, and a significant increase in surface roughness is indicated by the increase in high pass RMS.

In application to the monitoring of wheel dressing, the pneumatic sensor is still able to respond to the dressing process and show a clear and significant increase in high pass RMS in response to the increase in surface roughness. By monitoring the surface it may be possible to determine if the dressing process has reach an equilibrium and grain exposure has halted abrasion of the bond surface, or if the dressing process is too aggressive and is over exposing grains. In the case of equilibrium it would be expected that the PB RMS curve would remain unchanged with further dressing, while over dressing would see measurement points sliding down the curve, indicating that the surface is receding but not getting any rougher.

4.4.1.1 Relative Change in High Pass RMS

For the example shown in Fig. 4-51, interpolated high pass RMS values were taken for a constant value of average back pressure, but no instruction was given on how to select that constant value. It is worth investigating if the choice of average back pressure value has any influence on the interpolated results.

Using Fig. 4-51 as an example, high pass RMS values can be interpolated for multiple average back pressures. Fig. 4-52 shows this for four back pressure values, and plots the interpolated high pass RMS as a function of the length of dressing stick consumed. The values on each curve are also colour coded to match the wheel conditions shown in Fig. 4-51.

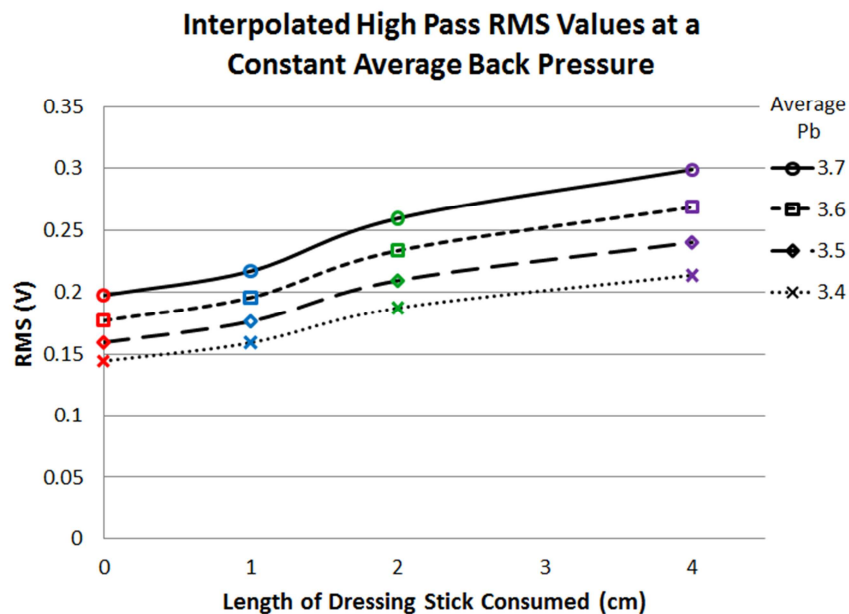


Figure 4-52: Interpolating High Pass RMS at multiple Pb values

Obviously the high pass RMS values are different for each constant back pressure. However, examining the relative change in high pass RMS it can be shown that any constant back pressure can be used, Fig. 4-53

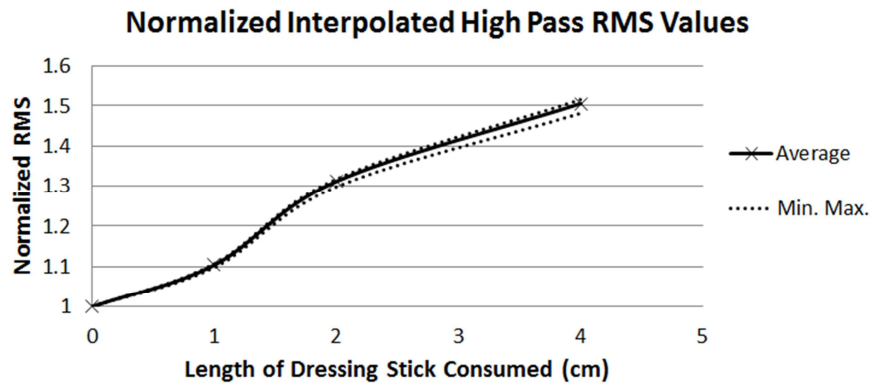


Figure 4-53: High Pass RMS Normalized by initial surface value.

As can be seen, any average back pressure may be selected for use in interpolating high pass RMS values, with little influence on the relative change in those values. The only constraint is that an interpolated value exists for all surface conditions.

It should be noted that the use of a constant back pressure value in this current method is a considerable improvement over the method proposed by Maksoud *et al.* [23], which reported only high frequency RMS values as an indication of surface roughness. The fault in the results is that the method made no account for the influence of stand-off distance or average back pressure on those RMS values.

4.4.2 Vitrified Wheel Dressing

Dressing a vitrified grinding wheel produces sharp, free cutting grains by opening up the wheel surface and by fracturing or removing worn grains. The cross feed rate of the dressing tool can be used to change the openness of the vitrified grinding wheel surface, and is typically varied between 50% to 100% of the grain size per revolution. Monitoring the dressing of a vitrified grinding wheel is challenging because the dressing process for a finely or coarsely dressed wheel only affects the fracture or removal of grains at the outer most wheel surface. Comparing to dressed surfaces means comparing two rough surfaces with the same underlying structure, composed of the same grains and with the volume of pores and bonding material.

To investigate the response of the sensor to changes in wheel surface roughness, the sensor was applied to contrasting wheel dressings. The grinding wheel was divided into two halves, each prepared with a different cross feed rate. The pneumatic sensor was configured according to table 3-4 (pg. 50), and used to take measurements at three stand-off distances and at multiple axial locations. The cross feed rates were then applied to the opposite halves, and the experiment repeated. Dividing of the wheel surface is illustrated in Fig. 4-54 on the next page. The grinding wheel was tested in this way for coarse, moderate and fine dressings, corresponding to cross feed rates of 0.255, 0.191 and 0.127 mm/rev. Dressing and monitoring was conducted with a surface velocity of 20 m/s.

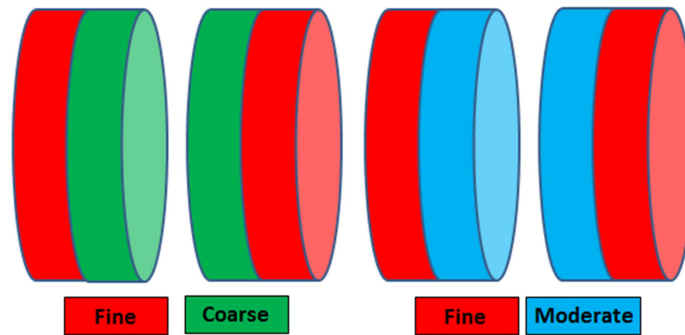


Figure 4-54: Differential dressing of a vitrified grinding wheel.

The results of this dressing experiment show that the sensor can distinguish between the more closed surface of a fine dressed wheel and the open surfaces of a moderate and coarsely dressed wheels, Fig. 4-55. The dotted and solid curves on the graph are results of measurements that were taken together as halves of the grinding wheel.

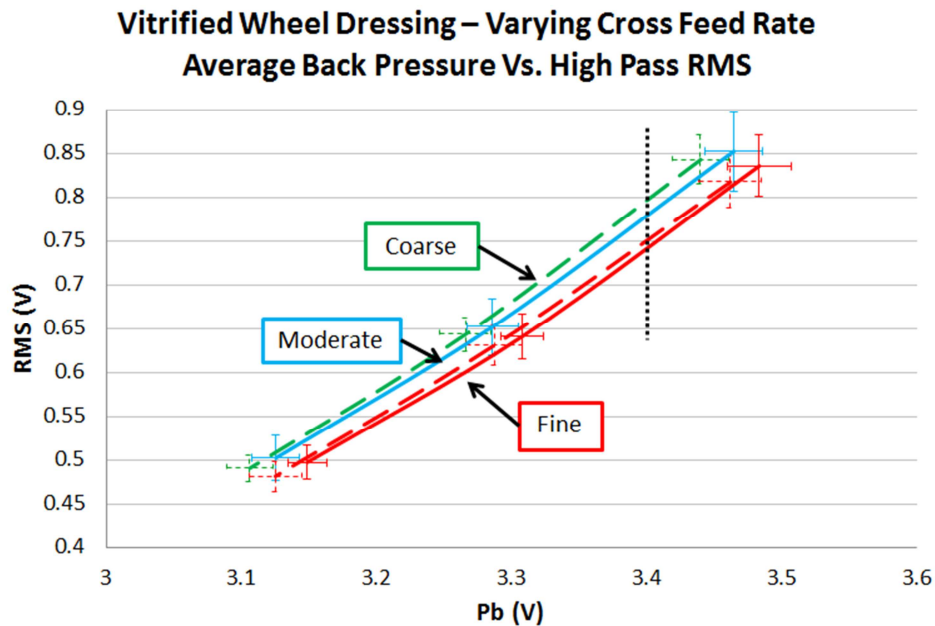


Figure 4-55: Pb-RMS curve for differential dressing of a vitrified wheel.

Fig. 4-55 is formed in the same way as Fig. 4-51, and each curve represents 48 measurements, taken at 3 stand-off distances (5, 41, and 76 μm). There are 16 axial locations taken per stand-off distance and the error bars represent the standard deviation for each stand-off distance.

As with Fig. 4-51, values of high pass RMS should be compared for a constant average back pressure value. The high pass RMS is then used to indicate how energetic the dynamic signal is, and is indicative of the surface roughness for each dressing condition. In Fig. 4-55 the high pass RMS increases with increasing dressing cross feed rate. This is logical, as higher cross feed rates produce a rougher and more open wheel surface. As covered in section 2.2.1 (pg. 19), research into the topography of the vitrified grinding wheel surface after dressing by Davis [17] showed that finer dressing parameters can leave the wheel surface in a semi-glazed condition. A finer dressing operation can leave bond material and partial grains blocking or reducing the size of pores at the wheel surface. Coarser dressing parameters produce higher forces and high degree of fracture of grain and bond material to leave the wheel surface more open, with greater exposure of both grain edges and pores.

Further information about the change in wheel surface condition can be gained by examining the change in the average back pressure. Operating the pneumatic sensor in the traditional sense as a displacement sensor, a change in average back pressure can be used to indicate a difference in the effective stand-off distance. Fig. 4-56 shows with black lines the average back pressure for each

surface condition, and clearly shows that for each case from Fig. 4-54, the moderate and coarse dressing results in a lower average back pressure when compare to the fine dressing. With the same stand-off distance of $5\text{ }\mu\text{m}$ used for each surface condition, the change in average back pressure can only be caused by differences in the porosity of the wheel surface for each condition

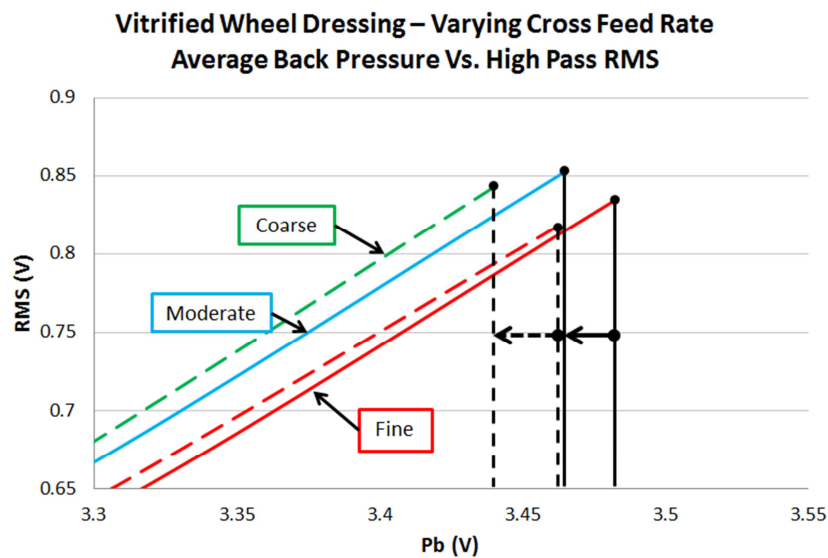


Figure 4-56: Changing average back pressure with dressing.

In this relatively simple experiment both high pass RMS and the change in average back pressure can be connected to the expected change in surface condition imposed on the grinding wheel by the varying dressing operation. The results of the vitrified wheel dressing experiment also shows that the response of the sensor is not a linear relationship to the cross feed rate, and is more sensitive in changes at lower cross feed rates.

4.5 Wear

To investigate the response of the sensor to wear of the grinding wheel surface the sensor was applied to the surfaces of the metal bond and vitrified bond grinding wheels. Experiments were created for each wheel to accelerate the rate of wear, which was monitored by the pneumatic sensor by taking samples of the dynamic pressure transducer signal and average back pressure at multiple axial locations and at multiple stand-off-distances from the original surface. Unlike the dressing experiments in which the change to the wheel surface condition was known qualitatively, to understand the response of the sensor to the wear, the worn wheel surface was examined separately using a digital microscope.

4.5.1 Metal Bond Wheel

Wear of the diamond abrasive grains in the metal bond grinding wheel occurs by the mechanisms of both mechanical and chemical wear, resulting in the development of wear flats on grains at the outer most surface, higher forces and eventual grain loss [22]. Grain loss is also brought on by the deterioration of the bonding material ahead of each grain by chips generated during grinding [17]. To test the response of the sensor to the wearing of this wheel an experiment was set up to accelerate the wheel wear, with the objective of observing the response of the sensor.

For the experiment a piece of tool steel was used for the workpiece. A steel workpiece will accelerate the dissolution of carbon from the abrasive

diamond grains, as well as creating high cutting forces and erosion of the bond material. The experiment begins with a dressed wheel that is incrementally worn by three sets of fifteen grinding passes over the workpiece. The surface is measured by the sensor in the same method used for the dressing experiments, with the sensor configuration listed in table 3-4 (pg. 50). Using the initial dressed wheel surface, 3 stand-off distances are set, and measurements are taken at 6 axial locations per stand-off distance. Measurements were taken for the dressed surface, as the initial surface condition, as well as after each wear set. The experiment was stopped after the third wear set showed a significant decrease in average back pressure.

The results of the measurements are shown in Fig 4-54. Analysis of the results follows in the same manner used to detect differences in vitrified wheel dressing, in section 4.4.2. The change in high pass RMS can be evaluated for any constant value of average back pressure, with the condition that a value can be interpolated for each surface condition. This boundary is indicated by the vertical black dotted lines on Fig. 4-54. Evaluation of the change in high pass RMS clearly shows an increase as the wheel surface condition progresses from initial dressed state and is incrementally worn.

Table 4-1: Grinding parameters for metal bond grinding wheel wear.

Wheel Surface Speed (RPM)	Table Feed	Depth of Cut	Workpiece length
20 m/s (1894)	1 m/min	10 μ m	95 mm

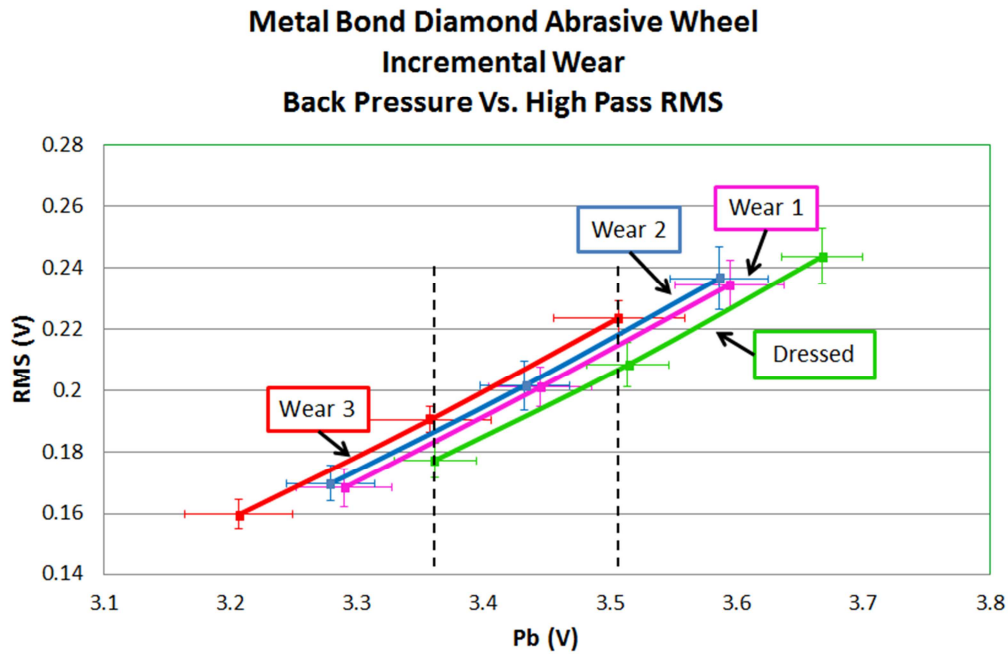


Figure 4-57: Pb-RMS curve for the incremental wear of the metal bond grinding wheel.

A change in the average back pressure can be observed in Fig. 4-57, comparing the four surface conditions for one stand-off distance value. Measurements taken at a stand-off distance of 5 μm , set in reference to the initial dressed surface, show a general trend of decreasing average back pressure as the wheel surface is progressively worn. This trend is shown clearly in Fig. 4-58, and indicates the effective stand-off distance is increasing and that the average wheel surface was receding from the nozzle.

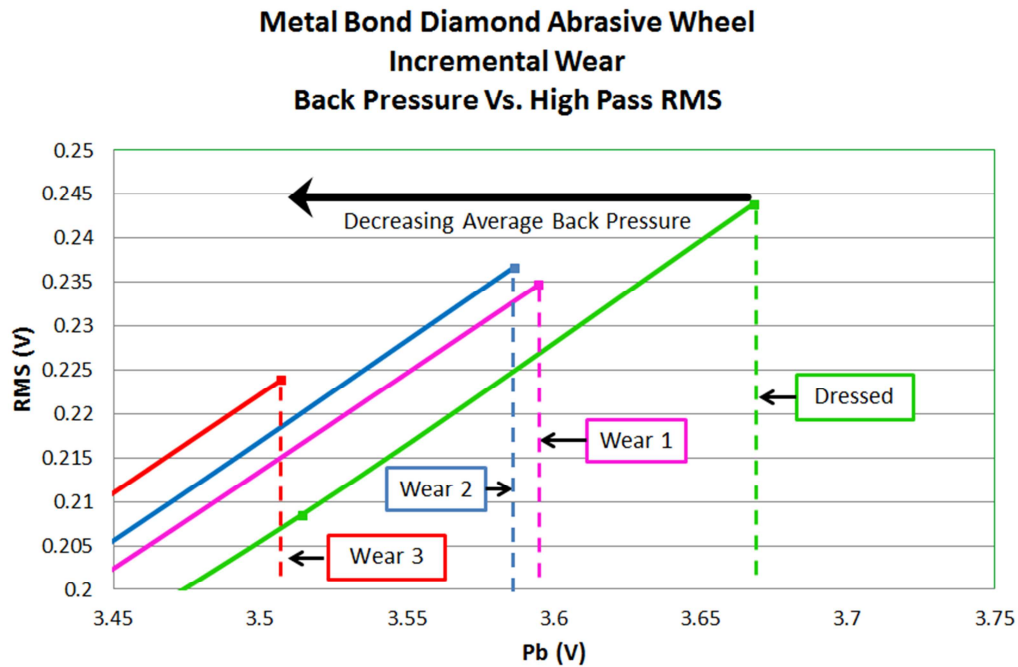


Figure 4-58: Changing average Pb with wear.

Results from the RMS-Pb curves indicate that as the surface of the grinding wheel was worn the average surface retracted from the sensor nozzle tip and became slightly rougher. These results do not appear logical at first, because it is expected that wheel wear would cause grinding wheel surface would be worn smooth by the development of wear flats on the abrasive grains. However, wheel wear can also result in grain loss and abrasion of bond material, which can create features in the wheel surface. A closer look at the worn grinding wheel surface can provide insight to the change in surface condition.

Examining the worn surface of the grinding wheel by digital microscope shows that wheel wear has caused grain loss from the wheel surface, leaving pores, Fig. 4-59. The extent of grain loss may be compared to the edge of the

wheel on the left hand side, which was not engaged in grinding. Some of these pores are also very near in size to the nominal grain size of 170-grit, which suggests that at least some of the grains pulled from the surface were protruding by half a grain diameter or less.

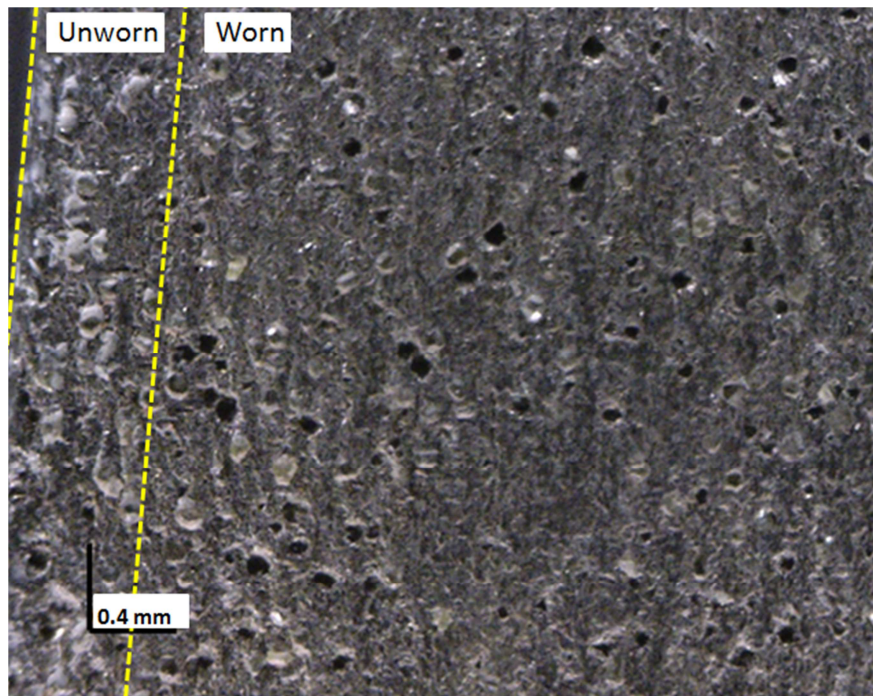


Figure 4-59: Photograph of the worn grinding wheel surface.

Elsewhere on the wheel surface it is possible to see more prominent effects of bond erosion producing larger surface features and evidence of loose pulled grains scraping along the surface of the grinding wheel. In Fig. 4-60 the recent loss of one grain appears to have caused the loss of a second. In Fig. 4-61, the abrasion of the wheel surface by debris has created a substantial feature.

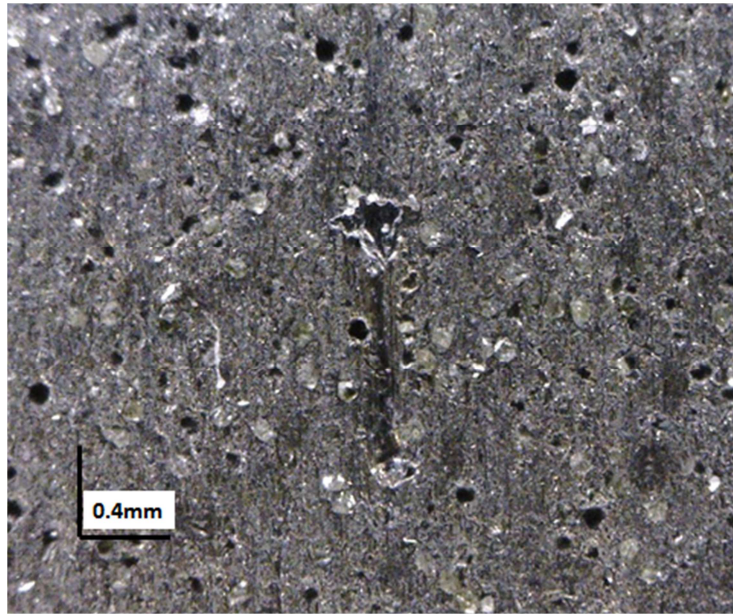


Figure 4-60: Pulled grains produce a new, large feature.

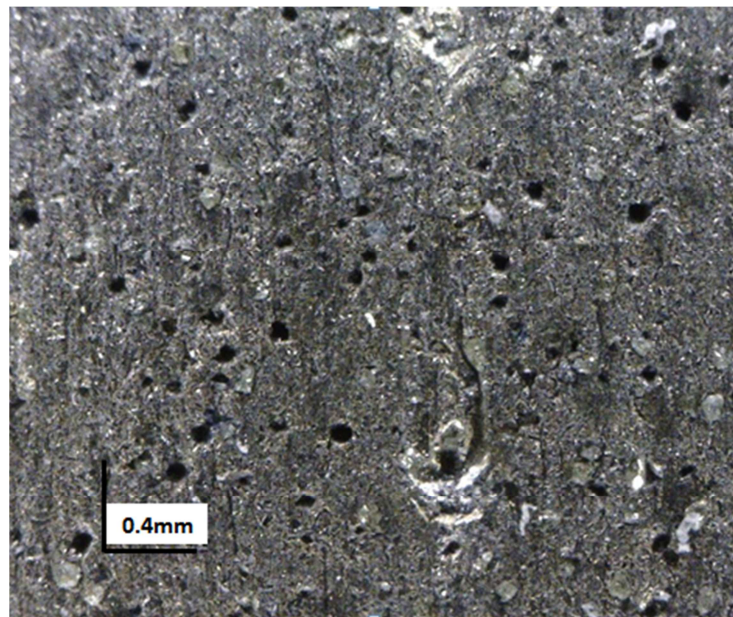


Figure 4-61: Abrasion of bond material by chips.

The loss of a great many diamond grits is confirmed by photographs of the workpiece surface Fig. 4-62, where many diamond grits of varying size can be. There is also evidence of the pull out of large grains, as the one seen to the right of center, and further contact of that grain with other grains in the wheel surface, as is evident from the trail of small diamond particles.

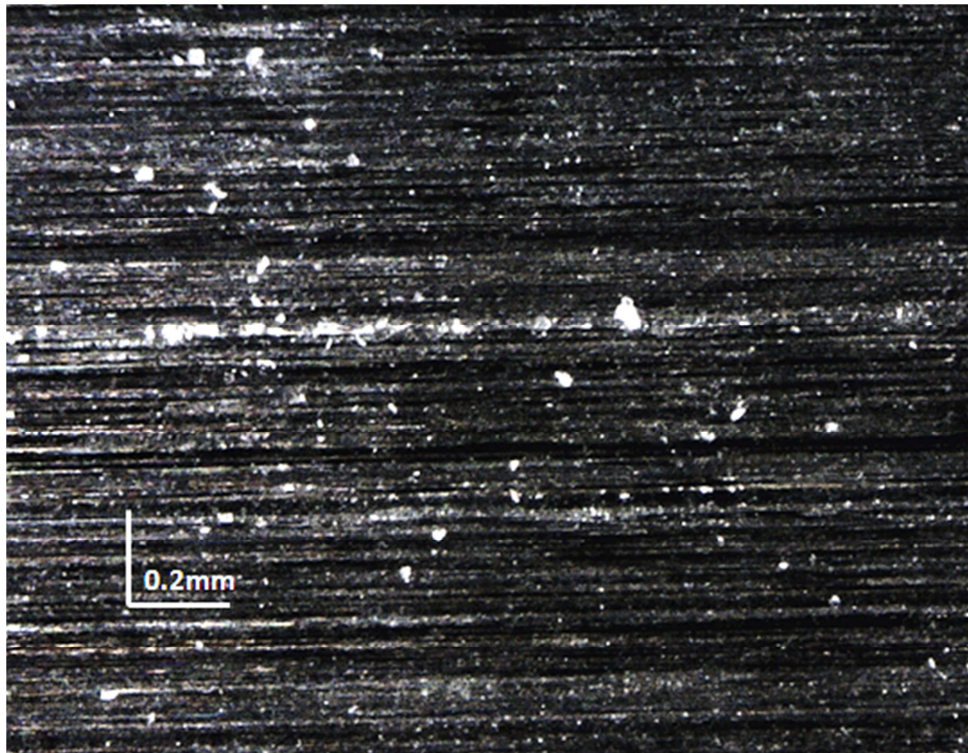


Figure 4-62: Ground workpiece surface after completion of the third set of grinding passes.

Upon examining the surfaces of both the grinding wheel and workpiece surface, the response of the pneumatic sensor follows logically for the grain loss and abrasion of the bond layer surface. The decrease in average back pressure and increase in high pass RMS are the result of an increase in the effective SOD, and an increase in surface roughness.

4.5.2 Vitrified Wheel

As detailed in section 2.2.1 (pg. 22), a vitrified grinding wheel may wear microscopically by attrition of the abrasive grains resulting in wear flats, grain loss or may wear by loading of the wheel surface. In some cases the continued wear can lead to some self-sharpening effects by increasing cutting and normal forces and fracturing the peripheral grains to create new edges, or by bond fracture causing grain loss, exposing new sharp grains and renewing the wheel surface. In cases where the wheel surface is not cleared of dull grains and debris the excessive wear can result in thermal damage to the workpiece, or grinding burn that can ruin a workpiece.

The experimental investigation into the response of the sensor to the changing surface condition of a vitrified grinding wheel undergoing wear was done in two parts. In the first experiment discussed below the wheel was worn until the workpiece shown signs of grinding burn. This experiment allows a comparison of the dressed surface section to a section worn by grinding burn, and no longer suitable for use. The second experiment applies more sustainable grinding parameters and the pneumatic sensor is applied periodically as the wear to the grinding wheel surface develops. The objective of this second experiment is to investigate the response of the sensor as the wear slowly develops wear flats, loads and fractures.

4.5.2.1 Grinding Burn

The high degree of wheel wear inherent to the grinding burn provides an example surface condition where the wheel has reached a point of failure. For investigating the response of the pneumatic sensor to a grinding wheel surface worn by grinding burn, the wear was allowed to progress only to the point where slight discoloration was visible on the workpiece surface. The grinding parameters for this experiment are given in table 4-2. The workpiece material was tool steel, and was ground to a total depth of 0.1 mm, when the workpiece became discoloured from grinding burn.

Table 4-2: Grinding parameters for vitrified wheel grinding burn.

Wheel Surface Speed (RPM)	Table Feed	Depth of Cut	Workpiece length
20 m/s (1338)	10 m/min	25 μ m	95 mm

With the grinding wheel width at 38.1 mm and the workpiece width at 12.7 mm, the workpiece was ground using only the center with of the grinding wheel. The resulting sections of dressed and worn wheel surfaces are shown in Fig 4-63, with a dressed wheel surface on each side of the worn area.

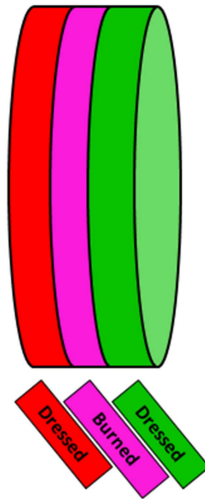


Figure 4-63: Grinding wheel section worn by grinding burn.

Measurements were taken at 3 stand-off distances, set in reference to the initial dressed surface at 5, 41 and 76 μm . For each stand-off distance measurements were made at multiple axial locations. Specifically, five axial locations for each dressed side and 8 axial locations across the burned section for a total of 54 measurements. Initially measurements were only made of the worn wheel section and the first dressed section, shown in red. Measurements of the dressed wheel surface shown in green were taken at stand-off distances of 20, 56, and 91 μm , and align well with the results of the first set of dressed surface measurements. This second set of dressed surface measurements were taken after comparison of initial dressed and burned wheel surface measurement resulting showed a significant increase in high pass RMS, Fig. 4-64.

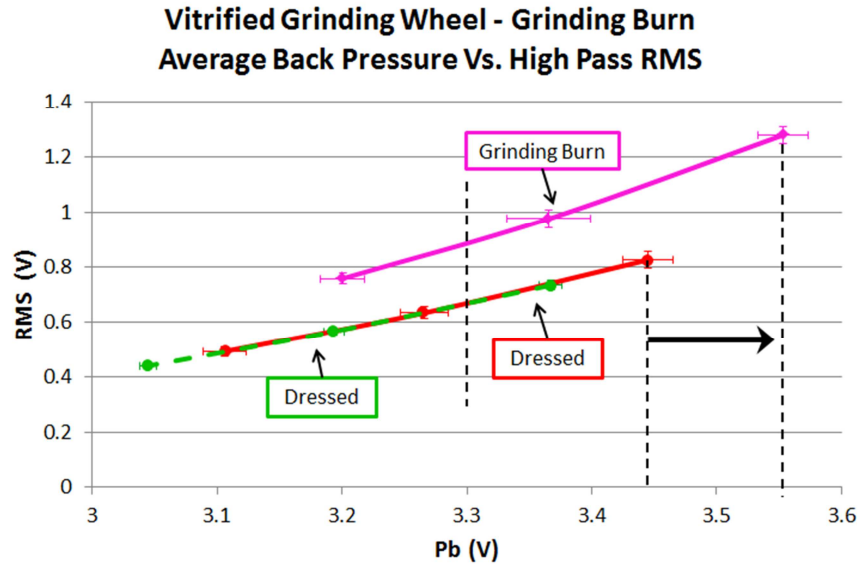


Figure 4-64: Pb-RMS curve of grinding burn by vitrified wheel.

Interpolating values of high pass RMS for each surface condition for a constant average back pressure, the result in Fig. 4-64 is encouraging. Measurements of the high pass RMS from the dynamic pressure transducer signal and the average back pressure are consistently higher for the surface worn by grinding burn than for the dressed surfaces, shown in red and green.

It is of interest to determine the cause of this change in high pass RMS, as wear has resulted in a more energetic signal. Typically wheel wear should result in a more closed wheel surface. In Fig. 4-55, dressing tests showed that the finer, more closed surface of a fine dressed wheel surface produced a lower high pass RMS value than the more open, coarse dressed wheel surface.

Comparing to the dressed surface results the wheel surface worn by grinding burn shows a great increase in average back pressure for the same SOD.

Comparing values for the 5 μm distance, shown on Fig. 4-64 by the black dotted lines on the right hand side, the increase in average back pressure corresponds to decrease in SOD of 19 μm . This is of course not physically possible. Logically the increase in average back pressure means that material must have been added to the wheel surface in the section worn by grinding burn.

Using a digital microscope, Fig. 4-65 shows a magnified view of the wheel surface at the edge between the dressed and worn sections. Immediately it is obvious that debris has been gathered in the worn wheel surface, and has done so in non-uniform manner. A closer inspection of the surface shows the buildup of chips occurs around only the outer most grains, blocking the small gaps between them and other grains nearby while larger pores are left open.

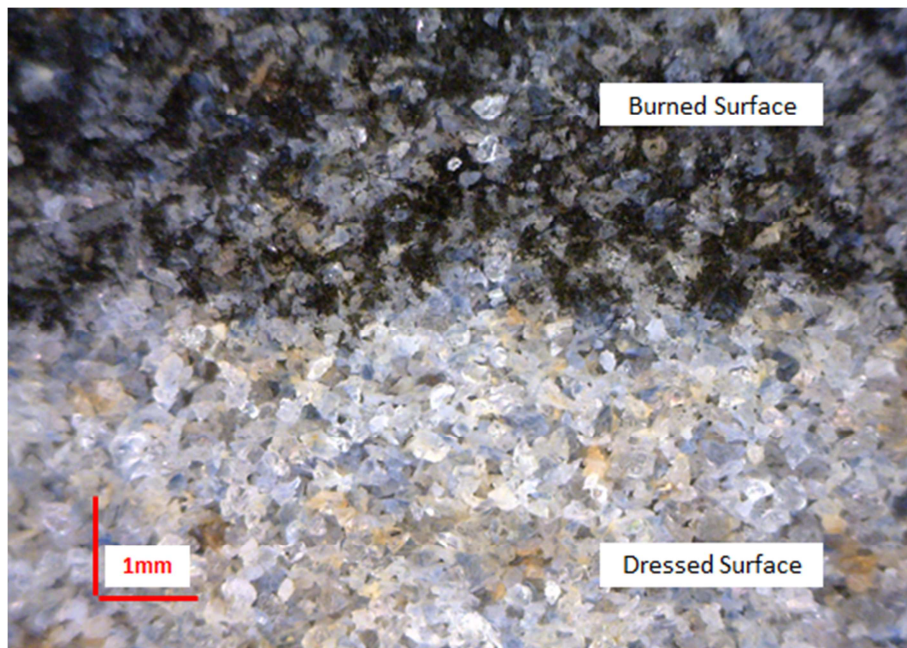


Figure 4-65: The grinding wheel surface as dressed and as worn with grinding burn.

Figure 4-66 shows the uneven collection of chips and debris in the wheel surface. The chips appear to collect around grains clusters, while the larger pores remain open. Some grains with wear flats are also visible and are surrounded by debris.

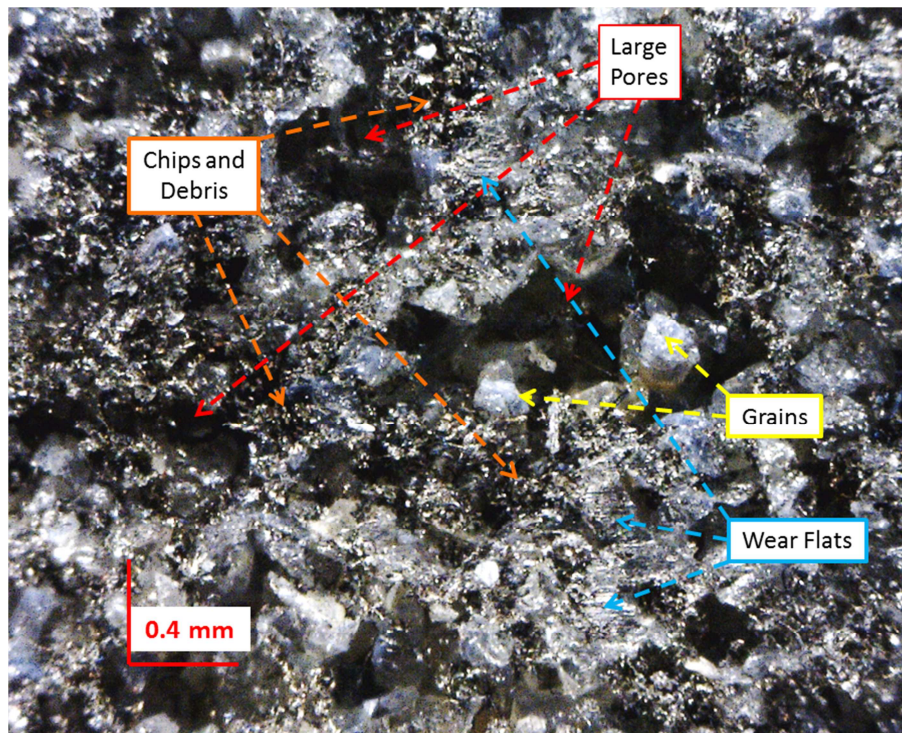


Figure 4-66: Wear flats and loading of the vitrified wheel by grinding burn.

Ultimately the increased values for the high pass RMS and average back pressure for the worn wheel surface is likely due to the buildup of chips in the wheel surface occurring only in areas around the outer most grains. The buildup makes those areas less permeable to air flow, while larger pores and recessed grains are relatively unaffected. The result is the restriction of air flow from the

nozzle is enhanced for the peripheral grains and grain clusters with chip loading, therefore increasing the signal energy and average back pressure.

4.5.2.2 Long Term Wear

Using more representative grinding parameters, an extended experiment was conducted to test the response of the sensor as the condition of the wheel surface evolved from the initial dressed state. The sensor was applied periodically throughout the experiment, which lasted for 400 passes of the grinding wheel over the workpiece. Additionally the grinding process was monitored using a dynamometer, measuring and recording the normal force between the workpiece and the grinding wheel.

The workpiece, a piece of unhardened tool steel measuring 25 mm wide, was ground using the parameters given in the table 4-3. Data was collected by the pneumatic sensor in the same manner used previously. Measurements were taken at SOD values set from the original dressed surface at 5, 41, and 76 μm , using seven axial locations. In this test the grinding and all data collection was conducted with a wheel surface speed of 30 m/s, in line with the use of representative testing parameters.

Table 4-3: Parameters for vitrified wheel long term wear testing.

Wheel Surface Speed (RPM)	Table Feed	Depth of Cut	Workpiece length
30 m/s (1977)	10 m/min	10 μm	330 mm

The results from the pneumatic sensor are shown and Pb-RMS curves in Fig 4-67. The area in the dotted outline is shown again to provide a clear view of

the results. The curves reflect the pneumatic sensor measurement sets taken for the dressed wheel surface and after 10, 100, 200 and 400 passes of the grinding wheel. Other measurement sets were taken during the experiment but are not shown for image clarity, as they show no deviation from the trends discussed.

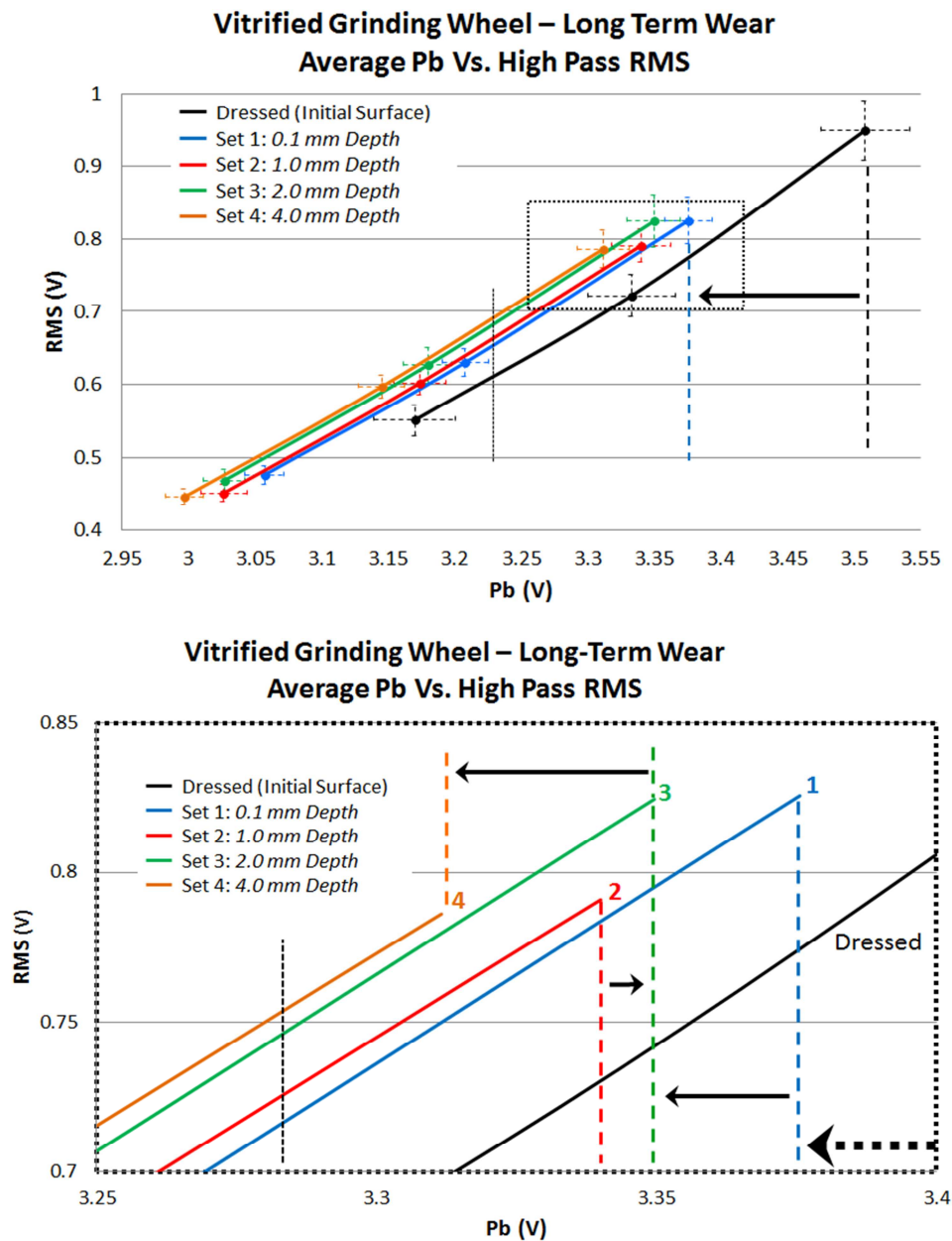


Figure 4-67: Long term wear testing Pb-RMS curve.

The discussion of the measurement results from the pneumatic sensor is oriented to the Pb-RMS curve shifting in three ways. These shifts are the large initial change from the dressed state to measurement set 1, the ‘sliding’ of measurements to lower values along a previous measurement set’s Pb-RMS curve as seen from set 1 to 2, and from set 3 to 4, and lastly the jump in RMS and Pb made from set 2 to 3.

The large initial change in the pneumatic sensor measurements from the dressed condition to after just ten grinding passes, measurement set 1, shows a significant increase in high pass RMS and a large decrease in the average back pressure. This is during a period of wheel wear when the great change to the wheel surface has been documented, [17,18,19]. For a vitrified grinding wheel trued and dressed by a single point diamond dressing tool, as in this research, the method of rolling the wheel over a carbon coated glass surface showed that peripheral grains are cut to zero clearance, exist in continuous groups of more than one grit having zero clearance and are shrouded by a layer of bond material cut flush with the surface of each grit. These experiments are supported by dynamometer results showing an early peak in grinding forces. Grisbrook concludes that the wheel surface as dressed is in this way loaded by the bond material, resulting in higher cutting forces until the bond material at the edge breaks away, leaving edges unsupported and exposed [18].

The dynamometer results are shown in Fig 4-68. The numbered and colour coded lines correspond to the measurement sets from Fig. 4-67, and show high normal force was produced by the initial grinding passes. The loss of bond material and any inadequately supported abrasive, edges or entire grains, accounts for both the large decrease in average back pressure and the increase in high pass RMS, as the effective SOD increases and the wheel surface opens up.

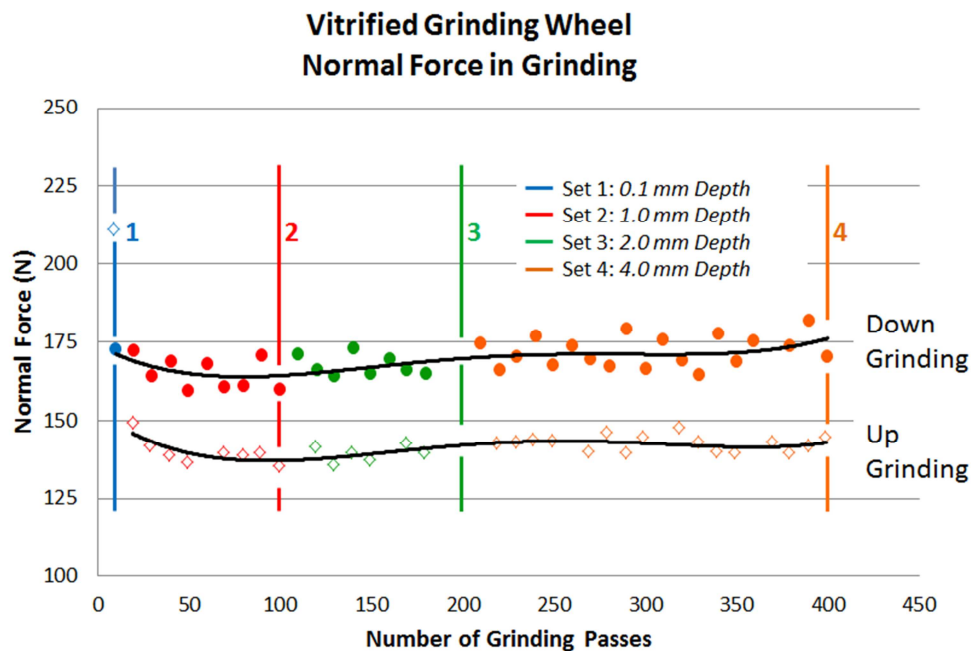


Figure 4-68: Dynamometer measurements of normal force.

True sliding of Pb-RMS curves can be seen in Fig. 4-64 for the measurement sets of the two dressed surfaces. The data points of the second measurement set, in green, fall on the curve formed by the first measurement set. The only difference being the increase in SOD values used for the second set. Referring to Fig. 4-67, from measurement set 1 to set 2, a significant decline in

the average back pressure occurs with a small increase in the high pass RMS. While not a true slide, as in Fig. 4-64, the transition is similar and may be described as such.

The decrease in average back pressure corresponds to an increase in effective SOD of just 7 μm , approximately, which is a small fraction the 250 μm nominal grain diameter. The minor change in high pass RMS indicates that while the average wheel surface is receding from the sensor the surface is maintaining similar topography while a small amount of material is lost from the surface.

The dynamometer results between measurement sets 1 and 2 show that the normal force continued to decline at a diminishing rate for a short time before reaching a relatively steady value. This supports the observations from the pneumatic sensor results, as during this time surface of the grinding wheel experiences micro-scale changes as fracture of the peripheral grains creates new sharp cutting edges and some grain and bond material is expelled.

The sliding of the Pb-RMS curve from set 3 to 4 similarly corresponds to decrease in the average back pressure and only a small increase in the high pass RMS is observed. The change in average back pressure corresponds to approximately 8 μm . Again this sliding action is indicative that the surface roughness is maintained, and the normal force measurements from the dynamometer show only a small degree of change over the course of the wear passes. This second sliding transition does have some differences from the first, most notably the high pass RMS is greater and the normal force measurements are

higher on average. The progression of this sliding transition is significantly slower than before, involving over twice as many grinding passes.

The transition from measurement set 2 to 3 is a jump in both the high pass RMS as well as the average back pressure. As in the grinding burn experiment this can only be caused by the addition of material to the wheel surface, and thus is indicative of chips collecting in the area around the outer most grains. While the wheel surface condition was not compromised to the point of causing grinding burn the dynamometer results show a small increase in the normal force from an average of 140 N to 143 N for up grinding, and from 164 N to 172 N for down grinding. It should be noted that the last two force measurements for this period were compromised by an equipment malfunction for both up and down grinding, and cannot be included.

Change in effective SOD is calculated using a back pressure curve, generated at operating speed for the vitrified grinding wheel with a coarse dressing.

The long term wear experiment demonstrates that measurement from the pneumatic sensor can be reflective of the wheel surface condition. Changes known to occur to the condition of the surface of the grinding induce a logical and apt response from the pneumatic sensor in the form of changes to the high pass RMS value of the dynamic pressure transducer signal and average back pressure.

4.6 Measurement Variation by Axial Position of the Sensor

Shifting the axial position of the pneumatic sensor on a grinding wheel surface will alter the response of the sensor. This is because the surface of a grinding wheel is non-deterministic, and the topography will change with axial position. Therefore, for a consistent surface condition, such as a dressed wheel surface, the pneumatic sensor is presented with a distinct surface topography at each axial measurement location. The specific topography at each location will have a direct influence on the values of average back pressure and high pass RMS. The following section examines the effect of axial position on the average back pressure and high pass RMS values, and the validity of the progression in wheel surface condition portrayed by pneumatic sensor monitoring results.

The average back pressure responds to changes in the size of the escape area between the nozzle tip and the wheel surface. Because the escape area is dependent on the topography of the wheel surface, it is expected that the average back pressure will be affected by the axial position of the sensor.

The dynamic response of the pneumatic sensor is also dependent on the topography of the target surface. The specific surface topography presented to the sensor determines what frequencies and corresponding amplitudes are generated. Additionally, in cases where the average back pressure is increased, the amplitude of the dynamic signal will also increase.

In the calculation of the high pass RMS, the amplitude of the dynamic signal is partially a function of the frequencies generated, because the sensitivity

of the sensor changes over different frequency bands. Therefore it is expected that the amplitude of the dynamic signal and the high pass RMS will be affected by the axial position of the sensor.

Examining the effect of axial position during monitoring, measurement variation can be observed in the incremental monitoring of wear for the metal bond, diamond abrasive grinding wheel, in Fig. 4-57, (pg. 132). Fig. 4-69 (a) compares the response of the pneumatic sensor to the initial, dressed surface and after one set of grinding passes, for two of the axial measurement locations. It is clear from the responses to the dressed surface in Fig. 4-69 (a), that even for a consistent surface condition, set by the dressing process, the axial position of the sensor is the source of a large variation in the values of average back pressure and high pass RMS.

Fig 4-69 (b) and (c) show the complete response of the pneumatic sensor for the incremental wear test, for two axial positions. As wear progresses at each axial location, the average back pressure and high pass RMS values for location A are consistently higher than those from location B. However, the general trend of decreasing average back pressure and increasing high pass RMS as wheel wear progresses is clearly visible at both measurement locations, and in agreement with the results shown and discussed in section 4.5.1, and Fig. 4-57 (pg. 132).

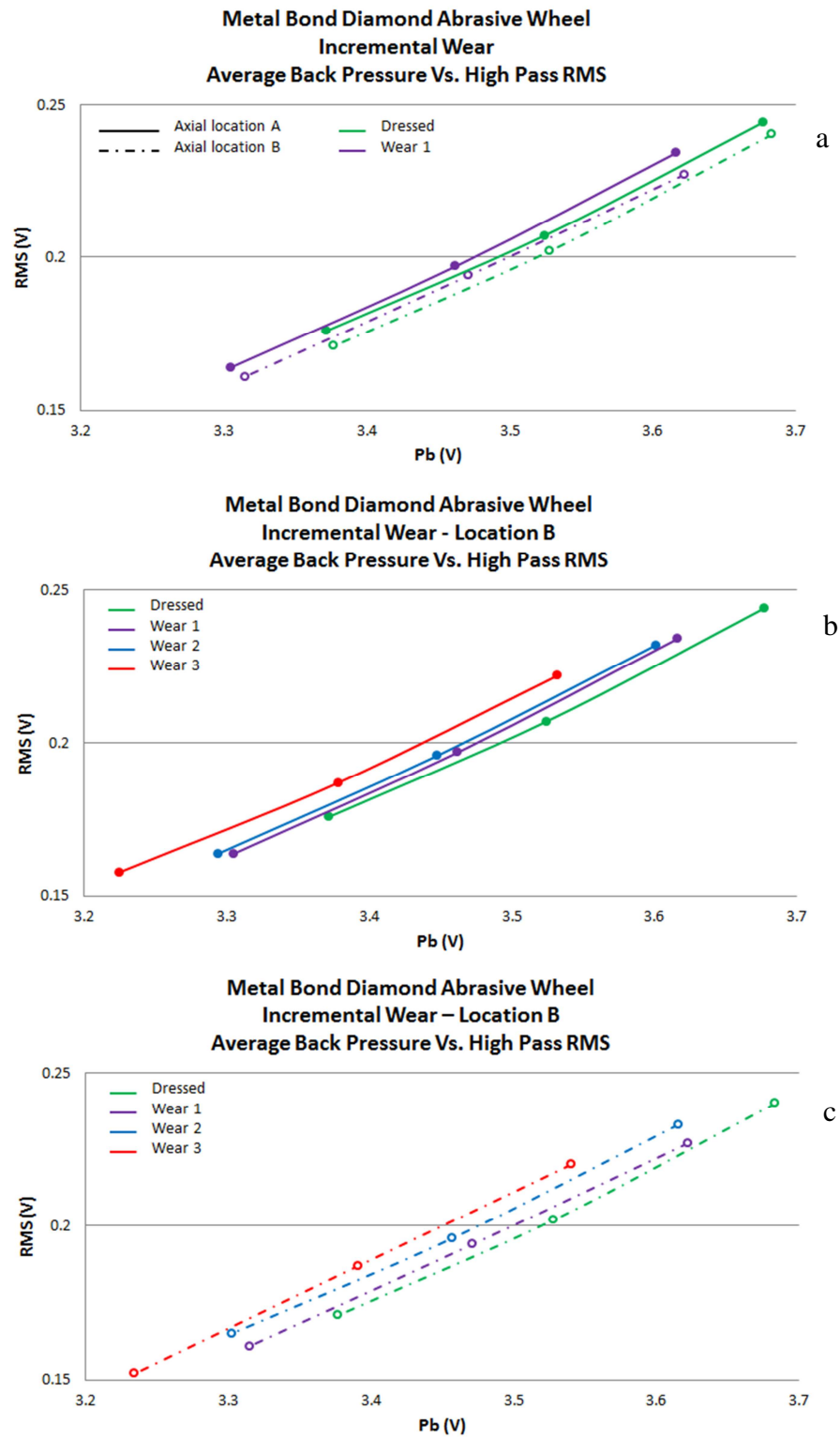


Figure 4-69: Pneumatic sensor measurements for two axial locations

The monitoring method described for this research includes the use of multiple axial measurement positions for the pneumatic sensor. As a result, the pneumatic sensor response for a given surface condition include a range of values, such as those shown for the progression of wear to a metal bond, diamond abrasive grinding wheel in Fig. 4-69. This section has established the axial position of the sensor as the major source of the variations, and shown that the results from the pneumatic sensor and prescribed monitoring method are therefore representative of the general progression of the wheel surface condition.

4.7 Effect of Coolant

The presence of coolant and debris from the grinding process are a major source of interference for direct measurement methods, and often require the use of additional cleaning air jets or protection for the sensors employed. It is proposed that such additional equipment is not required for a pneumatic sensor, as the constant flow of compressed air issuing from the nozzle tip clears the surface ahead of the sensor, leaving the wheel surface relatively unobstructed. In order to verify this, a series of experiments were conducted to investigate what effect the presence of coolant might have on the operation and performance of the sensor.

In a hypothetical production setup, the pneumatic sensor would be positioned at the wheel surface and away from the workpiece and grinding zone. An example of this positioning is shown in the diagram below with the sensor highlighted in red, Fig. 4-70. In addition to the spray generated by both the

coolant nozzle and the grinding wheel, the possibility of a fluid on or in the wheel surface was considered. To investigate what effect the presence of coolant might have on the pneumatic sensor, a simple experiment was constructed using a lathe and shaft mounted aluminum disk. The setup, shown in Fig. 4-71, provided coolant from the lathe as well as an additional air jet to rapidly clear the surface of the disk

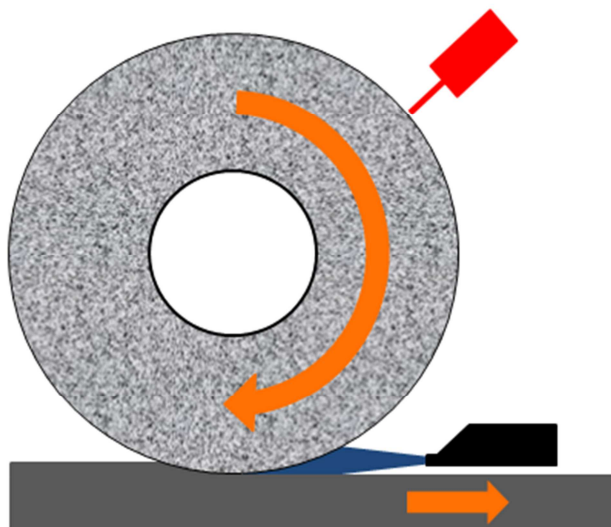


Figure 4-70: Illustration of in-process setup.

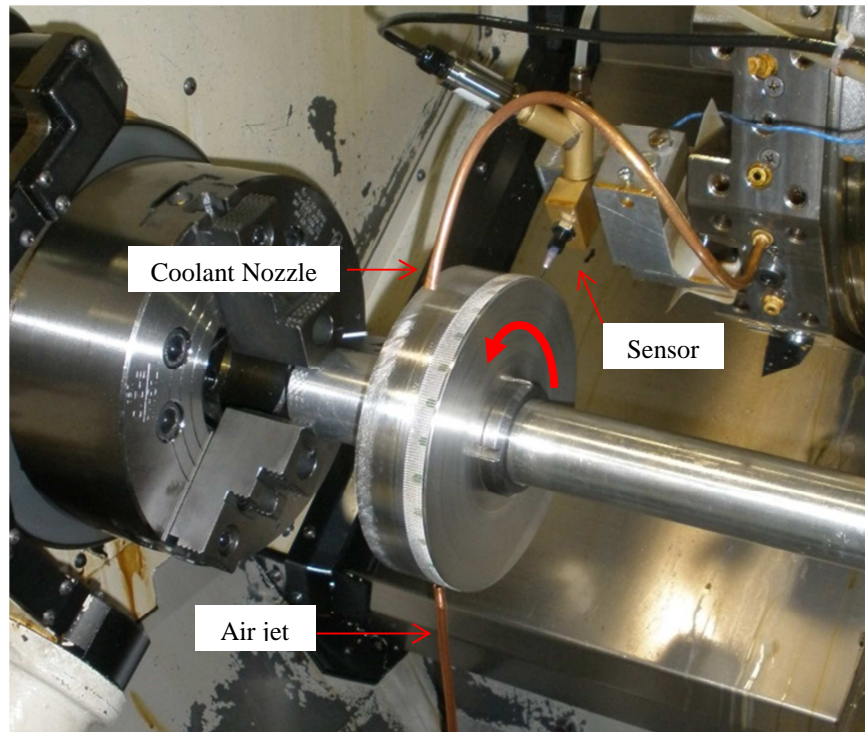


Figure 4-71: Indirect coolant application in lathe.

Applying the sensor to a section of large straight knurls at 20 m/s surface speed, measurements were taken with and without coolant, using a fixed SOD and supply pressure. The resulting dynamic pressure transducer signals are shown in the frequency domain, Fig. 4-72, and show an increase in signal amplitude for the frequencies created in response to the wheel surface. Most notably the frequency peak corresponding to the knurls, at 13 070 Hz, increases from 0.9 to about 1.0 V.

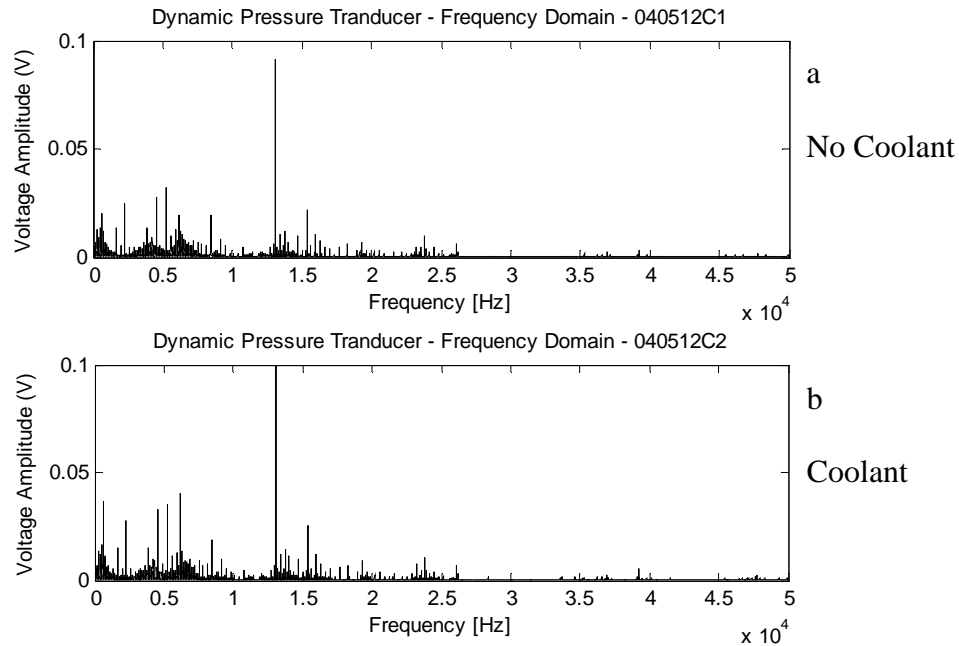


Figure 4-72: Straight knurls with no coolant (a) and with coolant (b).

This response is favourable as the frequency response of the sensor was unchanged except for an increase in signal strength. During the experiment it was noted that the average back pressure was increased by the presence of coolant. The effect of coolant on the average back pressure was further investigated as it directly influences the dynamic behaviour of the sensor. Using the auxiliary air jet to intermittently clear the surface of the disk of coolant confirmed that the presence of a coolant layer immediately increases the average back pressure, Fig. 4-73. This was established for both knurled and smooth disk surfaces.

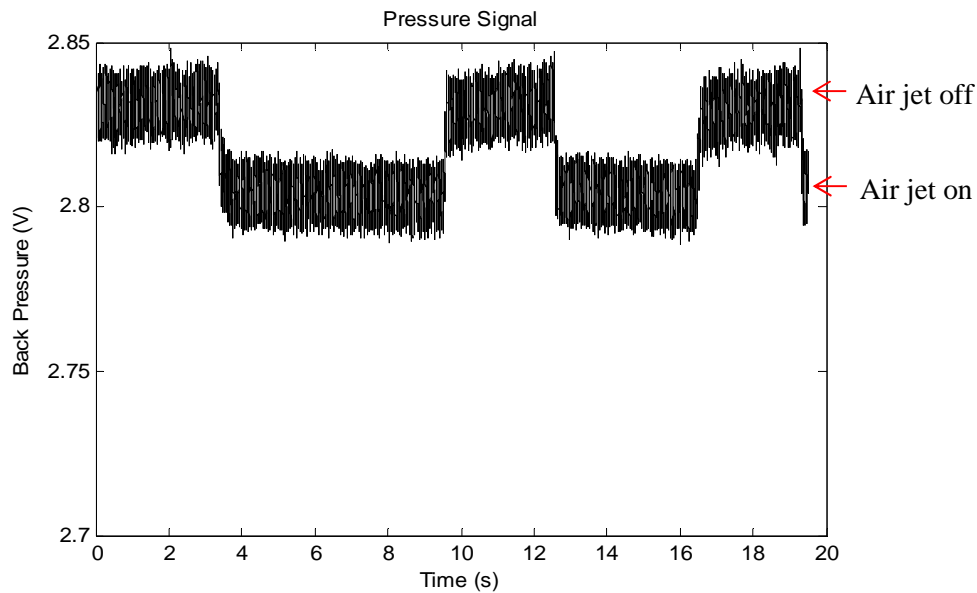


Figure 4-73: Back pressure with coolant and intermittent clearing by the auxiliary air jet.

With respect to grinding these simple tests suggest that the sensor should still be able to respond to the grinding wheel surface topography, with only a change in amplitude, as observed for the disk section with straight knurls. The effect of coolant on the monitoring of the grinding wheel surface was tested on the vitrified grinding wheel, at a surface velocity of 20 m/s. The coolant nozzle of the grinding machine was directed into the surface of the wheel so as to generously coat the surface directly ahead of the pneumatic sensor nozzle. Measurements of the grinding wheel surface were then taken at 3 stand-off distances. For the vitrified grinding wheel with no modification made to the wheel surface, the presence of coolant creates a sliding of the Pb-RMS curve, Fig. 4-74. Interpolating values of high pass RMS for each condition at a constant average back pressure show little change in the dynamic response of the sensor to the

presence of coolant. However, for the same stand-off distance the average back pressure is increased by the presence of coolant. While it may become difficult to accurately gauge a change in the effective SOD, the high pass RMS values that indicate surface roughness are very close for an equal average back pressure.

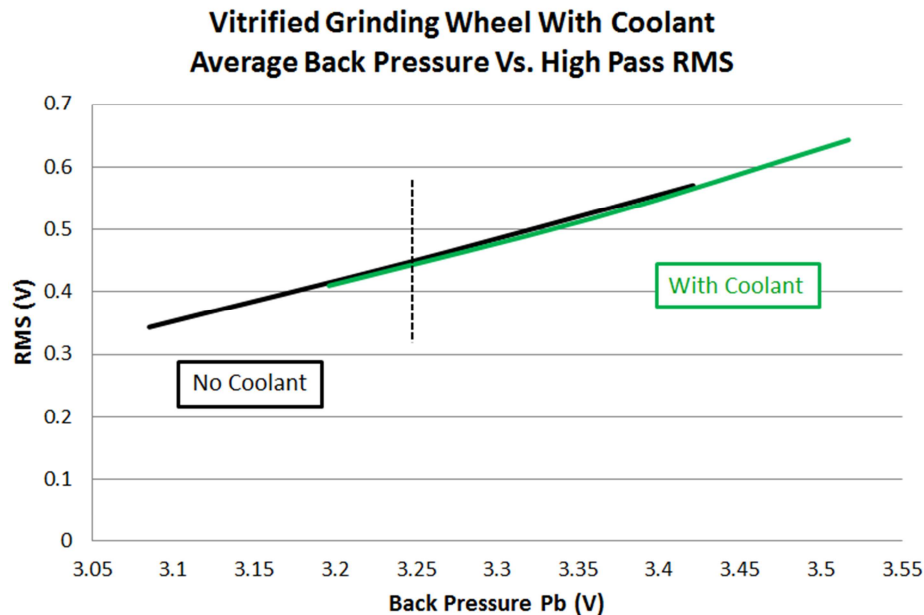


Figure 4-74: Effect of coolant on vitrified wheel measurements

It should be noted that when testing the effect of coolant the amplification of the raw signal from the dynamic pressure transducer was reduced by 30%, in reference to the dry wheel tests. This was necessary to prevent saturation of the sensor due to the increase in dynamic response amplitude caused by coolant. As a result, when comparing the Pb-RMS curves from this chapter to those in previous chapters, the high pass RMS reported here are lower.

In the case of the metal bond diamond abrasive grinding wheel, the effect of coolant is much more pronounced. When repeating the vitrified wheel

experiment on a trued surface measurements were taken at stand-off distances of 5, 15 and 25 μm . Fig. 4-75 shows the Pb-RMS curve was altered significantly. In addition to the increase in back pressure, the shape of the Pb-RMS curve is altered, and contrary to the results from the dry test indicates a higher high pass RMS value for a larger stand-off distance.

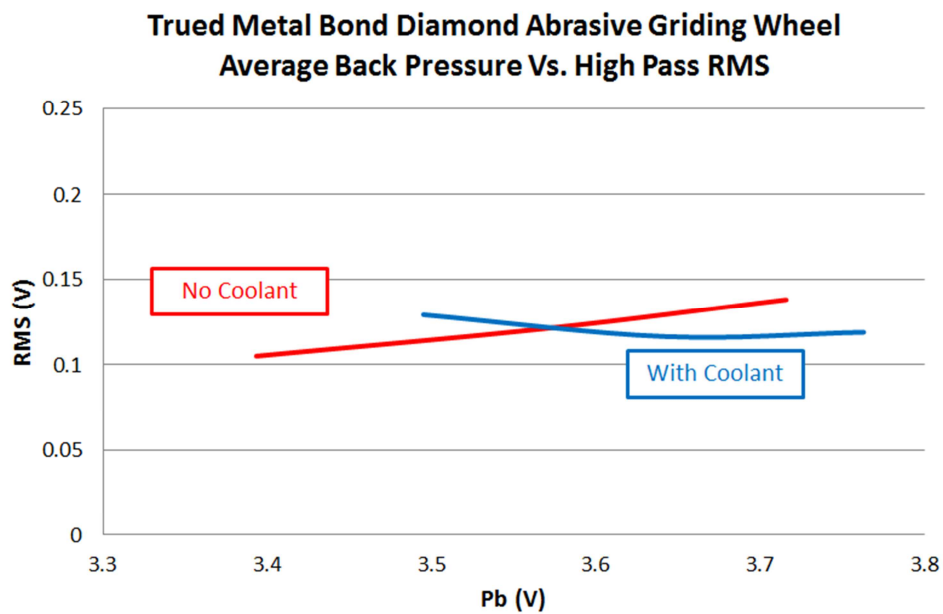


Figure 4-75: Effect of coolant on metal bond wheel measurements.

It is possible that changes in the pneumatic sensor setup, as shown in table 3-4 (pg. 50), are in part responsible for the dramatic interference from coolant. In order to more effectively monitor the finer surface of the diamond abrasive wheel, both the control orifice and nozzle diameters were 50% smaller than those used for either the knurled disk tests or the vitrified grinding wheel. This change resulted in a much reduced air flow rate and diminished capacity to clear coolant. Additionally the solid bond structure of the wheel provides no pores, which would

have aided the evacuation of coolant. In spite of this impedance it is still possible for the pneumatic sensor to detect an increase in surface roughness when the diamond abrasive wheel is dressed, Fig. 4-76.

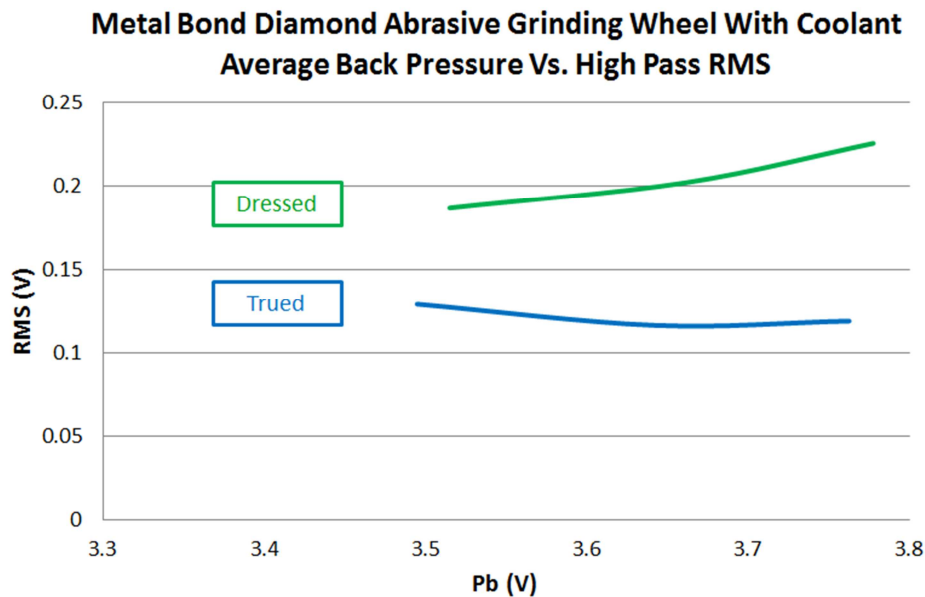


Figure 4-76: Metal bond wheel dressing in the presence of coolant.

The results shown in Fig. 4-76 demonstrate that while the presence of coolant alters the response of the pneumatic sensor to the wheel surface, the increase in surface roughness caused by the dressing process is still easily detectable.

Tests on both vitrified and metal bond grinding wheels show the pneumatic sensor is capable of responding to the wheel surface condition in the presence of coolant. Clearing of the coolant by the air flow in the vitrified wheel test allowed the nozzle to respond to the grains and pores of the of target wheel surface, which impinged or relieved the flow of air as during dry testing. In the case of the metal bond diamond abrasive wheel, the altered response of the sensor

suggests that the wheel surface is partially obstructed by the applied coolant. The sensor is still capable of detecting the change in surface condition caused by dressing and it is possible improvements may be made to the sensor setup to increase the robustness of the monitoring system.

5 Conclusions and Future Work

The pneumatic sensor has been investigated as a possible means to directly monitor the surface condition of a grinding wheel at operating speeds and conditions. This chapter reviews the results of the developmental completed and details possibilities for future work.

5.1 Conclusions

The simplicity and robustness of the pneumatic sensor, together with a known ability to measure displacement and topography of a moving surface, made it an attractive possible solution to an application where no single monitoring method has achieved widespread acceptance. This research work was focused on linking the response of the pneumatic sensor to the topography of a high velocity, rotating surface, and demonstrating that it is possible to use a pneumatic sensor to monitor the surface of a grinding wheel. The results of the experiments that explored and developed the capabilities of the pneumatic sensor and monitoring method are summarised here.

5.1.1 High Frequency Response

Progressive experiments have shown that the topography of a rotating surface with a surface velocity of up to 30 m/s is reflected in dynamic pressure fluctuations in the back pressure. Confirmed by controlled changes to both

grinding wheels and knurled test surfaces, the high frequency response of the sensor is dependent on the surface passing by the nozzle tip.

5.1.2 Dynamic Response and Maximum SOD

It has been experimentally shown on both knurled test surfaces and on grinding wheels that, to generate a dynamic response the pneumatic sensor must be positioned within a maximum stand-off distance from the wheel surface. It was discovered that the maximum distance for measuring dynamic pressure fluctuations is much less than the range used to monitor displacement. The limit can be established by monitoring the change in the high pass RMS value of the dynamic pressure transducer signal while increasing the stand-off distance.

Testing of the wheel-specific pneumatic sensor setups found the maximum distance from the grinding wheel surface for dynamic measurements was approximately 0.2 mm for a porous vitrified grinding wheel, and 0.05 mm for the metal bond, diamond abrasive grinding wheel. In comparison, the maximum displacement measurement range for each wheel was 0.35 and 0.1 mm respectively.

The relatively smaller grit size of the diamond abrasives lead to the use of a smaller nozzle and control orifice in the sensor. For the metal bond wheel, the reduced maximum distance for both dynamic and displacement measurements is the result of these differences in the wheel topography and corresponding sensor setup.

5.1.3 Monitoring Grinding Wheels

Under the proposed method the signals from the dynamic pressure transducer are quantified by high pass RMS values and are made comparable by simultaneous monitoring of the average back pressure at multiple stand-off distances. Experiments designed to explore the response of the pneumatic sensor to changes in the surface condition of a grinding wheel have shown that the relative change in the dynamic signal as well as the average back pressure progress in a manner that is logical and consistent with the changes known to occur on the wheel surface. Promising results were achieved on both metal bond and vitrified wheel constructions for both dressing and wear of the wheel surface.

5.1.4 Effect of Coolant

The effect of coolant was very different for vitrified and solid bond wheel structures, and their respective pneumatic sensor setups. Measurements of the vitrified grinding wheel surface showed that the presence of coolant increased the average back pressure but did not otherwise alter measurements of the wheel surface. The presence of coolant on the solid bond grinding wheel caused some impedance, altering both the dynamic response of the sensor and the response to displacement. In light of this, changes to the wheel surface by first truing then dressing were still detectable as indicated by relative changes in measurements of each surface condition.

5.2 Future Work

The following section details suggestions for future investigation and possible improvements to the current monitoring method.

5.2.1 Improved Dynamic Response

When testing the effect of changing surface velocity the dynamic pressure signal from the pneumatic sensor was sampled at 2 MS/s. The test showed that both 20 and 30 m/s surfaces generated similar maximum frequencies (Fig. 4-43), suggesting that the maximum was not property of the surface, but rather a property of the sensor. The implication of this is that the current pneumatic sensor is not capable of capturing all of the possible dynamic pressure fluctuations from the surface, and thus does not capture all the possible information about the surface.

With a maximum frequency range of 100 kHz, on a surface moving at 20 m/s the current pneumatic sensor is limited to describing surface features with a wavelength of 200 μm or greater, or about the same size as an 80 grit grain. It is possible that higher frequencies may contain more information about the wheel surface and the condition of the abrasive grains.

Improvements to the dynamic response of the pneumatic sensor can be made by alterations to the physical setup of the sensor. It may be useful to refine the construction of the pneumatic sensor to simplify the interior chamber and reduce its volume to improve the response time of the sensor. Additionally, it has

been reported by Rucki *et al.* [11] that a reduction of the nozzle wall thickness would also improve dynamic response.

5.2.1.1 Wheel Runout and Circularity

While this project has focused on the high frequency response of the pneumatic sensor and surface topography, the pneumatic sensor remains an excellent measurement tool for displacement. While Wager [10] proposed that the pneumatic sensor be used to assess the position of a grinding wheel surface, the use of dynamic pressure fluctuations can provide even more information. Applying a low pass filter to the signal from the dynamic pressure transducer, the radius of a wheel may be measured as it rotates. Fig. 5-1 shows the low frequency fluctuation from a dressed wheel. While the fluctuations appear great the wheel surface is in fact correctly trued and dressed. Because this application was never fully investigated, it is difficult to estimate the true waviness of the wheel surface.

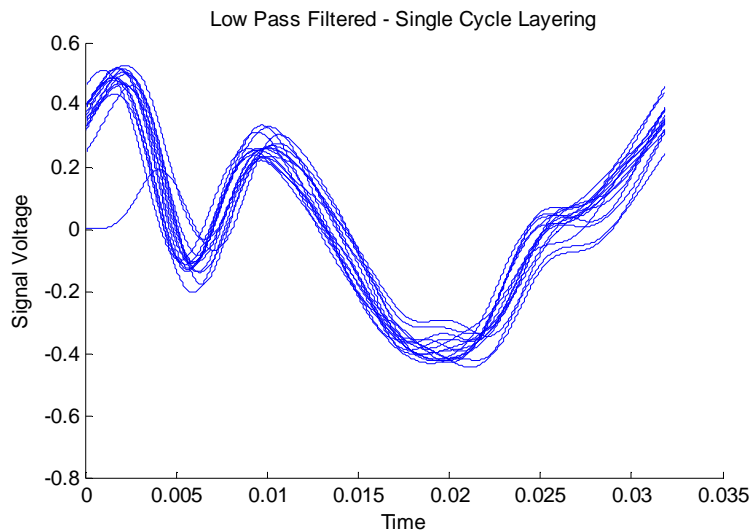


Figure 5-1: Low pass filtered dynamic response.

With further development it may be possible that the same pneumatic sensor used for monitoring wheel topography could also be used to monitor waviness and the wheel profile. Application for such a capability at fully operating speed and conditions go beyond wheel surface preparation, and may find use in the detection of grinding chatter.

In conclusion this work has shown that there is a clear connection between the response of the pneumatic sensor and surface of a grinding wheel. The simple operation of this type of sensor has proven useful and viable in operating conditions and operating speed typical of grinding operations, and application to both solid bond and porous vitrified grinding wheels has been demonstrated. These developments are promising not only to the application of grinding, but also to the monitoring of other rough, high velocity surfaces.

6 References

- [1] Europa Lehrmittel, Fachkunde Metall, 2010.
- [2] “Cylindrical Grinding Wheels,” *Norton Abrasives*, N.p. n.d. Web. April 28, 2013. <www.nortonindustrial.com>.
- [3] E. Brinksmeier, and F. Werner, “Monitoring of Grinding Wheel Wear,” *Annals of the CIRP*, vol. 41, pp. 373-376, 1992.
- [4] G. Byrne, D. Dornfeld, I. Inasaki, G. Ketteler, W. König, and R. Teti, “Tool Condition Monitoring (TCM) – The Status of Research and Industrial Application,” *Annals of the CIRP*, vol. 44, pp. 541-567, 1995.
- [5] B. Karpuschewski, M. Wehmeier, and I. Inasaki, “Grinding Monitoring System Based on Power and Acoustic Emission Sensors,” *Annals of the CIRP*, vol. 49, pp. 235-240, 2000.
- [6] J.F.G. Oliveira, E.J. Silva, C. Guo, and F. Hashimoto, “Industrial challenges in grinding,” *Annals of the CIRP*, vol. 58, pp. 663-680, 2009.
- [7] J. Webster, I. Marinescu, R. Bennett, and R Lindsay, “Acoustic Emission for Process Control and Monitoring of Surface Integrity during Grinding,” *Annals of the CIRP*, Vol. 43, pp. 299-304, 1994.
- [8] Z. Wang, P. Willett, P.R. DeAguiar, and J. Webster, “Neural network detection of grinding burn from acoustic emission,” *International Journal of Machine Tools and Manufacture*, vol. 41, pp. 283-309, 2001.

- [9] I. Menzies, and P. Koshy, “In-process detection of surface porosity in machined castings,” *International Journal of Machine Tools and Manufacture*, vol. 49, pp. 530-535, 2009.
- [10] J.G. Wager, “Surface Effects in Pneumatic Gauging,” *International Journal of Machine Tool Design and Research*, vol. 7, pp. 1-14, 1967.
- [11] M. Rucki, and B. Barisic, “Response Time of Air Gauges with Different Volumes of the Measurement Chambers,” *Metrology and Measurement Systems*, vol. 16, pp. 289-298, 2009.
- [12] M. Rucki, and C.J. Jermak, “Dynamic Properties of Small Chamber Air Gages,” *Journal of Dynamic Systems, Measurement, and Control*, Vol. 134, pp. 1-6, 2012.
- [13] D. Grandy, P. Koshy, and F. Klocke, “Pneumatic non-contact roughness assessment of moving surfaces,” *Annals of the CIRP*, vol. 58, pp. 515-518, 2009.
- [14] P. Koshy, D. Grandy, and F. Klocke, “Pneumatic non-contact Topography characterization of finish-ground surfaces using multivariate projection methods,” *Precision Engineering*, vol. 35, pp. 282-288, 2011.
- [15] S. Malkin, *Grinding Technology: Theory and Applications of Machining with Abrasives*, 1st ed. Dearborn, USA: Society of Manufacturing Engineers, 1989.
- [16] E. Oberg, F.D. Jones and H.L. Horton *Machinery’s Handbook*, Revised 21st ed. New York, USA: Industrial Press Inc., 1981.

- [17] C.E. Davis, “The Dependence of Grinding Wheel Performance on Dressing Procedure,” *International Journal of Machine Tool Design and Research*, vol. 14, pp. 33-52, 1974.
- [18] H. Grisbrook, “Precision Grinding Research,” *The Journal of the Institution of Production Engineers*, vol. 39, pp. 251-269, 1960.
- [19] H. Grisbrook, “Precision Grinding Research (Part 2),” *The Journal of the Institution of Production Engineers*, vol. 39, pp. 341-346, 1960.
- [20] P. Koshy, V.K. Jain, and G.K. Lal, “A model for the topography of diamond grinding wheels,” *Wear*, vol. 169, pp. 237-242, 1993.
- [21] “Brake-Controlled Truing Devices,” *Norton Abrasives*, N.p. n.d. Web. <www.nortonindustrial.com>.
- [22] W. Graham, and A.Y.C. Nee, “The grinding of tool steels – a comparison between diamond and cubic boron nitride,” *The Journal of the Institution of Production Engineers*, vol. 53, pp. 186-191, 1974.
- [23] T.M.A. Maksoud, A.A. Mokbel, and J.E. Morgan, “In-process detection of grinding wheel truing and dressing conditions using a flapper nozzle arrangement,” *Journal of Engineering Manufacture*, vol. 211, pp. 305-343, 1997.
- [24] E.O. Doebelin, *Measurement Systems: Application and Design*, 3rd ed. New York, USA: McGraw Hill Inc., 1983.